



National Technical University of Athens

School of Naval Architecture and Marine Engineering

Shipbuilding Technology Laboratory

# Corrosion behavior of Super-hydrophobic film on Copper in seawater



***FELIOS ATHANASIOS***

***Supervisor, Professor D.I PANTELIS***

*Athens 2012*



## Acknowledgments

For this project, which took me one year complete, I have been supported and assisted by many people, who I would like to thank and express my gratitude.

Firstly, I would like to thank my supervisor, Professor D.I. Pantelis, for his trust and his support and encouragement throughout my entire effort.

I would like to thank a lot Mrs. Tsiourva for her trust, support and guidance in this year, Dr A. Kontos and Dr. I Karatasios from National Center of Scientific Research, Demokritos for the contact angle measurements, and also Mrs. Korali and Prof. D. Manolakos from Laboratory of Manufacturing Technology in School of Mechanical Engineering for the AFM measurements. During my experimental work I received a great deal of help from the technical staff of the laboratory to whom I express my gratitude. I also would like to thank Dr A. Karantonis, Lecturer, in the School of Chemical Engineering for his valuable contribution in the study of electrochemical experiments and Dr. Ch. Papadopoulos, Lecturer for the participation in the examining committee.

Last but not least i want to thank my parents Iraklis and Aliki and my sister Aspa for supporting and encouraging me all the time. I want to thank Santra, without her I could not have made it, and all my beloved friends who understood and supported me.



## TABLE OF CONTENTS

Acknowledgments .....	i
Summary.....	vii
Περίληψη.....	viii
Συμπεριφορά σε διάβρωση υπέρ-υδρόφοβων επιφανειών χαλκού σε θαλασσινό νερό .....	viii
Εισαγωγή.....	ix
THEORETICAL PART .....	1
1 BIOMIMETIC .....	1
1.1 Introduction.....	1
1.2 Definition of Biomimetic .....	2
1.2.1 Some of the most known biomimetic designs .....	3
1.2.1.1 Mercedes-Benz bionic car .....	3
1.2.1.2 Velcro.....	4
1.2.1.3 Whalepower Wind Turbine .....	5
1.2.1.4 Shinkansen bullet train.....	6
1.2.1.5 Lotus Effect Hydrophobia .....	7
1.3 Hydrophobicity & Superhydrophobicity .....	8
1.3.1 Contact angle .....	8
1.3.1.1 Thermodynamics .....	10
1.3.1.2 Contact angle measurements.....	12
1.4 Fabrication of Superhydrophobic Surfaces .....	16
1.4.1 Anodic Oxidation .....	16
1.4.2 Electrodeposition and Chemical Etching.....	16
1.4.3 Plasma Etching.....	17
1.4.4 Laser Treatment .....	17
1.4.5 Electrospinning .....	18
1.4.6 Chemical Vapour Deposition .....	19
1.4.7 Sol–gel Processing .....	19
1.5 Applications for Superhydrophobic Materials .....	20
1.5.1 Problems that can be solved with Superhydrophobic Materials .....	20
i. Biofouling.....	20
ii. Corrosion .....	20
iii. Deicing .....	21
1.5.2 Tested Applications with Superhydrophobic Materials .....	22

i. Anti-Icing.....	22
ii. Anti-Corrosion .....	22
iii. Anti-Salination .....	23
2 COPPER .....	24
2.1 Introduction.....	24
2.2 Basic Properties of Coppers.....	26
2.2.1 Properties of copper:.....	28
General properties .....	28
Physical properties .....	28
Atomic properties.....	28
2.3 Copper and its Alloys .....	29
2.4 Applications of Copper and Copper Alloys .....	30
Property.....	30
Industry/Type of application .....	30
Reference .....	30
Property.....	31
Industry/Type of application .....	31
Reference .....	31
2.5 Marine Environments Applications of Copper and Copper Alloys .....	34
3 AQUEOUS CORROSION .....	36
3.1 Introduction.....	36
3.2 Thermodynamics of Aqueous Corrosion .....	37
3.2.1 Free Energy.....	40
3.3 Cell Potentials and the Electromotive Force Series.....	43
3.3.1 Table of Electromotive force series.....	44
3.3.3 Potential Measurements With Reference Electrodes .....	48
3.3.4 The Three-Electrode System .....	49
3.4.1 The kinetics of corrosion reactions .....	50
3.5.1 Mixed Potential Theory .....	56
EXPERIMENTAL PART.....	61
4 Experimental Procedure .....	62
4.1 Introduction.....	62
4. 2 Raw Material .....	63
4.2.1 Nominal Chemical Composition % by weight.....	64

4.2.2 Material Properties.....	64
4.2.3 Mechanical Properties.....	64
4.2.4 Physical Properties .....	65
4.2.5 Fabrication Properties .....	65
4.3 Cutting off Process.....	66
4.4 Cold Mounting Process.....	67
4.5 Grinding Process.....	67
4.5.1 Plane Grinding .....	68
4.5.2 Fine Grinding .....	68
4.6 Polishing Process .....	69
4.7 Etching Process [23].....	70
4.8 The Metallurgical Microscope .....	71
4.8.1 The Microscope .....	73
4.8.2 The Basic Metallurgical Microscope.....	73
Inverted microscope.....	74
4.8.3 The Mechanical System.....	74
4.8.4 The Optical System .....	76
4.9 Stereo microscope .....	76
4.10 The Microhardness Tester .....	77
4.11 The Scanning Electron Microscope (SEM) .....	79
4.12 Optical Tensiometry Contact Angle Measurements .....	83
4.13 Electrochemical Measurements .....	84
4.13.1 Three Electrode Cells.....	84
4.13.1.1 The working electrode.....	84
4.13.1.2 The Counter Electrode.....	85
4.13.1.3 The Reference electrode .....	85
4.13.1.4 The Source of Potential .....	86
4.13.1.5 The Electrolyte.....	86
4.13.2 E/log(i) Plots .....	88
4.14 The Atomic force microscopy (AFM).....	91
4.14.1 AFM Probe Deflection .....	91
4.14.2 Measuring Forces .....	91
4.14.3 AFM Modes of Operation.....	92
4.14.3.1 Contact Mode.....	92

4.14.3.2 Lateral Force Microscopy .....	93
4.14.3.3 Noncontact mode.....	93
4.14.3.4 Dynamic Force / Intermittant-contact / “tapping mode” AFM.....	93
4.14.3.5 Force Modulation .....	94
4.14.3.6 Phase Imaging.....	94
4.15 Preparation of Super-hydrophobic Surfaces .....	94
5 Results and Discussion .....	95
5.1 Introduction.....	95
5.2 Metallographic Study .....	95
5.3 Microhardness Measurements .....	102
5.4 Contact Angle Measurements.....	104
5.5 Atomic Force Microscopy.....	107
5.6 Scanning Electron Microscopy .....	109
5.7 Electrochemical Experiments .....	114
5.7.1 Open Circuit Experiments.....	114
5.7.2. Potentiodynamic Experiments .....	122
5.8 Anticorrosion mechanism .....	136
Conclusions.....	137
Bibliography.....	138



## Summary

A novel strategy for, the formation of a composite interface composed of the flower-like surface nanostructures, and how that innovative super-hydrophobic film affects corrosion behavior of the material, was studied within the present Thesis.

The film was formed on the fresh copper surface. The super-hydrophobic film was pretreated by myristic acid (*n*-tetradecanoic acid),  $(\text{CH}_3(\text{CH}_2)_{12}\text{COOH})$  chemically adsorbed onto the copper wafer. The film structure was probed with contact angle measurement (CA), scanning electron microscopy (SEM), and atomic force microscopy (AFM). Moreover, the corrosion resistances of bare and modified samples in seawater were investigated by Open Circuit and Potentiodynamic Polarization Measurements (PPM). Experimental results show that the corrosion resistance of Cu with super-hydrophobic surface was improved remarkably, because of its unique nanostructure.

All experimental results proved that the super-hydrophobic surface can improve the corrosion resistance of copper significantly. The air trapped in the nano-crevices of the film was suggested to be responsible for the superior water-repellent property.

## Περίληψη

### Συμπεριφορά σε διάβρωση υπέρ-υδρόφοβων επιφανειών χαλκού σε θαλασσινό νερό

Στην παρούσα διπλωματική εργασία μελετήθηκε μια καινοτόμος διεργασία, για το σχηματισμό σύνθετης οργανικής επίστρωσης σε υπόστρωμα χαλκού, με τη μορφή λουλουδιών «flower-like», η οποία έχει υπερ-υδρόφοβες ιδιότητες, καθώς και η επίδρασή της στην επιδεκτικότητα σε διάβρωση του χαλκού.

Το στρώμα σχηματίστηκε πάνω σε ενεργή επιφάνεια του χαλκού, η οποία προηγουμένως είχε λειανθεί έως 1500 SiC και προσβληθεί με HNO<sub>3</sub>, για την απομάκρυνση τυχόν οξειδίων. Η υπέρ-υδρόφοβη σχηματίστηκε με την εμβάπτιση των δοκιμίων για διάστημα δέκα (10) ημερών σε διάλυμα μυριστικού οξέος (CH<sub>3</sub>(CH<sub>2</sub>)<sub>12</sub>COOH) 0.06M, σε αιθανόλη, το οποίο προσροφάται χημικά πάνω στην επιφάνεια του χαλκού. Για τη μελέτη της υπερ-υδρόφοβης επιφάνειας που προέκυψε, πραγματοποιήθηκαν μετρήσεις της Γωνίας Επαφής (Contact Angle), παρατηρήσεις στο Ηλεκτρονικό Μικροσκόπιο Σάρωσης (SEM), και σε Μικροσκόπιο Ατομικής Δύναμης (AFM). Η συμπεριφορά σε διάβρωση μελετήθηκε με ηλεκτροχημικές μετρήσεις Ανοιχτού Κυκλώματος, καθώς και Ποτενσιοδυναμικές Καμπύλες, σε διάλυμα NaCl 3.5%.

Όλα τα πειραματικά αποτελέσματα απέδειξαν σαφή βελτίωση της συμπεριφοράς σε διάβρωση των υπερ-υδρόφοβων επιφανειών. Ο παγιδευμένος αέρας στις νάνο-εσοχές της οργανικής επίστρωσης που δημιουργήθηκε θεωρείται ότι παρέχει τις υπέρ-υδρόφοβες ιδιότητες των χημικά προσβεβλημένων επιφανειών.

## Εισαγωγή

Στόχος της παρούσας διπλωματικής εργασίας ήταν η δημιουργία υπερ-υδρόφοβων επιφανειών χαλκού, η μελέτη των επιφανειών αυτών, καθώς και η διερεύνηση της επιδεκτικότητάς τους στη διάβρωση.

Για το λόγο αυτό δοκίμια χαλκού, λειάνθηκαν και προσβλήθηκαν προκειμένου να επικαθήσει ευκολότερα η επίστρωση. Τα δοκίμια του καθαρού χαλκού μελετήθηκαν μεταλλογραφικά (Κεφ.5.2) και μετρήθηκε η μικρο-σκληρότητά τους (Κεφ.5.3). Στη συνέχεια βυθίστηκαν σε διάλυμα μυριστικού οξέως ( $\text{CH}_3(\text{CH}_2)_{12}\text{COOH}$ ) 0.06M, σε αιθανόλη για διάστημα 10 ημερών. Οι υπερ-υδρόφοβες επιφάνειες που σχηματίστηκαν μελετήθηκαν αρχικά ως προς τη μεταβολή της Γωνίας Επαφής τους, σε σχέση με τα γυμνά δοκίμια του χαλκού (Κεφ.5.4). Το ανάγλυφο των υπερο-υδρόφοβων επιφανειών μελετήθηκε στο Μικροσκόπιο Ατομικής Δύναμης (AFM) (Κεφ. 5.5) και στη συνέχεια έγιναν παρατηρήσεις στο Ηλεκτρονικό Μικροσκόπιο Σάρωσης (SEM) (Κεφ. 5.6). Για τη μελέτη της διάβρωσης πραγματοποιήθηκαν μετρήσεις Ανοιχτού Κυκλώματος (Open Circuit) και ελήφθησαν Ποτενσιοδυναμικές Καμπύλες (Potentiodynamic Curves) (Κεφ. 5.7). Όλα τα αποτελέσματα συγκρίθηκαν και σχολιάστηκαν με τα υπάρχοντα πρόσφατα στοιχεία της διεθνούς βιβλιογραφίας και διατυπώθηκαν σχετικά συμπεράσματα (Κεφ. 6). Τέλος, παρατίθεται αναλυτικά η βιβλιογραφία που χρησιμοποιήθηκε (Κεφ.7).

Η παρούσα εργασία εκπονήθηκε στο Εργαστήριο Ναυπηγικής Τεχνολογίας της Σχολής Ναυπηγών Μηχανολόγων Μηχανικών, ενώ οι μετρήσεις Γωνίας Επαφής στο Ινστιτούτο Φυσικοχημείας του Δημόκριτου, και οι μετρήσεις στο Μικροσκόπιο Ατομικής Δύναμης στο Εργαστήριο Κατεργασιών των Υλικών της Σχολής Μηχανολόγων Μηχανικών.

# **THEORETICAL PART**

# 1 BIOMIMETIC [13]

## 1.1 Introduction

Nature has gone through evolution over the 3.8 Gyr (gigayear, i.e. a billion ( $10^9$ ) years) since life is estimated to have appeared on the Earth (Gordon 1976). Nature has evolved objects with high performance using commonly found materials. These function on the macroscale to the nanoscale. The understanding of the functions provided by objects and processes found in nature can guide us to imitate and produce nanomaterials, nanodevices and processes. Biologically inspired design or adaptation or derivation from nature is referred to as '**biomimetics**'. The Lotus effect is a project coming from the field of biomimetics and exemplifies how nature can solve some major problems as are **corrosion, fouling, clotting** and others.

## 1.2 Definition of Biomimetic

**Biomimetic.** It means mimicking biology or nature. Biomimetic is derived from the Greek word biomimesis. The word was coined by polymath Otto Schmitt in 1957, who, in his doctoral research, developed a physical device that mimicked the electrical action of a nerve. Other words used include bionics (coined in 1960 by Jack Steele of Wright-Patterson Air Force Base in Dayton, OH), biomimicry and biognosis. The field of biomimetics is highly interdisciplinary. **It involves the understanding of biological functions, structures and principles of various objects found in nature by biologists, physicists, chemists and material scientists, and the design and fabrication of various materials and devices of commercial interest by engineers, material scientists, chemists and others.** Biological materials are highly organized from the molecular to the nanoscale, microscale and macroscale, often in a hierarchical manner with intricate nanoarchitecture that ultimately makes up a myriad of different functional elements. Nature uses commonly found materials. Properties of the materials and surfaces result from a complex interplay between the surface structure and the morphology and physical and chemical properties. Many materials, surfaces and devices provide multifunctionality. Molecular-scale devices, superhydrophobicity, self-cleaning, drag reduction in fluid flow, energy conversion and conservation, high adhesion, reversible adhesion, aerodynamic lift, materials and fibres with high mechanical strength, biological self-assembly, antireflection, structural coloration, thermal insulation, self-healing and sensoryaid mechanisms are some of the examples found in nature that are of commercial interest.

*So what are the most known biomimetic designs?*

## 1.2.1 Some of the most known biomimetic designs

### 1.2.1.1 Mercedes-Benz bionic car

The concept models of the Mercedes-Benz bionic car are appearing as part of the "Design and the Elastic Mind" exhibition at New York's Museum of Modern Art (MoMA), which showcases innovations in the fields of design and science.

One of the highlights of the exhibition is the Mercedes-Benz bionic car, which was first unveiled in June 2005 at the Innovation Symposium organized by Daimler AG in the US capital, Washington DC.



Figure 1 : Boxfish design

Engineers, designers and biologists at Mercedes-Benz worked hand in hand to develop the Mercedes-Benz bionic car. Its template was a sea dweller from tropical latitudes: *Ostracion Cubicus*, more commonly known as the **boxfish**. Despite

Shape	Drag Coefficient
Sphere	0.47
Half-sphere	0.42
Cone	0.50
Cube	1.05
Angled Cube	0.80
Long Cylinder	0.82
Short Cylinder	1.15
Streamlined Body	0.04
Streamlined Half-body	0.09
Measured Drag Coefficients	

its unusual-looking shape, the fish is extremely aerodynamic and can therefore move using a minimal amount of energy. Low drag helps the fish swim up to six body lengths per second, stabilized by the keel-like edges of its carapace.

In free flow, its body has an outstandingly low  $c_d$  value of **0.06**. These characteristics are also ideal ingredients for a car designed to achieve the best possible levels of energy efficiency and passenger safety.

The result is a two-door vehicle with four comfortable, individual seats and a drop-shaped design that is 4.24 meters long, 1.82 meters wide and 1.59 meters high.

With a drag coefficient ( $c_d$ ) of **0.19**, the Mercedes-Benz bionic car is one of the world's

most aerodynamic compact cars in its class. Today, this figure still stands as a benchmark for the aerodynamic optimization of car bodies.

### 1.2.1.2 Velcro



Figure 2 : Velcro idea came from burrs (seeds)

The most famous example of biomimicry was the invention of Velcro brand fasteners. The word Velcro is a portmanteau of the two French words velours ("velvet"), and crochet ("hook"). Hook-and-loop fasteners consist of two components: typically, two lineal fabric strips (or, alternatively, round "dots" or squares) which are attached (e.g., sewn, adhered, etc.) to the opposing surfaces to be fastened. The first component features tiny hooks; the second features even smaller and "hairier" loops. When the two components are pressed together, the hooks catch in the loops and the two pieces fasten or bind temporarily. When separated, by pulling or peeling the two surfaces apart, the velcro strips make a distinctive "ripping" sound.

The hook-and-loop fastener was invented in 1941 by Swiss engineer, Georges de Mestral who lived in Commugny, Switzerland. The idea came to him one day after returning from a hunting trip with his dog in the Alps. He took a close look at the burrs (seeds) of burdock that kept sticking to his clothes and his dog's fur. He examined them under a microscope, and noted their hundreds of "hooks" that caught on anything with a loop, such as clothing, animal fur, or hair. He saw the possibility of binding two materials reversibly in a simple fashion if he could figure out how to duplicate the hooks and loops.

Velcro is strong enough that a **5 cm<sup>2</sup> piece is enough to support a 175-pound (79 kg)**. The strength of the bond depends on how well the hooks are embedded in the loops, how much surface area is in contact with the hooks, and the nature of the force pulling it apart. If Velcro is used to bond two

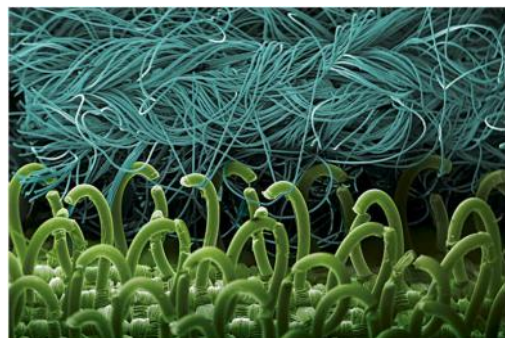


Figure 3 : Velcro

rigid surfaces, e.g. auto body panels and frame, the bond is particularly strong because any force pulling the pieces apart is spread evenly across all hooks. Also, any force pushing the pieces together is disproportionately applied to engaging more hooks and loops. Vibration can cause rigid pieces to improve their bond.



NASA makes significant use of Velcro. Each space shuttle has ten thousand inches of a special Velcro made of Teflon loops, polyester hooks, and glass backing. Velcro is used everywhere, from the astronauts' suits, to anchoring equipment. In the near weightless conditions in orbit, Velcro is used to temporarily hold objects and keep them from floating away. A Velcro patch is used inside astronauts' helmets where it serves as a nose scratcher. During mealtimes astronauts use trays that attach to their thighs using spring and Velcro fasteners. The US Army is another big user.



Figure 4 : NASA use Velcro

### 1.2.1.3 Whalepower Wind Turbine

Learn about a bio-mimicry concept that helps in harnessing the wind energy in a better way.

One of the most beneficial ways of increasing the efficiency of a wind turbine is to modify the design of the turbine blades. Although there are already many types of blade designs already in the market, only a few designs have turned out to be useful.



Figure 5 : Whalepower Wind Turbine



Figure 6 : Whale fin

Whalepower, a Canadian company that uses bio-mimicry, a concept of adapting the designs of nature into developing mechanical machine, has changed the design of the conventional turbine blades from flat smooth blades to a ridged design similar to that of whale fins. The blades of whale power turbine features a series of ridges just like the tubercles or bumps found on the humpback whale fins.

The whale power turbine uses tubercle technology, inspired from the whales, to harness

wind energy. Humpback whales move their fins at a specific angle to achieve a better lift in the water. The tilting of the blades is beneficial only if the steep angle is kept within a particular limit. This means that if the tilt is more a reverse action takes place which

leads to stalling, an effect that causes loss in lift. The tubercles on the whale's fins help to reduce this stalling, thus helping in getting steeper fin angles (**8% rise in lift**). This not only prevents stalling, but also prevents drag (**32% less drag**).



Figure 7 : Whalepower Wind Turbine

Steeper angled wind blades can be extremely beneficial in generating power, especially in low wind speed. Thus, the blades help in generating more power even in lower wind speeds. Moreover, it has been proved that adding tubercle bumps to the fins helps in pushing the **stall angle by 40 %**, making them better at moving the air around. Moreover, experiments on the whale turbine models have also helped in reducing the power usage by **20%**.

These specially designed blades if applied extensively, promises to increase annual electrical production by **20%**. One more advantage of these blades is that they greatly help in reducing the noise level. They are also more efficient and more reliable.

#### 1.2.1.4 Shinkansen bullet train

Shinkansen bullet train travelling at over 200 miles per hour, and is the fastest in the world. However the first design had one small problem, noise. Every time the train came out of a tunnel, it would produce an extremely loud bang because of the change in air pressure. Eiji Nakatsu, the train's chief engineer and an avid bird-watcher looked to nature for an answer. They found a similar situation in the kingfisher, which dives from air into water with little splashing. They redesigned the front end of the train using the beak of the kingfisher as a model and were able to create a much quieter train. The redesign also helped the train go **10% faster and use 15% less energy**.



Figure 8 : Shinkansen bullet train

### 1.2.1.5 Lotus Effect Hydrophobia



Figure 9 : Lotus effect

Lotus plants (*Nelumbo nucifera*) stay dirt-free, an obvious advantage for an aquatic plant living in typically muddy habitats, and they do so without using detergent or expending energy. The plant's cuticle, like that of other plants, is made up of soluble lipids embedded in a polyester matrix – wax – but the degree of its water repellency is extreme (superhydrophobic). This is accomplished

through the micro-topography of their leaf surfaces, which while showing a variety of structures, all share a similar mathematical set of proportions associated with superhydrophobicity.

Lotus leaves, for example, exhibit extensive folding (i.e., papillose epidermal cells) and epicuticular wax crystals jutting out from the plant's surface, resulting in a roughened microscale surface. As water and air adhere less well than water and solids, roughened surfaces tend to reduce adhesive force on water droplets, as



Figure 10 : Lotus effect

trapped air in the interstitial spaces of the roughened surface result in a reduced liquid-to-solid contact area. This allows the self-attraction of the polar molecule of water to express more fully, causing it to form spheres. Dirt particles on the leaf's surface stick to these droplets, both due to natural adhesion between water

and solids and because contact with the leaf surface is reduced by

over 95% from the leaf's micro-topography. The slightest angle in the surface of the leaf (e.g., caused by a passing breeze) then causes the balls of water to roll off due to gravity, taking the attached dirt particles with them and cleaning the leaf without using detergent or expending energy.

*Let's take a closer look to lotus effect and the meaning of Hydrophobia and Superhydrophobia.*

## 1.3 Hydrophobicity & Superhydrophobicity [22]

Hydrophobicity comes from the Greek words hydro, meaning water, and phobos, meaning fear. Is the physical property of a molecule (known as a hydrophobe) that is repelled from a mass of water. Hydrophobic molecules tend to be non-polar and, thus, prefer other neutral molecules and non-polar solvents. Hydrophobic molecules in water often cluster together, forming micelles. **Water on hydrophobic surfaces will exhibit a high contact angle.**

Superhydrophobic surfaces are highly hydrophobic, extremely difficult to wet. The **contact angles** of a water droplet **exceeds 150°** and the **roll-off angle** is **less than 10°**. This is also referred to as **the Lotus effect**, after the superhydrophobic leaves of the lotus plant.

*Let's define the meaning of **Contact angle**.*

### 1.3.1 Contact angle [28]

Contact angle,  $\theta$ , is a quantitative measure of the wetting of a solid by a liquid. It is defined geometrically as the angle formed by a liquid at the three phase boundary where a liquid, gas and solid intersect as shown below:

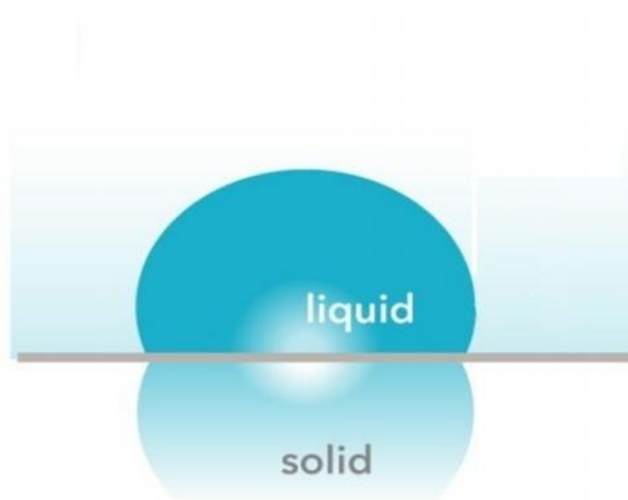


Figure 11 : Contact angle

If the molecules of a liquid are strongly attracted to the molecules of a solid (for example water on a strongly hydrophilic solid) then a drop of the liquid will completely spread out on the solid surface, corresponding to a contact angle of 0°.

Weaker attractions between liquid and solid molecules will result in higher contact angles. On many **low hydrophilic** surfaces, water droplets will exhibit contact angles of **0° to 30°**.

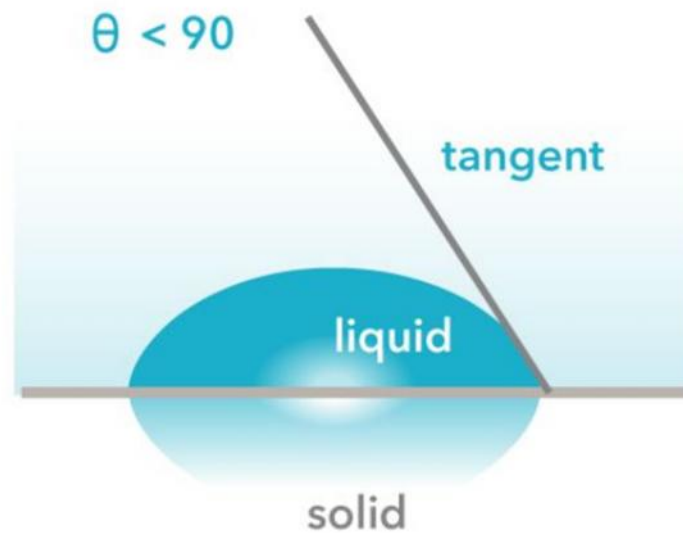


Figure 12 : Low hydrophilic surfaces

If the solid surface is **hydrophobic**, the water contact angle will be **larger than 90°**. Highly hydrophobic surfaces made of low surface energy (e.g. fluorinated) materials may have water contact angles as high as  $\sim 120^\circ$ . Some materials with highly rough surfaces may have a water contact angle even **greater than 150°**, due to the presence of air pockets under the liquid drop. These are called **superhydrophobic** surfaces.

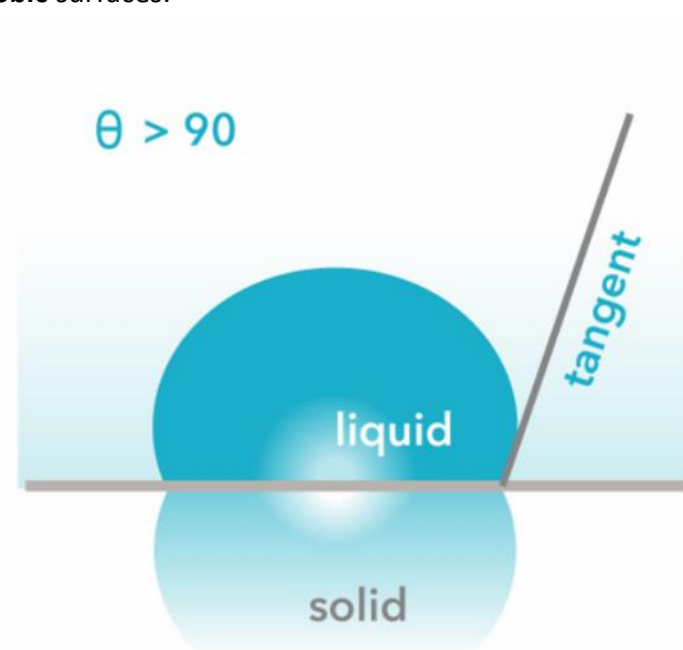


Figure 13 : Hydrophilic surfaces

The measurement of a single static contact angle to characterize the interaction is no longer thought to be adequate. For any given solid/ liquid interaction there exists a range of contact angles which may be found. The value of static contact angles are found to depend on the recent history of the interaction. **When the drop has recently expanded the angle is said to represent the 'advanced' contact angle. When the drop has recently contracted the angle is said to represent the 'receded' contact angle.** These angles fall within a range with advanced angles approaching a maximum value and receded angles approaching a minimum value.

If the three phase (liquid/solid/vapor) **boundary is in actual motion** the angles produced are called **Dynamic Contact Angles** and are referred to as 'advancing' and 'receding' angles. The difference between 'advanced' and 'advancing', 'receded' and 'receding' is that in the static case motion is incipient in the dynamic case motion is actual. Dynamic contact angles may be assayed at various rates of speed. Dynamic contact angles measured at low velocities should be equal to properly measured static angles. **The difference between the maximum (advanced/advancing) and minimum (receded/receding) contact angle values is called the contact angle hysteresis.** A great deal of research has gone into analysis of the significance of hysteresis. It has been used to help characterize surface heterogeneity, roughness and mobility. Briefly, for surfaces which are not homogeneous there will exist domains on the surface which present barriers to the motion of the contact line. For the case of chemical heterogeneity these domains represent areas with different contact angles than the surrounding surface. For example when wetting with water, hydrophobic domains will pin the motion of the contact line as the liquid advances thus increasing the contact angles. When the water recedes the hydrophilic domains will hold back the draining motion of the contact line thus decreasing the contact angle. From this analysis it can be seen that, when testing with water, advancing angles will be sensitive to the hydrophobic domains and receding angles will characterize the hydrophilic domains on the surface.

### 1.3.1.1 Thermodynamics

The theoretical description of contact arises from the consideration of a thermodynamic equilibrium between the three phases: the liquid phase of the droplet (**L**), the solid phase of the substrate (**S**), and the gas/vapor phase of the ambient (**G**) (which will be a mixture of ambient atmosphere and an equilibrium concentration of the liquid vapor). The gaseous phase could also be another (immiscible) liquid phase. At equilibrium, the chemical potential in the three phases should be equal. It is convenient to frame the discussion in terms of the interfacial energies. If we denote the solid–vapor interfacial energy as  $\gamma_{SG}$  the solid–liquid

interfacial energy as  $\gamma_{SL}$  and the liquid–vapor interfacial energy as simply  $\gamma$ , we can write an equation that must be satisfied in equilibrium (known as the **Young Equation**):

$$\gamma_{SG} + \gamma_{SL} + \gamma \cdot \cos\theta_c = 0$$

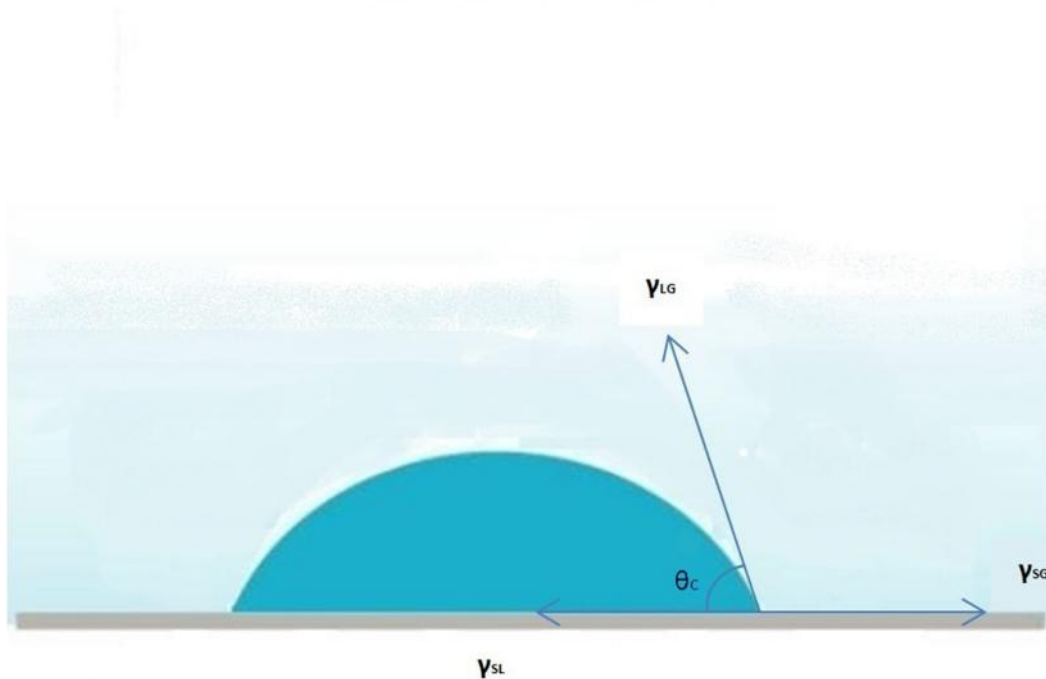


Figure 14 : Contact angle Young Equation

Where  $\theta_c$  is the equilibrium contact angle. The Young equation assumes a perfectly flat and homogeneous surface, and in many cases surface roughness and impurities cause a deviation in the equilibrium contact angle from the contact angle predicted by Young's equation.

Even in a perfectly smooth surface a drop will assume a wide spectrum of contact angles between the highest (advancing) contact angle,  $\theta_A$  and the lowest (receding) contact angle,  $\theta_R$ . The equilibrium contact angle ( $\theta_c$ ) can be calculated from  $\theta_A$  and  $\theta_R$  as was shown theoretically by Tadmar and confirmed experimentally by Chibowski:

$$\theta_c = \arccos \frac{r_A \cos \theta_A + r_R \cos \theta_R}{r_A + r_R}$$

Where,

$$r_A = \sqrt[3]{\frac{3 \sin^3 \theta_A}{2 - 3 \cos \theta_A - \cos^3 \theta_A}}$$

and,

$$r_R = \sqrt[3]{\frac{sr^3\theta_R}{2 - 3\cos\theta_R + \cos^3\theta_R}}$$

The contact angle can also be used to determine an interfacial energy (if other interfacial energies are known). This equation can be rewritten as the **Young-Dupre equation**:

$$\Delta W_{SLV} = \gamma(1 + \cos\theta_c)$$

Where  $\Delta W_{SLV}$  is the adhesion energy per unit area of the solid and liquid surfaces when in the medium V.

*How is contact angle measured?*

### 1.3.1.2 Contact angle measurements

Two different approaches are commonly used to measure contact angles of non-porous solids, **optical tensiometry** (goniometry) and **force tensiometry**. Optical tensiometry involves the observation of a sessile drop of test liquid on a solid substrate. Force ensiometry involves measuring the forces of interaction as a solid is contacted with a test liquid.

In the case of porous solids, powders and fabrics another approach is commonly used. This technique involves the Washburn method. It is the method of choice when your sample contains a porous architecture which absorbs the wetting liquid.

#### Optical tensiometry

Analysis of the shape of a drop of test liquid placed on a solid is the basis for optical tensiometry (goniometry). The basic elements of an optical tensiometer (also called contact angle meter) include light source, sample stage, lens and image capture. Contact angle can be assessed directly by measuring the angle formed between the solid and the tangent to the drop surface.

The production of drops with advanced and receded edges involves one of two strategies. Drops can be made to have advanced edges by addition of liquid.



Receded edges may be produced by allowing sufficient evaporation or by withdrawing liquid from the drop. Alternately, both advanced and receded edges are produced when the stage on which the solid is held is tilted to the point of incipient motion. Using an instrument with high speed image capture capabilities shapes of drops in motion may be analyzed.



Figure 15 : Optical tensiometry

### *Advantages*

Optical tensiometry can be used in many situations where force tensiometry cannot. You can use a great variety of solid substrates provided they have a relatively flat portion for testing. Substrates with regular curvature, such as contact lenses are also easily analyzed. Testing can be done using very small quantities of liquid. It is also easy to test high temperature liquids such as polymer melts.

### *Limitations*

The assignment of the tangent line which will define the contact angle is a factor which can limit the reproducibility of contact angle measurements. Conventional optical tensiometry relies on the consistency of the operator in

the assignment of the tangent line. This can lead to significant error, especially subjective error between multiple users.

### Force tensiometry

The force tensiometric method for measuring contact angles measures the forces that are present when a sample of solid is brought into contact with a test liquid. If the forces of interaction, geometry of the solid and surface tension of the liquid are known the contact angle may be calculated. The user first makes a measurement of the surface tension of the liquid using either a Wilhelmy plate or Du Noüy ring. The sample of the solid to be tested is then hung on the balance and tarred. The liquid is then raised to contact the solid. When the solid contacts the liquid the change in forces is detected and registers this elevation as zero depth of immersion. As the solid is pushed into the liquid the forces on the balance are recorded.

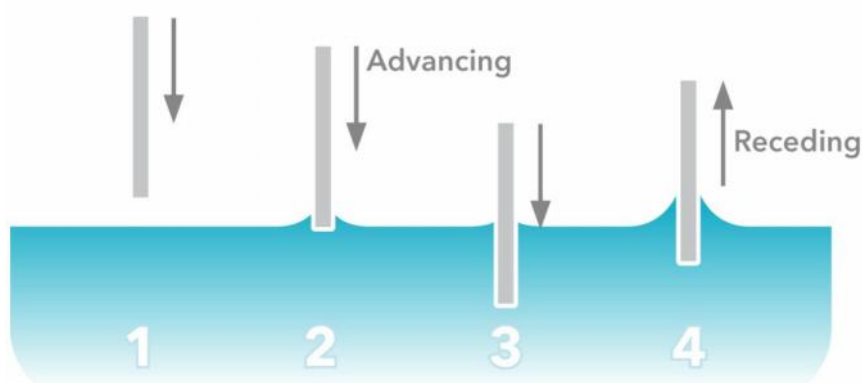


Figure 16 : Force tensiometric method

### Advantages

The use of force tensiometry for measurement of contact angle has several advantages over conventional optical tensiometry. At any point on the immersion graph, all points along the perimeter of the solid at that depth contribute to the force measurement recorded. Thus the force used to calculate  $\theta$  at any given depth of immersion is already an averaged value. You may calculate an averaged value for the entire length of the sample or average any part of the immersion graph data to assay changes in contact angle along the length of the sample.

This technique allows the user to analyze contact angles produced from wetting over an entire range of velocities from static to rapid wetting.

Because the contact angles are determined from the forces measured by the instrument there is no possibility of subjective error.

Analysis of fibers, very problematic for goniometry, is handled easily by your force tensiometer. A single fiber can also be analyzed with an optical tensiometer. You can find more information here about fiber wettability.

The graphs produced by this technique are very useful in studying hysteresis. Variations of contact angles, both advancing and receding, for the entire lengths of the sample tested are visualized on the same graph. In addition variations generated over multiple wetting/dewetting cycles can yield information on changes caused by wetting (such as absorption or surface reorientation).

### *Limitations*

There are two major limitations for the application of this technique. Firstly the user must have enough of the liquid being tested available so that he can immerse a portion of his solid in it. Secondly the solid in question must be available in samples which meet the following constraints. The sample must be formed or cut in a regular geometry such that it has a constant perimeter over a portion of its length. Rods, plates or fibers of known perimeter are ideal. The sample must have the same surface on all sides which contact the liquid.

It is also more difficult to use this technique in systems which are measured at high temperatures. Temperatures at or below 100 ° C are easily handled but for measurements above this range goniometry is recommended.

## 1.4 Fabrication of Superhydrophobic Surfaces [18] [19] [20] [21]

Inspired by the novel repellent properties of lotus leaves, scientists have created artificial super-hydrophobic surfaces by tailoring the surface topography and using techniques such as ***anodic oxidation, electrodeposition and chemical etching, plasma etching, laser treatment, electrospinning, chemical vapour deposition, sol-gel processing***, and so on. To fabricate a surface with a water contact angle larger than  $150^\circ$ , two key factors must be considered, Surface energy and Surface roughness. When the surface energy is lowered, the hydrophobicity is enhanced. However, even a material with the lowest surface energy gives a water contact angle of only around  $120^\circ$ . For higher hydrophobicity, providing an appropriate surface roughness is required.

### 1.4.1 Anodic Oxidation

Here we report the fabrication of self-organized nano- and microstructured surfaces with superhydrophobic properties by smart anodizing of certain thin-film valve metals covered by an aluminium layer. In this approach, the upper Al layer is first converted into its nanoporous oxide, then anodic oxidation of the underlying metal proceeds through the alumina barrier layer locally under the pores.

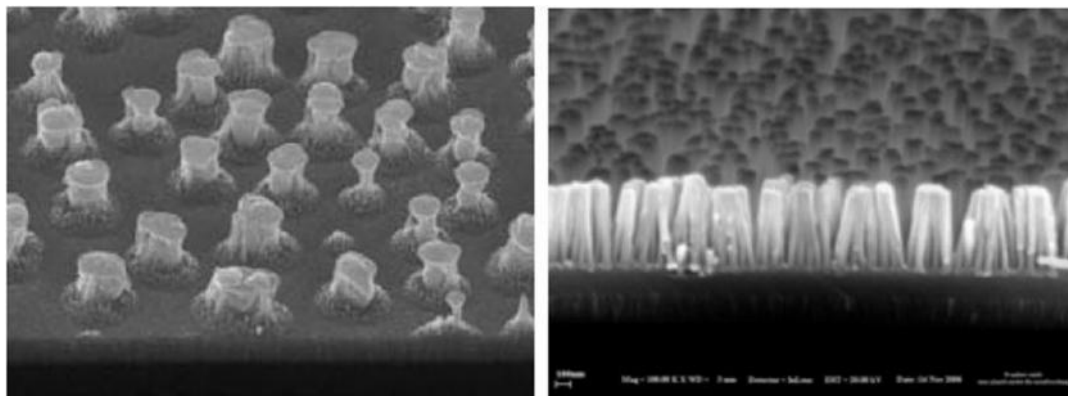


Figure 17 :Superhydrophobic structure with Anodic Oxidation

### 1.4.2 Electrodeposition and Chemical Etching

Electrodeposition it is analogous to a galvanic cell acting in reverse. The part to be plated is the cathode of the circuit. In one technique, the anode is made of the metal to be plated on the part. Both components are immersed in a solution called

an electrolyte containing one or more dissolved metal salts as well as other ions that permit the flow of electricity. A power supply supplies a direct current to the anode, oxidizing the metal atoms that comprise it and allowing them to dissolve in the solution. At the cathode, the dissolved metal ions in the electrolyte solution are reduced at the interface between the solution and the cathode, such that they "plate out" onto the cathode. The rate at which the anode is dissolved is equal to the rate at which the cathode is plated, vis-a-vis the current flowing through the circuit. In this manner, the ions in the electrolyte bath are continuously replenished by the anode.

### 1.4.3 Plasma Etching

Plasma etching is a form of plasma. It involves a high-speed stream of glow discharge (plasma) of an appropriate gas mixture being shot (in pulses) at a sample. The plasma source, known as etch species, can be either charged (ions) or neutral (atoms and radicals). During the process, the plasma will generate volatile etch products at room temperature from the chemical reactions between the elements of the material etched and the reactive species generated by the plasma. Eventually the atoms of the shot element embed themselves at or just below the surface of the target, thus modifying the physical properties of the target.

### 1.4.4 Laser Treatment

The first stage of the process involves creating a dispersion of nanoparticles (figure 18). Additives are employed to modify the properties of the dispersion so that it can subsequently be deposited on the substrate to form the required defect-free structure using an ink-jet printing process. In the final stage, the deposited film undergoes thermal post-treatment through exposure to laser radiation, which results in the specified sheet resistance through a combination of thermal compression and sintering.

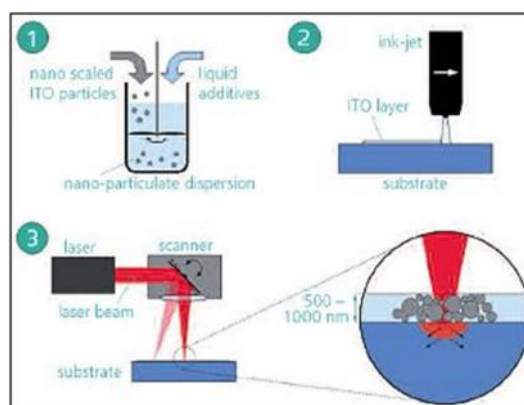


Figure 18 : Laser Treatment

### 1.4.5 Electrospinning

Electrospinning is a versatile technique for producing micro/nanofibers from many kinds of polymers. In a laboratory environment, electrospinning requires a high-power supply, a conducting substrate, and a syringe pump. The electrospinning process is initiated by a high electric field between the syringe (containing viscous polymer solution) and the conducting substrate. Because of the high electrical potential, a charged liquid jet is ejected from the tip of a distorted droplet, the so-called Taylor cone. The liquid jet experiences whipping and bending



Figure 19 : Superhydrophobic structure with Electrospinning

instabilities within a sufficient distance to evaporate its solvent thoroughly and, consequently, becomes a solid nonwoven micro/ nanofiber membrane on the substrate. Oriented polymer nanofibers can also be produced by modifying the ground electrode geometry and/or rotating it and by using a microfluidic chip to deliver the solution to the ejection tip. Electrospinning has been used to make membranes with rough surfaces, followed by the deposition of hydrophobic material, and to produce superhydrophobic membranes in a single-step process. In the former case, rough membranes are electrospun first and then coated with hydrophobic material by deposition techniques such as CVD and the layer-by-layer technique. In the latter case, the electrospun fiber itself can provide superhydrophobicity by electrospinning a blend of polymer and hydrophobic material and/or by introducing secondary structures such as pores and beads. Nanoparticles have also been introduced to increase roughness and to produce superhydrophobicity.

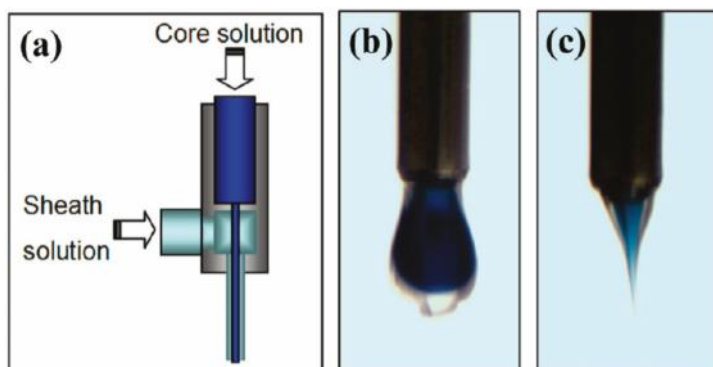


Figure 20: Coaxial electrospinning operation: (a) diagram of the coaxial nozzle (b) core-sheath droplet without bias (c) Taylor cone and coaxial jet formation.

### 1.4.6 Chemical Vapour Deposition

Chemical vapor deposition (CVD) is a chemical process used to produce high-purity, high-performance solid materials. The process is often used in the semiconductor industry to **produce thin films**. In a typical CVD process, the wafer (substrate) is exposed to one or more volatile precursors, which react and/or decompose on the substrate surface to produce the desired deposit. Frequently, volatile by-products are also produced, which are removed by gas flow through the reaction chamber.

Microfabrication processes widely use CVD to deposit materials in various forms, including: monocrystalline, polycrystalline, amorphous, and epitaxial. These materials include: silicon, carbon fiber, carbon nanofibers, filaments, carbon nanotubes, SiO<sub>2</sub>, silicon-germanium, tungsten, silicon carbide, silicon nitride, silicon oxynitride, titanium nitride, and various high-k dielectrics.

### 1.4.7 Sol-gel Processing

The sol-gel process is a wet-chemical technique widely used in the fields of materials science and ceramic engineering. Such methods are used primarily for the fabrication of materials (typically metal oxides) starting from a colloidal solution (sol) that acts as the precursor for an integrated network (or gel) of either discrete particles or network polymers. Typical precursors are metal alkoxides and metal salts (such as chlorides, nitrates and acetates), which undergo various forms of hydrolysis and polycondensation reactions.

With the viscosity of a sol adjusted into a proper range, both optical and refractory ceramic fibers can be drawn which are used for fiber optic sensors and thermal insulation, respectively. Thus, many ceramic materials, both glassy and crystalline, have found use in various forms from bulk solid-state components to high surface area forms such as thin films, coatings and fibers.

## 1.5 Applications for Superhydrophobic Materials [22]

- i. **Anti-corrosion**
- ii. **Anti-fouling**
- iii. **Anti-clotting**
- iv. **Anti-ice**
- v. **Anti-friction**
- vi. **Anti-condensation**
- vii. **Mildew and mold resistance**

*Some outstanding problems that can be solved with Superhydrophobic Materials.*

### 1.5.1 Problems that can be solved with Superhydrophobic Materials

#### i. **Biofouling:**

- Adds **330 lbs/meter<sup>2</sup>** in just **6 months**
- **\$70,000** – cost to clean a ship hull
- **40 –50%** increased fuel cost
- **\$2,1 billion** –annual cost to US Navy



Figure 21 : Biofouling problem on the hulls of ship

#### ii. **Corrosion:**

##### i. *Pipe Corrosion and Fouling:*

- **\$6 –8 billion** –transmission pipelines
- **\$276 billion** –residential plumbing costs



Figure 22 : Pipe Corrosion and Fouling



ii. *Bridge Corrosion:*

➔ Annual cost of US Bridges:  
**\$7 billion**



Figure 23 : Bridge Corrosion

iii. **Deicing:**

➔ Aircraft Deicing: **\$5.000**  
**per aircraft**



Figure 24 : Aircraft Deicing

➔ Power Lines : **One winter**  
**storm -\$5 billion**



Figure 25 : Power Lines Deicing

*Some Tested Applications with Superhydrophobic Materials.*

**1.5.2 Tested Applications with Superhydrophobic Materials**

**i. Anti-Icing:**

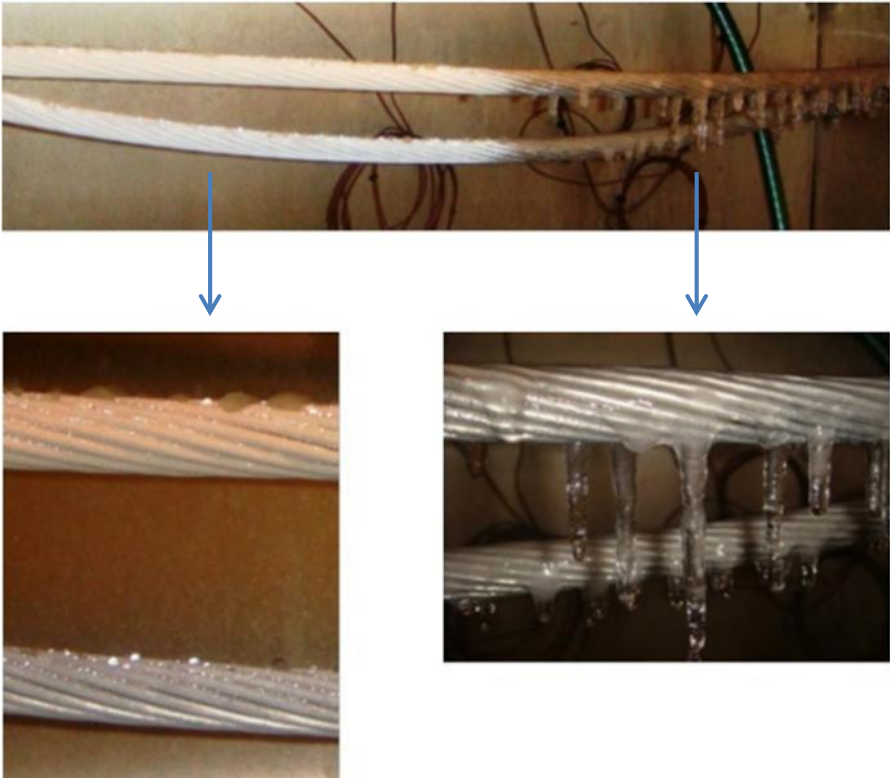


Figure 26 :Uncoated Cables & Coated Cables

**ii. Anti-Corrosion:**



Figure 27 :Steel Plate at day 1



Figure 28 :Steel Plate at day 60

iii. **Anti-Salination:**

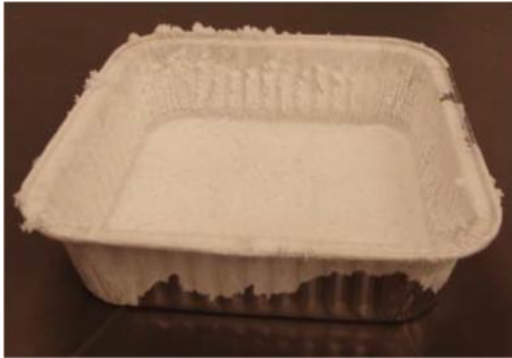


Figure 29 : Uncoated Aluminum Pan



Figure 30 : Aluminum Pan with Super Hydrophobic Coating

## 2 COPPER [1] [26]

### 2.1 Introduction

Copper was the first metal used by man in any quantity. The earliest workers in copper soon found that it could be easily hammered into sheets and the sheets in turn worked into shapes which became more complex as their skill increased. After the introduction of bronze, a wide



Figure 29 : Ancient Copper tools

range of castings also became possible. Many of the illustrations on this site serve to show man's progress as a metal-worker, culminating in the priceless inheritance of the Renaissance craftsmen. But copper and its principal alloys, bronze and brass, have always been more than a means of decorative embellishment. Although iron became the basic metal of every Western civilization from Rome onwards it was the copper metals which were used when a combination of strength and durability was required. The ability to resist corrosion ensured that copper, bronze and brass remained as functional as well as decorative materials during the Middle Ages and the successive centuries through the Industrial Revolution and on to the present day.

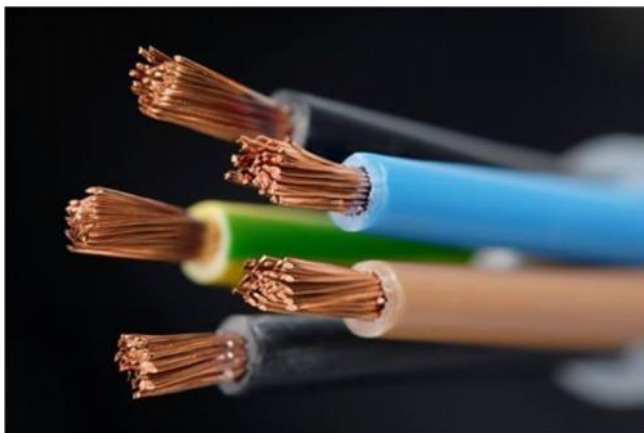


Figure 30 : Copper wires

Watt's steam engines, which ushered in the modern world, depended largely on iron and coal, with copper and its alloys making a lesser yet significant contribution, but with the subsequent development of electrical power copper proved to be the metal par excellence. The

early decades of the 19th Century saw the foundation of the Electrical Age and thereafter the demand for copper increased tremendously. Britain was the major producer for much of the 19th Century but new mines were opened

up in U.S.A., Chile, and later in Africa, until in 1911 the world's output of smelted copper for the first time exceeded a million tons per annum. With the increase in all branches of human activity which followed the Industrial Revolution new important uses were found for copper and advances in metallurgical knowledge led to the introduction of many new copper alloys.

Today more than 5 million tons of copper are produced annually and the copper metals are playing an increasingly vital part in many branches of modern technology. The ductility of copper, which led to its use for water piping in ancient Egypt, is illustrated by the countless thousands of miles of copper tube in contemporary plumbing and heating systems: the corrosion resistance of copper, which induced the Romans to use it for sheathing the roof of the Pantheon, is today verified by the thousands of copper roofs on modern buildings large and small; and the electrical conductivity of copper, which was utilized by Michael Faraday in his epoch-making experiments, remains the key to modern power generation.

These are but three of the examples outlined on this site where present applications are indissolubly linked with the past, but copper is also an essential material of the future. Solar heating, large-scale desalination of water, the linear motor are all innovations where copper will make an increasingly important contribution. The known reserves of copper ore are ample for all envisaged requirements, and continuous metallurgical research promises to provide new alloys possessing even superior properties to meet the exacting demands of the technology of the 21st Century.

*What are the basic properties and application of copper ?*



Figure 31 : Copper wire

## 2.2 Basic Properties of Coppers

Copper possesses the highest conductivity of any of the commercial metals. Hold a piece of copper and it will feel cold, an indication of how quickly hand heat can be conducted away. Each time you press a switch to light a room, think of the high electrical conductivity of the copper in the circuit that makes that simple operation possible. We take for granted the electrical power and also the metal essential for its efficient arrival at our homes. Lightning conductors in copper are a familiar sight protecting tall buildings - 200 years ago a conductor was attached to St Paul's Cathedral to lead lightning strikes safely to earth for that historic landmark.

Each time you turn on a water tap, think of the copper tubing that delivers the water hygienically within your home. Copper has excellent resistance to atmospheric and **marine corrosion** and good corrosion resistance when used in many industrial process environments. Add other elements to copper and we can get alloys that show good mechanical strength at low, ambient and elevated temperatures combined with high ductility and many other advantages.

The surface lustre and warm colour of copper and copper alloys makes them beautiful to look at and this means they find widespread use in architecture. The attractive green surface patina enhances the appearance of copper roofing. Bronze sculpture may have exquisite toning or patination. Jewellery and household ornaments and fittings gleam satisfyingly. If you look no further than your domestic surroundings, you will start to appreciate the huge role played by copper in the production of useful, attractive items that enhance our lives.

The word copper is used in everyday speech in the expression "a copper bottomed guarantee" as an assurance of long-term reliability.

Copper is a chemical element with the symbol Cu ( from **Latin: cuprum** ) and **atomic number 29**. It is a ductile metal with very high thermal and electrical conductivity. Pure copper is soft and malleable, a freshly exposed surface has a reddish-orange color.

In the Roman era, copper was principally mined on Cyprus, hence the origin of the name of the metal as **cyprium (metal of Cyprus)**, later shortened to cuprum. Its compounds are commonly encountered as copper(II) salts.

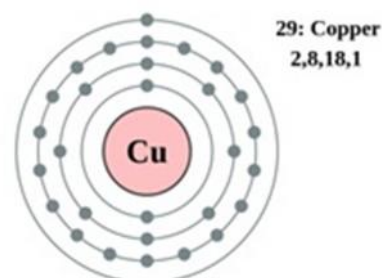


Figure 32 : Copper atom

Copper, silver and gold are in **group 11** of the periodic table, and they share certain attributes: they have one s-orbital electron on top of a filled d-electron shell and are characterized by high ductility and electrical conductivity. The filled d-shells in these elements do not contribute much to the interatomic interactions, which are dominated by the s-electrons through metallic bonds. Contrary to metals with incomplete d-shells, metallic bonds in



Figure 33 : Copper ore

copper are lacking a covalent character and are relatively weak. This explains the low hardness and high ductility of single crystals of copper. At the macroscopic scale, introduction of extended defects to the crystal lattice, such as grain boundaries, hinders flow of the material under applied stress thereby increasing its hardness. For this reason, copper is usually supplied in a fine-grained polycrystalline form, which has greater strength than monocrystalline forms.

**THE PERIODIC TABLE**

THE PERIODIC TABLE																		
1 IA																	18 VIIIA	
1 <b>H</b> 1.008 Hydrogen																		2 <b>He</b> 4.00 Helium
2 IIA												13 IIIA	14 IVA	15 VA	16 VIA	17 VIIA		
3 <b>Li</b> 6.94 Lithium	4 <b>Be</b> 9.01 Beryllium											5 <b>B</b> 10.81 Boron	6 <b>C</b> 12.01 Carbon	7 <b>N</b> 14.01 Nitrogen	8 <b>O</b> 16.00 Oxygen	9 <b>F</b> 19.00 Fluorine	10 <b>Ne</b> 20.18 Neon	
3 IIIB		4 IVB	5 VB	6 VIB	7 VIIB	8 VIII			9 VIIIB	10 VIIIB	11 IB	12 IIB						
11 <b>Na</b> 22.99 Sodium	12 <b>Mg</b> 24.31 Magnesium											13 <b>Al</b> 26.98 Aluminum	14 <b>Si</b> 28.09 Silicon	15 <b>P</b> 30.97 Phosphorus	16 <b>S</b> 32.07 Sulfur	17 <b>Cl</b> 35.45 Chlorine	18 <b>Ar</b> 39.95 Argon	
4 IIIB		4 IVB	5 VB	6 VIB	7 VIIB	8 VIII	9 VIIIB	10 VIIIB	11 IB	12 IIB								
19 <b>K</b> 39.10 Potassium	20 <b>Ca</b> 40.08 Calcium	21 <b>Sc</b> 44.96 Scandium	22 <b>Ti</b> 47.88 Titanium	23 <b>V</b> 50.94 Vanadium	24 <b>Cr</b> 52.00 Chromium	25 <b>Mn</b> 54.94 Manganese	26 <b>Fe</b> 55.85 Iron	27 <b>Co</b> 58.93 Cobalt	28 <b>Ni</b> 58.69 Nickel	29 <b>Cu</b> 63.55 Copper	30 <b>Zn</b> 65.39 Zinc	31 <b>Ga</b> 69.72 Gallium	32 <b>Ge</b> 72.61 Germanium	33 <b>As</b> 74.92 Arsenic	34 <b>Se</b> 78.96 Selenium	35 <b>Br</b> 79.90 Bromine	36 <b>Kr</b> 83.80 Krypton	
5 IIIB		4 IVB	5 VB	6 VIB	7 VIIB	8 VIII	9 VIIIB	10 VIIIB	11 IB	12 IIB								
37 <b>Rb</b> 85.47 Rubidium	38 <b>Sr</b> 87.62 Strontium	39 <b>Y</b> 88.91 Yttrium	40 <b>Zr</b> 91.22 Zirconium	41 <b>Nb</b> 92.91 Niobium	42 <b>Mo</b> 95.94 Molybdenum	43 <b>Tc</b> (97.9) Technetium	44 <b>Ru</b> 101.07 Ruthenium	45 <b>Rh</b> 102.91 Rhodium	46 <b>Pd</b> 106.42 Palladium	47 <b>Ag</b> 107.87 Silver	48 <b>Cd</b> 112.41 Cadmium	49 <b>In</b> 114.82 Indium	50 <b>Sn</b> 118.71 Tin	51 <b>Sb</b> 121.76 Antimony	52 <b>Te</b> 127.60 Tellurium	53 <b>I</b> 126.90 Iodine	54 <b>Xe</b> 131.29 Xenon	
6 IIIB		4 IVB	5 VB	6 VIB	7 VIIB	8 VIII	9 VIIIB	10 VIIIB	11 IB	12 IIB								
55 <b>Cs</b> 132.91 Cesium	56 <b>Ba</b> 137.33 Barium	57 <b>La</b> 138.91 Lanthanum	72 <b>Hf</b> 178.49 Hafnium	73 <b>Ta</b> 180.95 Tantalum	74 <b>W</b> 183.85 Tungsten	75 <b>Re</b> 186.21 Rhenium	76 <b>Os</b> 190.2 Osmium	77 <b>Ir</b> 192.22 Iridium	78 <b>Pt</b> 195.08 Platinum	79 <b>Au</b> 196.97 Gold	80 <b>Hg</b> 200.59 Mercury	81 <b>Tl</b> 204.38 Thallium	82 <b>Pb</b> 207.2 Lead	83 <b>Bi</b> 208.98 Bismuth	84 <b>Po</b> (209) Polonium	85 <b>At</b> (210) Astatine	86 <b>Rn</b> (222) Radon	
7 IIIB		4 IVB	5 VB	6 VIB	7 VIIB	8 VIII	9 VIIIB	10 VIIIB	11 IB	12 IIB								
87 <b>Fr</b> 223.02 Francium	88 <b>Ra</b> 226.03 Radium	89 <b>Ac</b> 227.03 Actinium	104 <b>Rf</b> (261) Rutherfordium	105 <b>Db</b> (262) Dubnium	106 <b>Sg</b> (263) Seaborgium	107 <b>Bh</b> (262) Bohrium	108 <b>Hs</b> (265) Hassium	109 <b>Mt</b> (266) Meitnerium	110 Unnamed Discovery 110 Nov. 1994	111 Unnamed Discovery 111 Nov. 1994	112 Unnamed Discovery 112 1996	114 Unnamed Discovery 114 1999	116 Unnamed Discovery 116 1999	118 Unnamed Discovery 118 1999				
ALKALI METALS												HALOGENS				NOBLE GASES		

The low hardness of copper partly explains its high electrical ( $59.6 \times 10^6 \text{ S/m}$ ) and thus also high thermal conductivity, which are the second highest among pure metals at room temperature. This is because the resistivity to electron transport in metals at room temperature mostly originates from scattering of electrons on thermal vibrations of the lattice, which are relatively weak for a soft metal. The maximum permissible current density of copper in open air is approximately  $3.1 \times 10^6$

$A/m^2$  of cross-sectional area, above which it begins to heat excessively. As with other metals, if copper is placed against another metal, galvanic corrosion will occur.

Together with osmium (bluish), and gold (yellow), copper is one of only three elemental metals with a **natural color** other than gray or silver. Pure copper is orange-red and acquires a reddish tarnish when exposed to air. The characteristic color of copper results from the electronic transitions between the filled 3d and half-empty 4s atomic shells – the energy difference between these shells is such that it corresponds to orange light. The same mechanism accounts for the yellow color of gold.

### 2.2.1 Properties of copper:

Table 1 : Properties of Copper

General properties		Physical properties		Atomic properties	
<i>Name, Symbol, Number</i>	Copper, Cu, 29	<i>Phase</i>	Solid	<i>Electronegativity</i>	1.90 (Pauling scale)
<i>Element category</i>	transition meta	<i>Density (near r.t.)</i>	8.96 g·cm <sup>-3</sup>	<i>Atomic radius</i>	128 pm
<i>Group, Period, Block</i>	11, 4, d	<i>Liquid density at m.p.</i>	8.02 g·cm <sup>-3</sup>	<i>Covalent radius</i>	132±4 pm
<i>Standard atomic weight</i>	63.546 (3)	<i>Melting point</i>	1084.6 °C	<i>Van der Waals radius</i>	140 pm
		<i>Boiling point</i>	2562 °C		
		<i>Heat of fusion</i>	13.26 kJ·mol <sup>-1</sup>		
		<i>Heat of vaporization</i>	300.4 kJ·mol <sup>-1</sup>		
		<i>Molar heat capacity</i>	24.440 J·mol <sup>-1</sup> ·K <sup>-1</sup>		



## 2.3 Copper and its Alloys

Copper forms alloys more freely than most metals, and with a wide range of alloying elements, Zinc, Tin, Nickel and Aluminium are the most common alloying additions and produce the following alloy types:

**COPPER** with:

- Tin makes **Bronze**
- Tin and Phosphorus makes **Phosphor bronze**
- Aluminium makes **Aluminium bronze**
- Zinc makes **Brass**
- Tin and Zinc makes **Gunmetal**
- Nickel makes **Copper-nickel**
- Nickel and Zinc make **Nickel silver**

Alloys based upon copper are classified as non-ferrous (ferrous materials are iron-base, for example, steel). Useful alloying additions of other elements to these alloys in small amounts can include *Aluminium, Arsenic, Beryllium, Cadmium, Chromium, Cobalt, Iron, Lead, Manganese, Nickel, Niobium, Oxygen, Phosphorus, Silicon, Silver, Sulphur, Tellurium, Tin, Zinc* and *Zirconium*. All are found in standard coppers and copper alloys and are added as required in small amounts to give specific properties suitable for many demanding applications. Some alloying elements have been in use with copper

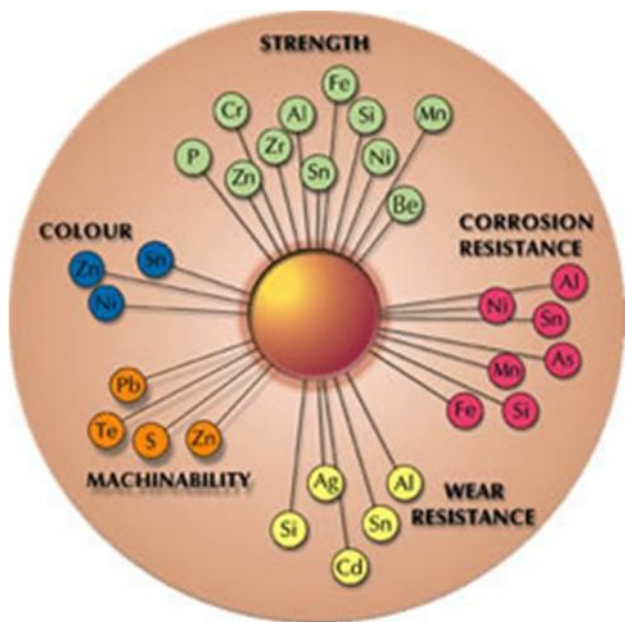





Figure 34 : Copper alloys


since early times. Initially there may have been no full understanding of what type of copper alloy had been produced and why it possessed its particular characteristics. However, the development of metallurgical and corrosion science knowledge has provided many answers and also led to the use of other alloying elements with copper. Further development of copper alloys is still taking place and will continue into the 21st century to meet modern application challenges.

## 2.4 Applications of Copper and Copper Alloys

The following table shows some of the reasons why copper and copper alloys are vital to the major types of application that benefit from combinations of the great many attributes available.

Table 2 : Applications of Copper and Copper Alloys

Property	Industry/Type of application	Reference
<i>Aesthetics</i>	<b>Architecture</b> <b>Sculpture</b> <b>Jewellery</b> <b>Clocks</b> <b>Cutlery.</b>	
<i>Bactericide</i>	<b>Door furniture</b> <b>Agricultural crop treatments.</b>	
<i>Bearing/antigalling properties</i> <i>Biofouling resistance</i>	<b>General and heavy engineering</b> <b>Metal working</b> <b>Aerospace</b> <b>Internal combustion engines</b> <b>Boat building</b> <b>Offshore oil and gas platforms.</b>	

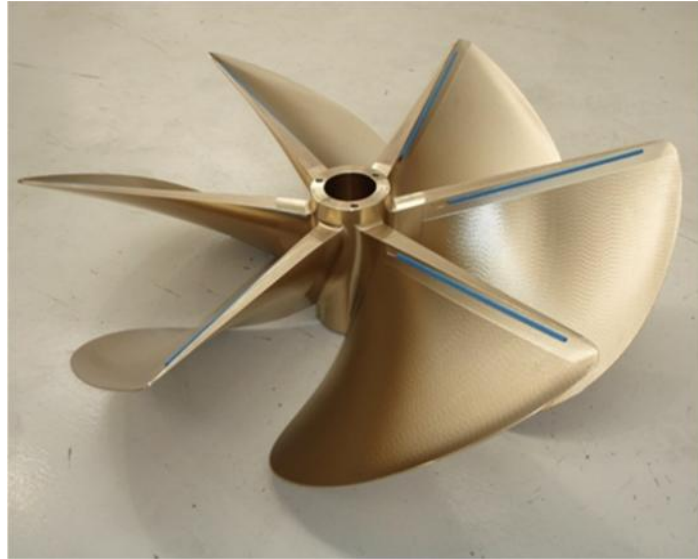
Property	Industry/Type of application	Reference
<i>Corrosion resistance</i>	<p>Plumbing tubes and fittings</p> <p>Roofing</p> <p>General and marine engineering</p> <p>Naval vessel and boat building</p> <p>Chemical engineering</p> <p>Industrial processes e.g. pickling, etching and distilling,</p> <p>Domestic plumbing</p> <p>Architecture</p> <p>Desalination</p> <p>Textiles</p> <p>Paper making.</p>	
<i>Ease of fabrication</i>	All of the above plus printing.	
<i>Environmental friendliness</i>	Vital for health of crops, animals and humans.	
<i>Fungicide</i>	<p>Agriculture</p> <p>Preservation of food and wood.</p>	
<i>Hardness</i>	<p>Non-sparking tools</p> <p>Springs.</p>	

<p><i>Electrical conductivity</i></p>	<p>Electrical engineering Communications Resistance welding Electronics.</p>	
<p><i>Low temperature properties</i></p>	<p>Cryogenics Liquid gas handling</p>	
<p><i>Mechanical strength/ductility</i></p>	<p>General engineering, Marine engineering Defence Aerospace.</p>	
<p><i>Non-magnetic</i></p>	<p>Instrumentation Geological survey equipment Mine counter-measure vessels Offshore drilling.</p>	
<p><i>Non-sparking</i></p>	<p>Mining tools Oxygen distribution.</p>	
<p><i>Resistance to hydrogen embrittlement</i></p>	<p>Offshore oil and gas (subsea), Boat/ship construction.</p>	

<p><i>Strength</i></p>	<p><b>Architectural fixings</b></p> <p><b>Engineering components.</b></p>	
<p><i>Springiness</i></p>	<p><b>Electrical springs and contacts</b></p> <p><b>Safety pins</b></p> <p><b>Instrument bellows.</b></p>	
<p><i>Thermal conductivity</i></p>	<p><b>Heat exchangers</b></p> <p><b>Automotive radiators</b></p> <p><b>Dies for plastics moulding</b></p> <p><b>Internal combustion engines</b></p> <p><b>Mining.</b></p>	
<p><i>Wear resistance</i></p>	<p><b>General and heavy engineering</b></p> <p><b>Shipbuilding</b></p> <p><b>Moulds and dies.</b></p>	

## 2.5 Marine Environments Applications of Copper and Copper Alloys

The excellent corrosion resistance in marine environments possessed by specially formulated copper alloys is combined with resistance to biofouling which confers a very useful advantage for desalination piping, pumps, valves, naval vessel components, boat propellers, shafts and rudders, yacht fittings, boat hulls, fish farming



cages, Offshore oil and gas equipment made in copper alloys includes pumps, splash zone and subsea bolting, drill collars, piping systems, valves, deluge system sprinklers and anti-fouling collars.

Figure 35 : Copper-Nickel propeller

The need for marine corrosion and biofouling resistance leads to the choice of copper-nickel. This confers the benefit of negligible material loss by corrosion attack and, in the case of a vessel hull, means that costly dry-docking for removal of biofouling is not needed. Higher speeds can consistently be achieved due to less resistance to movement through the water. It may also be possible to design with smaller engines, reduced size of fuel bunkers and increased cargo space. On offshore structures the use of copper-nickel clad steel means that it is possible to design with smaller corrosion factors and reduce allowances for the stresses caused when strong currents drag on extensive biofouling.

Ship components made of copper-nickel do not need active systems for their protection. Copper-nickel alloys form a protective shield against bio-fouling and emit very low amounts of poisonous copper ions. Weka, one supplier of boxcoolers made from copper-nickel tubes, has developed a protection system which manages to fully protect the ship and boxcooler from corrosion while at the same time eliminating the need for anode protection.

Protection against bio-fouling is necessary, but copper-nickel alloys is naturally protected. The left part of the picture shows a traditional coated boxcooler, the right part with tubes of copper-nickel

Dutch company **Weka**, the leading boxcooler company, has completely abandoned aluminium-brass and active anti-fouling systems in their boxcoolers. Weka's choice of copper-nickel alloys for the tubes in the boxcooler is based on economical and environmental reasons, says Cees de Kwant, head of Weka Boxcoolers BV:

“Copper-Nickel is a perfect material for boxcoolers. It has good manufacturing properties and is naturally protective against the fouling by animal. Earlier difficulties to adequately protect CuNi boxcoolers from galvanic corrosion, especially during welding at construction, have



Figure 36 : Copper-Nickel boxcooler

been solved. We regard the minimal issue of copper ions as a very strong argument for CuNi tubes, and we see yards and ship-owners increasingly prepared to accept the slightly higher initial cost. During the ship's operative life-time, the higher cost for CuNi tubes is paid back many times by lower maintenance costs.”

## 3 AQUEOUS CORROSION [2] [3] [4] [14] [15] [16] [17]

### 3.1 Introduction

Aqueous corrosion is an extremely complex physical phenomenon that depends on a multitude of factors including the metallurgy of the corroding metal, the chemistry of the corrosion-inducing aqueous phase, the presence of other – solid, gaseous, or non-aqueous liquid – phases, environmental constraints such as temperature and pressure, fluid flow characteristics, methods of fabrication, geometrical factors, and construction features. This inherent complexity makes the development of realistic physical models very challenging and, at the same time, provides a strong incentive for the development of practical models to understand the corrosion phenomena, and to assist in their mitigation. The need for tools for simulating aqueous corrosion has been recognized in various industries including oil and gas production and transmission, oil refining, nuclear and fossil power generation, chemical processing, infrastructure maintenance, hazardous waste management, and so on. The past three decades have witnessed the development of increasingly sophisticated modeling tools, which has been made possible by the synergistic combination of improved understanding of corrosion mechanisms and rapid evolution of computational tools.

Corrosion modeling is an interdisciplinary undertaking that requires input from electrolyte thermodynamics, surface electrochemistry, fluid flow and mass transport modeling, and metallurgy. In this chapter, we put particular emphasis on corrosion chemistry by focusing on modeling both the bulk environment and the reactions at the corroding interface. The models that are reviewed in this chapter are intended to answer the following questions:

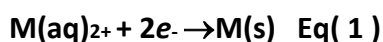
- i. What are the aqueous and solid species that give rise to corrosion in a particular system? What are their thermophysical properties, and what phase behavior can be expected in the system? These questions can be answered by thermodynamic models.
- ii. What are the reactions that are responsible for corrosion at the interface? How are they influenced by the bulk solution chemistry and by flow conditions? How can the interfacial phenomena be related to observable corrosion rates? These questions belong to the realm of electrochemical kinetics.

These models can be further used as a foundation for larger-scale models for the spatial and temporal evolution of systems and engineering structures subject to localized and general corrosion. Also, they can be combined with probabilistic and expert system-type models of corrosion.

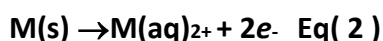


### 3.2 Thermodynamics of Aqueous Corrosion

In the discussion of chemical reactions and valence, the topic of electrochemical reactions is usually treated as a special case. Electrochemical reactions are usually discussed in terms of the change in valence that occurs between the reacting elements, that is, oxidation and reduction. Oxidation and reduction are commonly defined as follows. Oxidation is the removal of electrons from atoms or groups of atoms, resulting in an increase in valence, and reduction is the addition of electrons to an atom or group of atoms. Because electrochemical reactions or oxidation-reduction reactions can be represented in terms of an electrochemical cell with oxidation reactions occurring at one electrode and reduction occurring at the other electrode, electrochemical reactions are often further defined as cathodic reactions and anodic reactions. By definition, cathodic reactions are those types of reactions that result in reduction, such as:



Anodic reactions are those types of reactions that result in oxidation, such as:



Because of the production of electrons during oxidation and the consumption of electrons during reduction, oxidation and reduction are coupled events. If the ability to store large amounts of electrons does not exist, equivalent processes of oxidation and reduction will occur together during the course of normal electrochemical reactions. The oxidized species provide the electrons for the reduced species. The example stated above, like many aqueous corrosion situations, involves the reaction of aqueous metal species at a metal electrode surface. This metal/aqueous interface is complex, as is the mechanism by which the reactions take place across the interface. Because the reduction-oxidation reactions involve species in the electrolyte reacting at or near the metal interface, the electrode surface is charged relative to the solution, and the reactions are associated with specific electrode potentials. The charged interface results in an electric field that extends into the solution. This electric field has a dramatic effect on the solution near the metal. A solution that contains water as the primary solvent is affected by an electrical field because of its structure. The primary solvent -water--is polar and can be visualized as dipolar molecules that have a positive side (hydrogen atoms) and a negative side (oxygen atoms). In the electric field caused by the charged interface, the water molecules act as small dipoles and align themselves in the direction of the electric field. Ions that are present in the solution are also charged because of the loss or gain of electrons. The positive charged ions (cations) and negative charged ions (anions) also have an electric field associated with them. The

solvent (water) molecules act as small dipoles; therefore, they are also attracted to the charged ions and align themselves in the electric field established by the charge of the ion. Because the electric field is strongest close to the ion, some water molecules reside very close to an ionic species in solution. The attraction is great enough that these water molecules travel with the ion as it moves through the solvent. The tightly bound water molecules are referred to as the primary water sheath of the ion. The electric field is weaker at distances outside the primary water sheath, but it still disturbs the polar water molecules as the ion passes through the solution. The water molecules that are disturbed as the ion passes, but do not move with the ion, are usually referred to as the secondary water sheath. **Figure 39** shows a representation of the primary and secondary solvent molecules for a cation in water. Because of their smaller size relative to anions, cations have a stronger electric field close to the ion, and more water molecules are associated in their primary water sheath. However, anodic species have few, if any, primary water molecules.

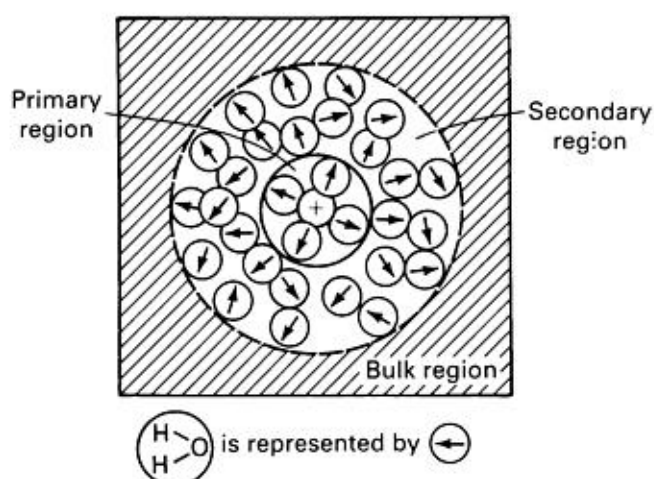


**Figure 37 :** Schematic of the primary and secondary solvent molecules for a cation in water

Because of the potential and charge established at the metal/aqueous interface of an electrode, ions and polar water molecules are also attracted to the interface because of the strong electric field close to the interface. Water molecules form a first row at the metal/aqueous interface. This row of water molecules limits the distance that hydrated ions can approach the interface. **Figure 40** shows a schematic diagram of a charged interface and the locations of cations at the surface. Also, the primary water molecules associated with the ionic species limit the distance the ions can approach. For example, the plane of positive charge of the cations that reside near the surface of a negatively charged interface is a fixed distance from the metal due to the water molecules that are between the surface and the ions. This plane of charge is referred to as the Outer-Heimholz Plane (OHP).

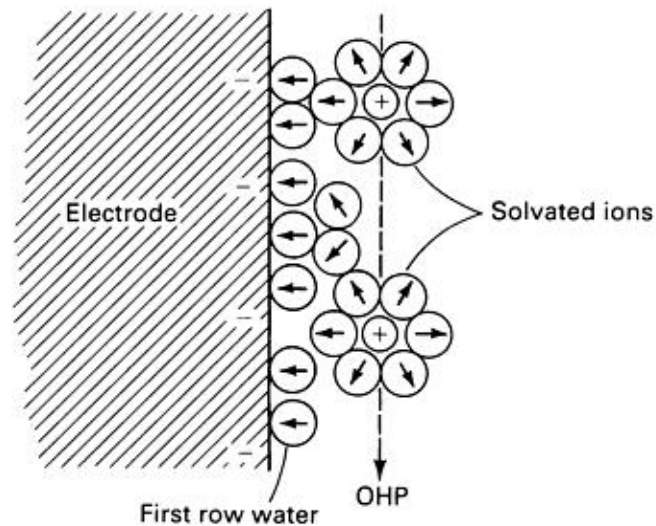


Figure 38 : Schematic of a charged interface and the locations of cations at the electrode surface

Because of the structure of the charged interface described above, it is often represented as a charged capacitor (**Fig. 41**). The potential drop across the interface is also often simplified as a linear change in potential from the metal surface to the OHP.

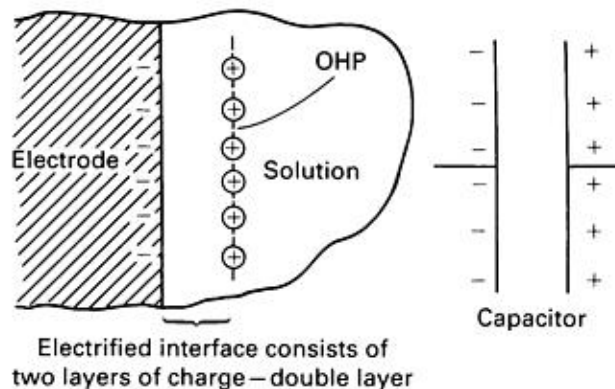


Figure 39 : Simplified double layer at a metal aqueous interface

The significance of the electronic double layer is that it provides a barrier to the transfer of electrons. If there were no difficulty in the transfer of electrons across the interface, the only resistance to electron flow would be the diffusion of aqueous species to and from the electrode. The surface would be nonpolarizable, and the potential would not be changed until the solution was deficient in electron acceptors and/or donors. This is of particular interest when dealing with the kinetics at the interface. The double layer results in an energy barrier that must be overcome. Thus, reactions at the interface are often dominated by activated processes, and activation polarization plays a significant role in corrosion. The key to controlling corrosion usually consists of minimizing the kinetics; this slows the reaction rates sufficiently that corrosion appears to be stopped. The object of chemical thermodynamics is to

develop a mathematical treatment of the chemical equilibrium and the driving forces behind chemical reactions. The desire is to catalog known quantitative data concerning equilibrium that can be later used to predict equilibria (perhaps even equilibria that has never been investigated by experimentation). The driving force for chemical reactions has been expressed in thermodynamic treatments as the balance between the effect of energy (enthalpy) and the effect of probability. The thermodynamic property that relates to probability is called entropy. The idea of entropy has been expressed as thermodynamic probability and is defined as the number of ways in which microscopic particles can be distributed among states accessible to them. The thermodynamic probability is an extensive quantity and is not the mathematical probability that ranges between **0** and **1**.

### 3.2.1 Free Energy

The driving force for chemical reactions depends not only on chemical formulas of species involved but also on the activities of the reactants and products. Free energy is the thermodynamic property that has been assigned to express the resultant enthalpy of a substance and its inherent probability. At constant temperature, free energy can be expressed as:

$$\Delta G = \Delta H - T\Delta S \quad \text{Eq( 3 )}$$

Where:

$\Delta G$  is the change in free energy (Gibbs free energy).

$\Delta H$  is the change in enthalpy.

$T$  is the absolute temperature.

$\Delta S$  is the change in entropy.

When reactions are at equilibrium and there is no apparent tendency for a reaction to proceed either forward or backward, it has been shown that:

$$\Delta G^\circ = -RT \ln K_{\text{eq}} \quad \text{Eq( 4 )}$$

Where:

$\Delta G^\circ$  is the free energy change under the special conditions when all reactants and products are in a preselected standard state.

$R$  is the gas constant.

$K_{\text{eq}}$  is the equilibrium constant.

The standard free energy of formations for an extensive number of compounds as a function of temperature have been cataloged; this allows the prediction of equilibrium constants over a wide range of conditions. It is necessary only to determine the standard free energy change for a reaction ( $\Delta G^\circ$ ) by subtracting the sum of the free energy of formations of the products at constant temperature.

If an electrochemical cell is constructed that can operate under thermodynamic reversible conditions (the concept of reversibility is described in more detail in the section, "Potential Measurements With Reference Electrodes") and if the extent of reaction is small enough not to change the activities of reactants and products, the potential remains constant, and the energy dissipated by an infinitesimal passage of charge is given by:

$$|\Delta G| = \text{charge passed} \cdot \text{potential difference}$$

or

$$|\Delta G| = nF \cdot |E| \quad \text{Eq( 5 )}$$

Where:

$n$  is the number of electrons per atom of the species involved in the reaction.

$F$  is the charge of 1 mol of electrons.

$E$  is the cell potential.

Because free energy has a sign that denotes the direction of the reaction, a thermodynamic sign convention must be selected. The common U.S. convention is to associate a positive potential with spontaneous reactions; thus, the reaction becomes:

$$\Delta G = -nFE \quad \text{Eq( 6 )}$$

If the reaction occurs under conditions in which the reactants and products are in their standard states, the equation becomes:

$$\Delta G^\circ = -nFE^\circ \quad \text{Eq( 7 )}$$

Combination with

$$\Delta G^\circ = -RT \ln K_{\text{eq}}$$

results in:

$$\ln K_{\text{eq}} = \frac{-nFE^{\circ}}{RT} \quad \text{Eq( 8 )}$$

Hus allowing the prediction of equilibrium data for electrochemical reactions.

### 3.3 Cell Potentials and the Electromotive Force Series

If a strip of zinc metal is placed in water, some zinc ions will be converted to aqueous zinc ions because of the relatively large tendency for zinc to oxidize. Because of the electrons remaining in the metal, the positively charged zinc ions will remain very close to the negatively charged zinc strip and thus will establish a double layer. The potential difference established between the solution and the zinc is of the order of 1 V, but because the double layer is very small, the potential gradient (change in potential with respect to distance) can be very high. A negative electrode potential (with respect to the standard hydrogen electrode discussed below) exists for a zinc electrode in a solution of zinc ions. However, if a copper strip is placed in a solution containing copper ions, a positive potential is established between the more noble copper strip and the solution. If, however, a metal is placed in a solution containing metal ions of a different nature, the first metal may dissolve, while the second metal deposits from its ions. A common example of this is the metal displacement reaction between zinc metal and copper ions, for which the complete oxidation-reduction reaction is:



If the reverse procedure is tried, that is, copper metal placed in a solution containing zinc ions, no reaction will take place to any measurable extent. For example, if the solution containing zinc ions has no copper ions present initially, the reaction will occur to a very small extent, with the reaction stopping when a certain very small concentration of copper ions has been produced. In the opposite case, zinc metal will react with copper ions almost to completion; the reaction will stop only when the concentration of copper ions is very small. The above experiment can be repeated with many combinations of metals, and the ability of one metal to replace another ion from solution can be used as a basis for tabulating the metals in a series. The table formed would show the abilities of metals to reduce other metal ions from solution. This electromotive force (**emf**) series for some common metals is shown in Table 3.

### 3.3.1 Table of Electromotive force series

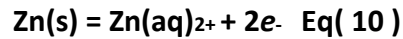
Table 3 : Table of Electromotive force series

$\text{Au}^{3+} + 3e^- \rightarrow \text{Au}$ 1.50	$\text{Au}^{3+} + 3e^- \rightarrow \text{Au}$ 1.50
$\text{Pd}^{2+} + 2e^- \rightarrow \text{Pd}$ 0.987	$\text{Pd}^{2+} + 2e^- \rightarrow \text{Pd}$ 0.987
$\text{Hg}^{2+} + 2e^- \rightarrow \text{Hg}$ 0.854	$\text{Hg}^{2+} + 2e^- \rightarrow \text{Hg}$ 0.854
$\text{Ag}^+ + e^- \rightarrow \text{Ag}$ 0.800	$\text{Ag}^+ + e^- \rightarrow \text{Ag}$ 0.800
2	2
$2 \text{Hg}^{2+} + 2e^- \rightarrow 2\text{Hg}$ 0.789	$2 \text{Hg}^{2+} + 2e^- \rightarrow 2\text{Hg}$ 0.789
$\text{Cu}^+ + e^- \rightarrow \text{Cu}$ 0.521	$\text{Cu}^+ + e^- \rightarrow \text{Cu}$ 0.521
$\text{Cu}^{2+} + 2e^- \rightarrow \text{Cu}$ 0.337	$\text{Cu}^{2+} + 2e^- \rightarrow \text{Cu}$ 0.337
$\text{Pb}^{2+} + 2e^- \rightarrow \text{Pb}$ -0.126	$\text{Pb}^{2+} + 2e^- \rightarrow \text{Pb}$ -0.126
$\text{Sn}^{2+} + 2e^- \rightarrow \text{Sn}$ -0.136	$\text{Sn}^{2+} + 2e^- \rightarrow \text{Sn}$ -0.136
$\text{Ni}^{2+} + 2e^- \rightarrow \text{Ni}$ -0.250	$\text{Ni}^{2+} + 2e^- \rightarrow \text{Ni}$ -0.250
$\text{Co}^{2+} + 2e^- \rightarrow \text{Ni}$ -0.277	$\text{Co}^{2+} + 2e^- \rightarrow \text{Ni}$ -0.277
$\text{Tl}^+ + e^- \rightarrow \text{Tl}$ -0.336	$\text{Tl}^+ + e^- \rightarrow \text{Tl}$ -0.336
$\text{In}^{3+} + 3e^- \rightarrow \text{In}$ -0.342	$\text{In}^{3+} + 3e^- \rightarrow \text{In}$ -0.342
$\text{Cd}^{2+} + 2e^- \rightarrow \text{Cd}$ -0.403	$\text{Cd}^{2+} + 2e^- \rightarrow \text{Cd}$ -0.403
$\text{Fe}^{2+} + 2e^- \rightarrow \text{Fe}$ -0.440	$\text{Fe}^{2+} + 2e^- \rightarrow \text{Fe}$ -0.440
$\text{Pb}^{2+} + 2e^- \rightarrow \text{Pb}$ -0.126	$\text{Pb}^{2+} + 2e^- \rightarrow \text{Pb}$ -0.126
$\text{Ga}^{3+} + 3e^- \rightarrow \text{Ga}$ -0.53	$\text{Ga}^{3+} + 3e^- \rightarrow \text{Ga}$ -0.53
$\text{Cr}^{3+} + 3e^- \rightarrow \text{Cr}$ -0.74	$\text{Cr}^{3+} + 3e^- \rightarrow \text{Cr}$ -0.74
$\text{Cr}^{2+} + 2e^- \rightarrow \text{Cr}$ -0.91	$\text{Cr}^{2+} + 2e^- \rightarrow \text{Cr}$ -0.91
$\text{Zn}^{2+} + 2e^- \rightarrow \text{Zn}$ -0.763	$\text{Zn}^{2+} + 2e^- \rightarrow \text{Zn}$ -0.763
$\text{Mn}^{2+} + 2e^- \rightarrow \text{Mn}$ -1.18	$\text{Mn}^{2+} + 2e^- \rightarrow \text{Mn}$ -1.18
$\text{Zr}^{4+} + 4e^- \rightarrow \text{Zr}$ -1.53	$\text{Zr}^{4+} + 4e^- \rightarrow \text{Zr}$ -1.53
$\text{Ti}^{2+} + 2e^- \rightarrow \text{Ti}$ -1.63	$\text{Ti}^{2+} + 2e^- \rightarrow \text{Ti}$ -1.63
$\text{Al}^{3+} + 3e^- \rightarrow \text{Al}$ -1.66	$\text{Al}^{3+} + 3e^- \rightarrow \text{Al}$ -1.66
$\text{Hf}^{4+} + 4e^- \rightarrow \text{Hf}$ -1.70	$\text{Hf}^{4+} + 4e^- \rightarrow \text{Hf}$ -1.70
$\text{U}^{3+} + 3e^- \rightarrow \text{U}$ -1.80	$\text{U}^{3+} + 3e^- \rightarrow \text{U}$ -1.80
$\text{Be}^{2+} + 2e^- \rightarrow \text{Be}$ -1.85	$\text{Be}^{2+} + 2e^- \rightarrow \text{Be}$ -1.85
$\text{Mg}^{2+} + 2e^- \rightarrow \text{Mg}$ -2.37	$\text{Mg}^{2+} + 2e^- \rightarrow \text{Mg}$ -2.37
$\text{Na}^+ + e^- \rightarrow \text{Na}$ -2.71	$\text{Na}^+ + e^- \rightarrow \text{Na}$ -2.71
$\text{Ca}^{2+} + 2e^- \rightarrow \text{Ca}$ -2.87	$\text{Ca}^{2+} + 2e^- \rightarrow \text{Ca}$ -2.87
$\text{K}^+ + e^- \rightarrow \text{K}$ -2.93	$\text{K}^+ + e^- \rightarrow \text{K}$ -2.93
$\text{Li}^+ + e^- \rightarrow \text{Li}$ -3.05	$\text{Li}^+ + e^- \rightarrow \text{Li}$ -3.05

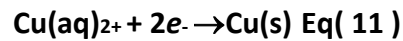
The reactions described in establishing an **emf** series are referred to as electrochemical reactions. Electrochemical reactions are those reactions that involve oxidation (increase in valence) and reduction (decrease in valence).



For the example of copper metal deposition using zinc metal, the oxidation reaction for producing electrons is:



Electrons are consumed by copper ion according to the following reduction reaction:



An electrochemical cell, such as the one shown and described in **Fig. 42**, can be constructed by using a copper electrode in a solution of copper sulfate as one electrode and a zinc electrode in a solution of zinc sulfate as the other electrode. If the external conduction path is short circuited, electrons will flow from the zinc electrode (anode) as zinc dissolves to the copper electrode (cathode); this causes the deposition of copper metal. This type of arrangement would demonstrate how some electrochemical reactions can take place with the reactants and products physically separated and how the overall process can be visualized as two separate reactions that occur together.

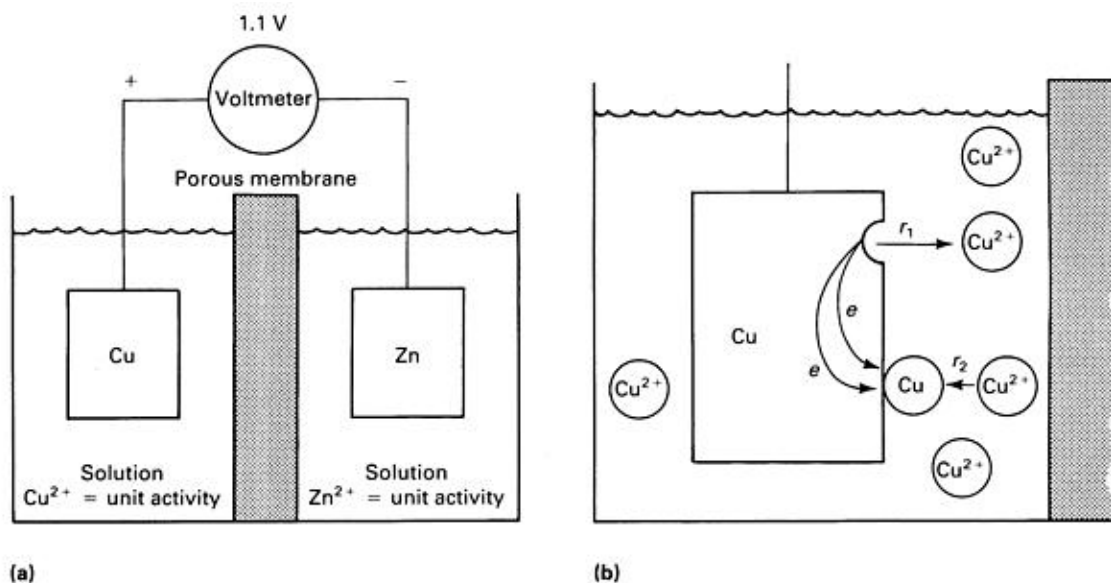


Figure 40 : Typical electrochemical cell (a) used to study the free energy change that accompanies electrochemical or corrosion reactions. In this example, the cell contains copper and zinc electrodes in equilibrium, with their ions separated by a porous membrane to mitigate mixing. For purposes of simplicity, the concentration of metal ions is maintained at unit activity; that is, each solution contains about 1 g atomic weight of metal ion per liter. The reactions taking place on each side of the cell are represented by Eq 10, and 11, and the half-cell reactions for copper and zinc electrodes are given in Table 1. The rates of metal dissolution and deposition must be the same as shown in (b), which illustrates copper atoms being oxidized to cupric ions and, at other areas, cupric ions being reduced to metallic copper. Equilibrium conditions dictate that the reaction rates  $r_1$  and  $r_2$  be equal.

The two reactions listed in **Eq 10**, and **11**, and shown schematically in **Fig. 42** are often referred to as half-cell reactions. This nomenclature is due to the requirement that oxidation and reduction occur simultaneously under equilibrium conditions. Therefore, the reaction given in **Eq 10** is defined as an oxidation half-cell reaction, and the reaction given in **Eq 11** is a reduction half-cell reaction. The reaction in **Eq 9** can be referred to as the overall electrochemical reaction and is the sum of the half-cell reactions given in **Eq 10** and **11**. Because specific, or absolute, potentials of electrodes cannot be measured directly, an arbitrary half-cell reaction is used as a reference by defining its potential as 0. All other half-cell potentials can then be calculated with respect to this zero reference. As described in the following section "**Potential Measurements With Reference Electrodes**" the hydrogen ion reaction  $2\text{H}^+ + 2e \rightarrow \text{H}_2$  is used as the standard reference point. It is not possible to make an electrode from hydrogen gas; therefore, the standard hydrogen electrode (**SHE**) potential is measured by using an inert electrode, such as **platinum, immersed in a solution saturated hydrogen gas at 1 atm**. All values of electrode potential, therefore, are with reference to **SHE**. The potentials given in **Table 1** are specifically the potentials measured relative to an **SHE** at **25 °C (77 °F)** when all concentrations of ions are **1 molal**, gases are at **1 atm** of pressure, and solid phases are pure. This specific electrode potential is referred to as the standard electrode potential and is denoted by  $E^\circ$ . The standard electrode potential for zinc- the accepted value for which is **-0.763 (Table 1)**- can be calculated by measuring the **emf** of a cell made up, for example, of a zinc and a hydrogen electrode in a zinc salt solution of known activity  $\text{Zn}^{2+}$  and  $\text{H}^+$  (**Fig. 43**). This procedure could be repeated by exchanging the zinc electrode with any other metal and by assigning the half-cell electrode potentials measured for the electrochemical cells to the proper reactions in **Table 1**. Changes in concentration, temperature, and partial pressure will change the electrode potentials and the position of a particular metal in the **emf** series. In a particular, the change in electrode potential as a function of concentration is given by the **Nernst equation**:

$$E = E^\circ - \frac{RT}{nF} \ln \frac{(ox)}{(red)} \quad \text{Eq( 12 )}$$

Where:

$E$  is the electrode potential.

$E^\circ$  is the standard electrode potential.

$R$  is the gas constant (1.987 cal/K mol).

$T$  is the absolute temperature (in degrees Kelvin).

$n$  is the number of moles of electrons transferred in the half-cell reaction.

$F$  is the Faraday constant ( $F = 23,060$  cal/volt equivalent).

**(ox)** and **(red)** are the activities of the oxidized and reduced species, respectively.

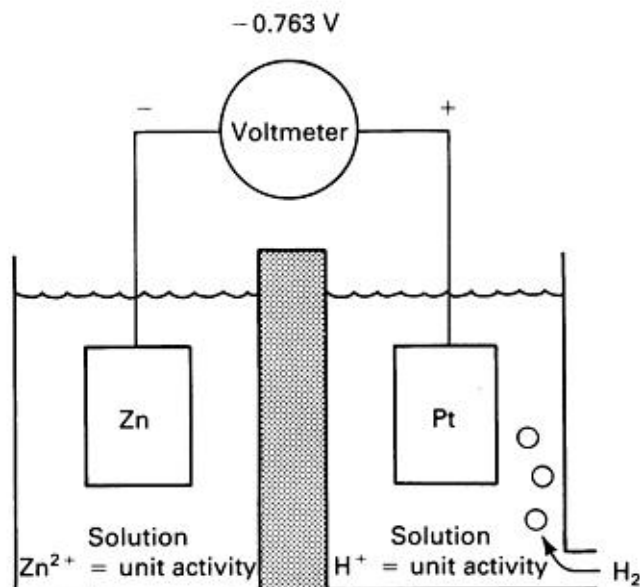
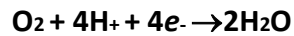


Figure 41 : Electrochemical cell containing a zinc electrode and hydrogen electrode

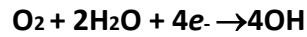
Electrode potentials, as described above, are always measured when zero current is flowing between the electrode and the **SHE**. The potential is thus a reversible measurement of the maximum potential that exists and an indication of the tendency for the particular reaction to occur. For example, metals listed in **Table 1** above molecular hydrogen are **more noble** and less resistant to oxidation than the metals listed below hydrogen when standard state conditions exist. This tendency is a thermodynamic quantity and does not take into account the kinetic factors that may limit a reaction because of such physical factors as protection by corrosion product layers. Care should be taken when using an **emf** series such as that shown in **Table 1**. These values are for a very specific condition (standard state) and may not apply to a specific corrosion environment. Returning to the example of an electrochemical cell with copper and zinc electrodes, it is apparent that the chemical energy that exists between the copper and zinc electrodes can be converted to electrical energy (as occurs in a battery). However, the external circuit can be replaced with a direct current (dc) power supply, which can be used to force electrons to go in a direction opposite to the direction they tend to go naturally. Both concepts are useful when dealing with corrosion because the oxidation of a metal will always be coupled to a cathodic reaction and because corrosion reactions are similar to the galvanic-type cell. Also, application of external potentials can be used to protect metals, as in cathodic protection. Corrosion processes are often viewed as the partial processes of oxidation and reduction previously described. The oxidation reaction (anodic reaction) constitutes the corrosion of the metallic phase, and the reduction reaction (cathodic reaction) is the result of the environment. Several different cathodic reactions are encountered in metallic corrosion in aqueous systems. The most common are:



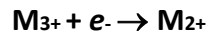
**Hydrogen ion reduction**



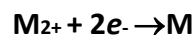
**Reduction of dissolved oxygen (acid media)**



**Reduction of dissolved oxygen (basic media)**



**Metal ion reduction**



**Metal deposition**

Hydrogen ion reduction is very common because acidic media is so often encountered, and oxygen reduction is very common because of the fact that aqueous solutions in contact with air will contain significant amounts of dissolved oxygen. Metal ion reduction and metal deposition are less common and are encountered most often in chemical process streams. All of the above reactions, however, share one attribute: they consume electrons.

### 3.3.3 Potential Measurements With Reference Electrodes

Electrode potential measurement is an important aspect of corrosion prevention. It includes determination of the **corrosion rate** of metals and alloys in various environments and **control of the potential** in **cathodic** and **anodic protection**. Many errors and problems can be avoided by intelligently applying electrochemical principles in the use of reference electrodes. Among the problems are the selection of the best reference for a specific case and selection of an adequate method of obtaining meaningful results. It is important to note that many different reference electrodes are available, and others can be designed by the users themselves for particular problems. Each electrode has its characteristic rest potential value, which can be used to convert the results obtained into numbers expressed with respect to other references. These conversions are frequently required for comparison and discussion, and this involves use of *E*-pH (Pourbaix) diagrams. The electrode selected must then be properly used, taking into account the stability of its potential value and the problem of resistance (*IR*) drop.

### 3.3.4 The Three-Electrode System

When a system is at rest and no significant current is flowing, the use of only one other electrode as a reference is sufficient to measure the test electrode potential. When a current is flowing spontaneously in a galvanic cell or is impressed to an electrolytic cell, reactions at both electrodes are not at equilibrium, and there is consequently an overpotential on each of them. The potential difference measured between these two electrodes then includes the value of the two overpotentials. The potential of only the test electrode cannot be determined from this measurement. To obtain this value, a third electrode, the auxiliary electrode, must be used (**Fig. 46**). In this way, the current flows only between the test and the auxiliary electrodes. A high-impedance voltmeter placed between the test and the reference prevents any significant current flow through the reference electrode, which then does not show any overpotential. Its potential remains at its rest value. The test electrode potential and its changes under electric current flow can then be measured with respect to a fixed reference potential (most references are not made to be polarized by a current flow). The three-electrode system is widely used in the laboratory and in field potential measurement.

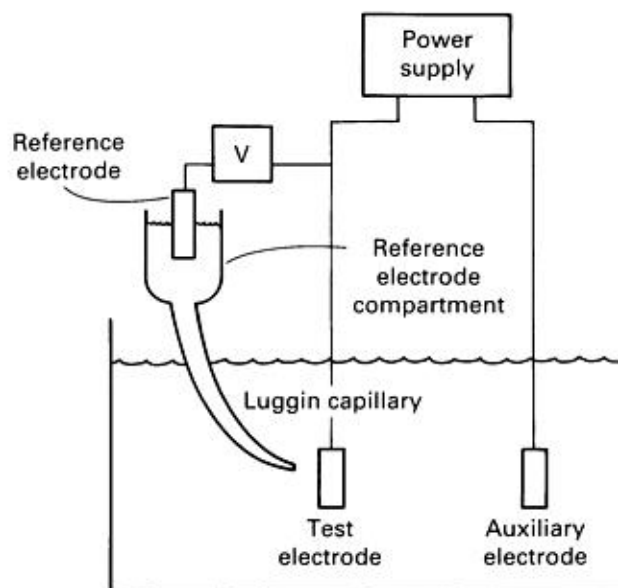


Figure 42 : Potential measurement with a luggin capillary. V, voltmeter

### 3.4.1 The kinetics of corrosion reactions

We have now been considering the thermodynamic implications of corrosion reactions, as evidenced by electrochemical potentials, but we have discovered that when a current flows the potential changes. This brings us back to the point that thermodynamics tells us only about the **tendency** of the system to corrode. Corrosion reactions not in equilibrium cause current flow and we must fully investigate the relationships between potential and current to appreciate corrosion kinetics

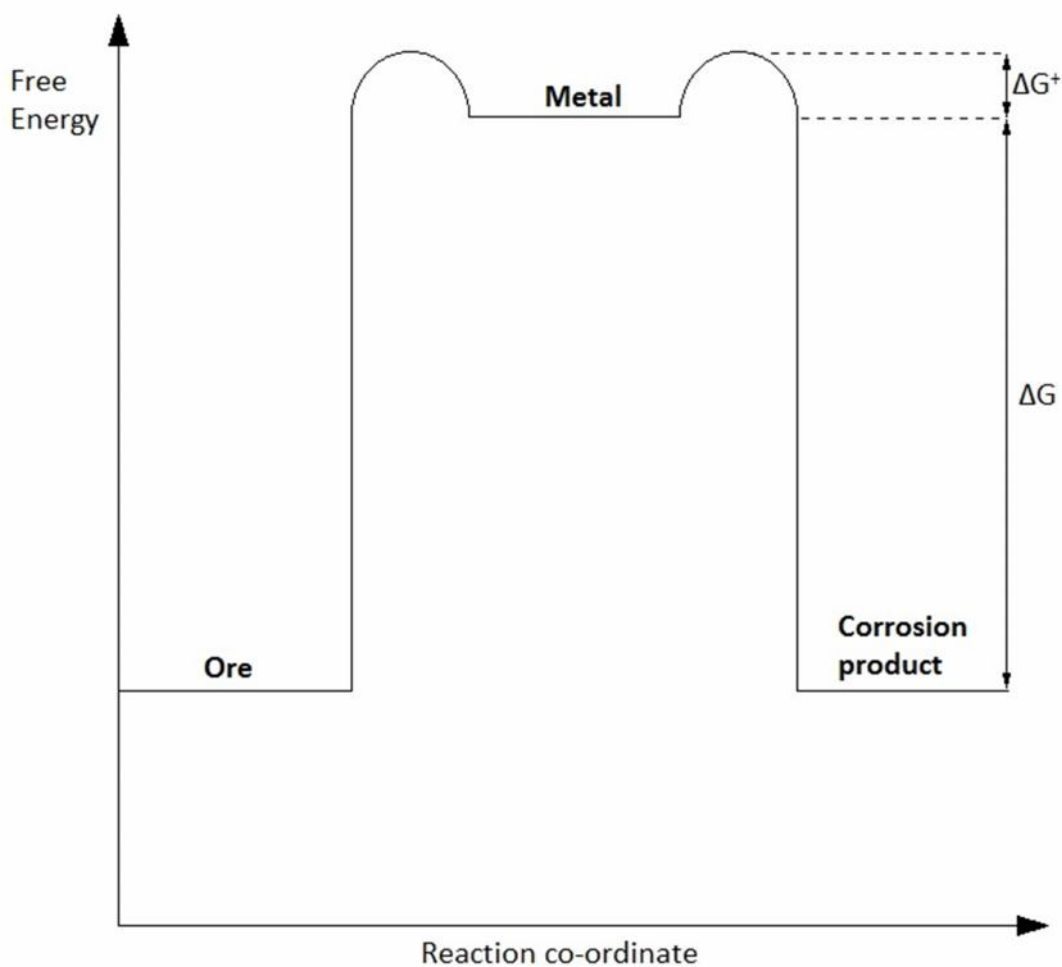


Figure 43 : A thermodynamic energy profile for metals and their compounds

Consider two pieces of metal, areas  $10 \text{ mm}^2$  and  $1 \text{ mm}^2$  such that they both corrode in separate cells and produces current of 10 electrons per second. It is easy to see that smaller piece will suffer corrosion damage 10 times worse ( if  $z = 1$  ) than the larger piece because the surface mass affected by corrosion is directly proportional to the rate of generation of electrons. When measuring corrosion currents we eliminate the effects of area by considering **current density**. Throughout

the discussions which follow we shall use  $I$  to represent an absolute current ( A ) and  $i$  to represent current density (  $A\ m^{-2}$  ). We shall always imply a flow of electrons as being the current ; conventional currents will not be used . we shall also use the symbols  $i_a$  and  $i_c$  to represent the magnitudes of anodic and cathodic current densities. When they need to be added, it is necessary to treat them as opposite signs because the currents flow in opposite directions.

We place a piece of pure copper of unit area in beaker of pure water. Immediately there applies a situation parallel to the energy profile of **Figure 45** and redrawn in **Figure 46**. Note that both  $\Delta G$  and  $\Delta G^\ddagger$  are treated as variable in this discussion because they are both upon the nature of the materials on each side of the metal/electrolyte interface and these materials change.

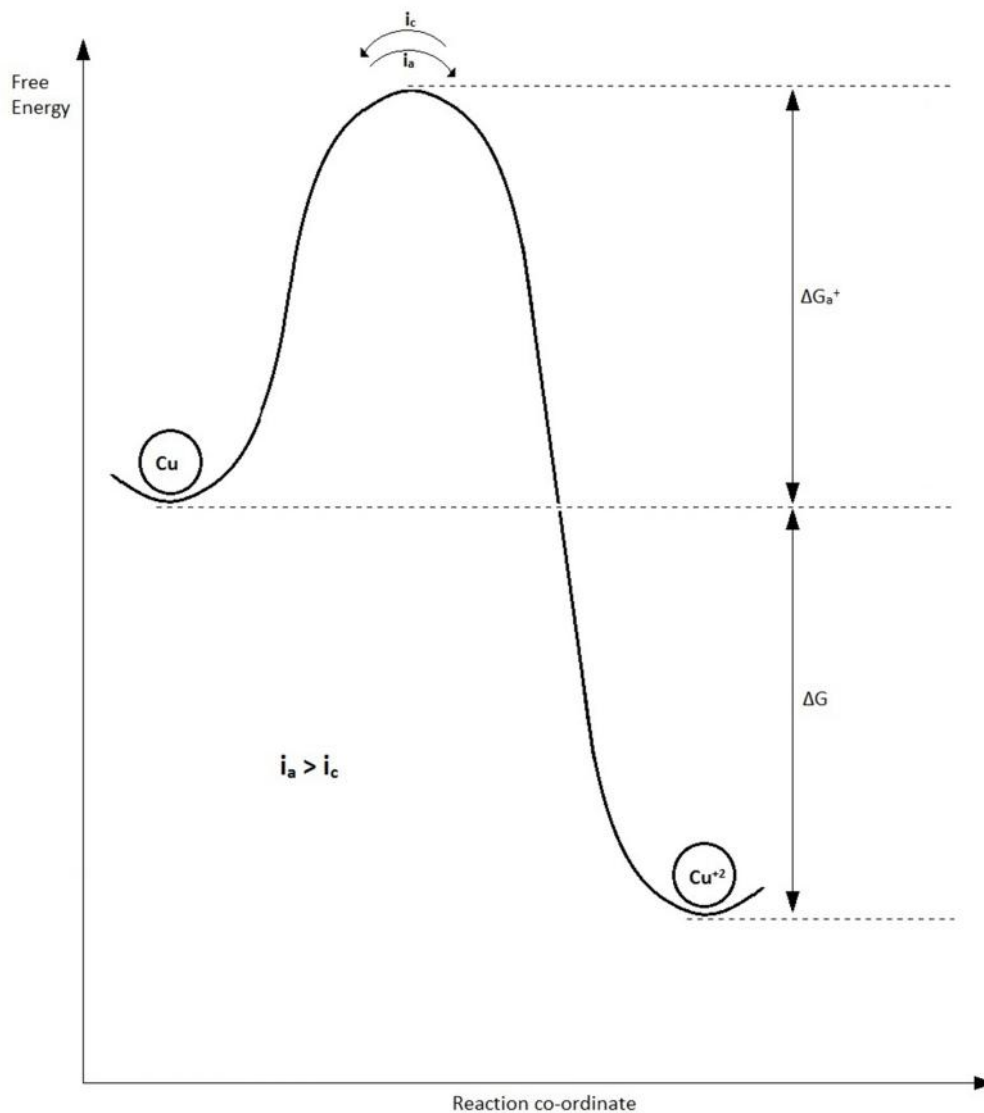


Figure 44 : An energy profile for copper in pure water  $i_a > i_c$

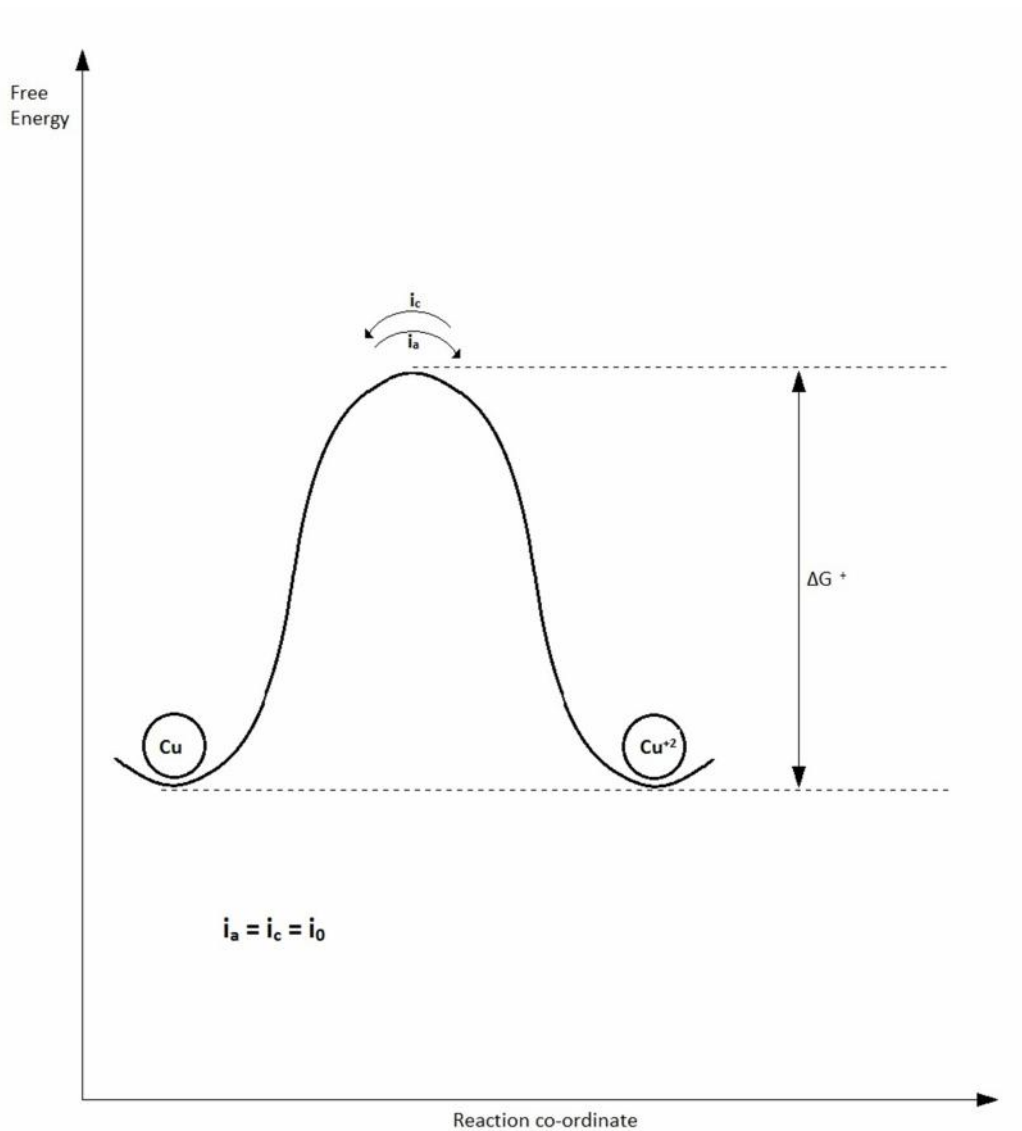


Figure 45 : An energy profile for copper in equilibrium with a solution of divalent ions,  $i_a = i_c = i_0$

There is sufficient available energy in the environment for a steady flow of copper atoms to 'pass over the energy barrier'  $\Delta G_a^+$ , and proceed to the  $\text{Cu}^{2+}$  ionic form. The copper begins to dissolve ( corrode ) and the concentration of copper ions in the water, initially zero, will slowly increase.



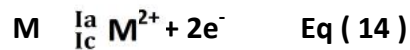
Remember that a single piece of metal placed in an electrolyte can act as its own anode, cathode and electrical connection. Individual areas of the metal can be anodic to others because of microvariations in the solid structure of the metal, or environmental differences over the surface as a whole .

The tendency of the copper to corrode decreases as the current increases from zero, and the value of the  $\Delta G$  diminishes, together with the potential, in



accordance with Faraday's Law. The thermodynamic energies of metal atoms and the assembly of adjacent ions tend to approach each other.

As soon as copper ions are present in solution, there is a possibility for them to 'pass back over the energy barrier' and replate onto the metal. The rate of this process is governed by the activation free energy in the reverse direction, (  $\Delta G + \Delta G_a^+$  ), a quantity initially greater than that for the forward reaction,  $\Delta G_a^+$ . However, this free energy barrier is reduced in magnitude as the energies of the two species approach each other, increasing the extent of the backward reaction of copper ions plating out. On the other hand, the rate of the forward reaction decreases because its activation free energy increases. The situation is thus obtained that the rate of the decreasing forward reaction and equilibrium is established **Figure 47** at an equilibrium value of free energy of activation  $\Delta G^+$ , and with  $\Delta G = 0$ . For a divalent metal, M we can rewrite **Eq ( 13 )** as:



When the state of equilibrium is reached,  $i_a = i_c$  the measured current density,  $i_{meas} = ( i_a - i_c )$  and no net current flows. There is current flowing, but it is equal and opposite and cannot be measured. It is called the **exchange current** and is denoted by  $I_0$ , or  $i_0$  when divided by area.

The non-homogeneous distribution of ions which has resulted from the immersion of a metal in an aqueous electrolyte is commonly referred to as the **double layer**. It is illustrated schematically in **Figure 48**. The double layer consists of **two parts: a compact layer** and a **diffuse layer**.

The compact layer, or **Helmholtz layer**, is closest to the surface in which the distribution of charge, and hence potential, changes linearly with the distance from the electrode surface. The more diffuse outer layer, the **Gouy-Chapman layer**, occurs where the potential changes exponentially.

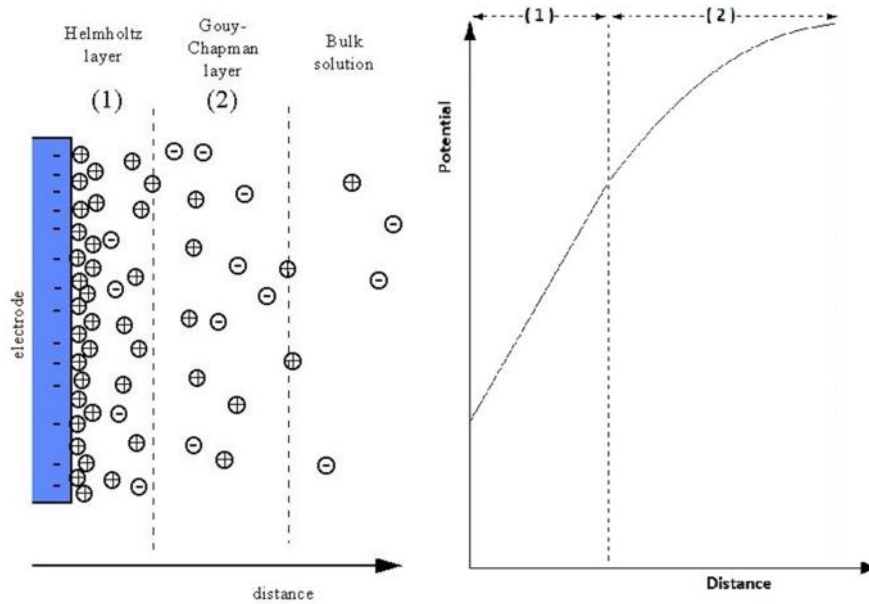


Figure 46 : The double layer : distribution of ions as a function of distance from an electrode behaving as an anode and variation of potential with distance for the model

The constitution of the double layer will parallel the changes of potential occurring at the electrode. It may also reach an equilibrium condition corresponding to the energy profile of **Figure 48**, or when the equilibrium is destroyed by an increase in either the forward or backward reaction, a new condition may be established in which a continuous flow of anions and cations in the electrolyte adjacent to the electrodes performs the bulk current-carrying requirement of the electrode reactions.

Faraday's Law of Electrolysis states that

$$Q = zFM$$

Where:

**Q** is the charge created by the ionization of **M** mol of material.

Differentiating with respect to time we get

$$\frac{dQ}{dt} = zF \frac{dM}{dt} \quad \text{Eq ( 15 )}$$

Now the rate of flow of charge is current, **I**, and if we consider the passage of charge across unit area of cross-section then we can use current density, **I**. then **dM/dt** becomes **J**, the flux of substance, and **Eq 15** becomes:

$$I = zFJ \quad \text{Eq ( 16 )}$$

The flux of substance is another name for corrosion rate by measurement of current density is a most important concept that current density and corrosion rate can be equated.

The ability to determine a corrosion rate by measurement of current density is a most important finding. However, in practical terms, to say that a metal is corroding at rate of **0,003 Am<sup>-2</sup>** is less helpful than a average rate of deterioration per unit area expressed as the **average depth of corrosion over a given area in a given time**. Thus, engineers prefer, for example, a corrosion rate of **2,5 mm per year**, meaning that in one year the metal will have corroded on average across the whole of its exposed area to depth of 2,5 mm. Millimeters per year is sometimes written mmpy. In the United States a corrosion rate expressed in mpy means milli-inches per year, sometimes referred to as mils.

A variety of other practical units are used to state corrosion rates. One commonly used unit is milligrams weight lost per square decimeter per day ( **mss** ). In certain forms of corrosion, such as crevice or pitting corrosion, these methods of considering corrosion rate are dangerous because an average corrosion rate is meaningless. Corrosion can be very rapid and penetrating over very small areas of a large exposed surface. It can also vary considerably over long periods such as a year.

### 3.5.1 Mixed Potential Theory

We can use a graph of potential versus current density to illustrate diagrammatically the typical polarization of both electrodes in a corrosion cell. By plotting current density on a logarithmic scale, the polarization lines will be linear, in accordance with the Tafel equation. The diagrams drawn in the way described below are commonly called **Evans diagrams**, after one of the founders of corrosion science, Ulick Evans.

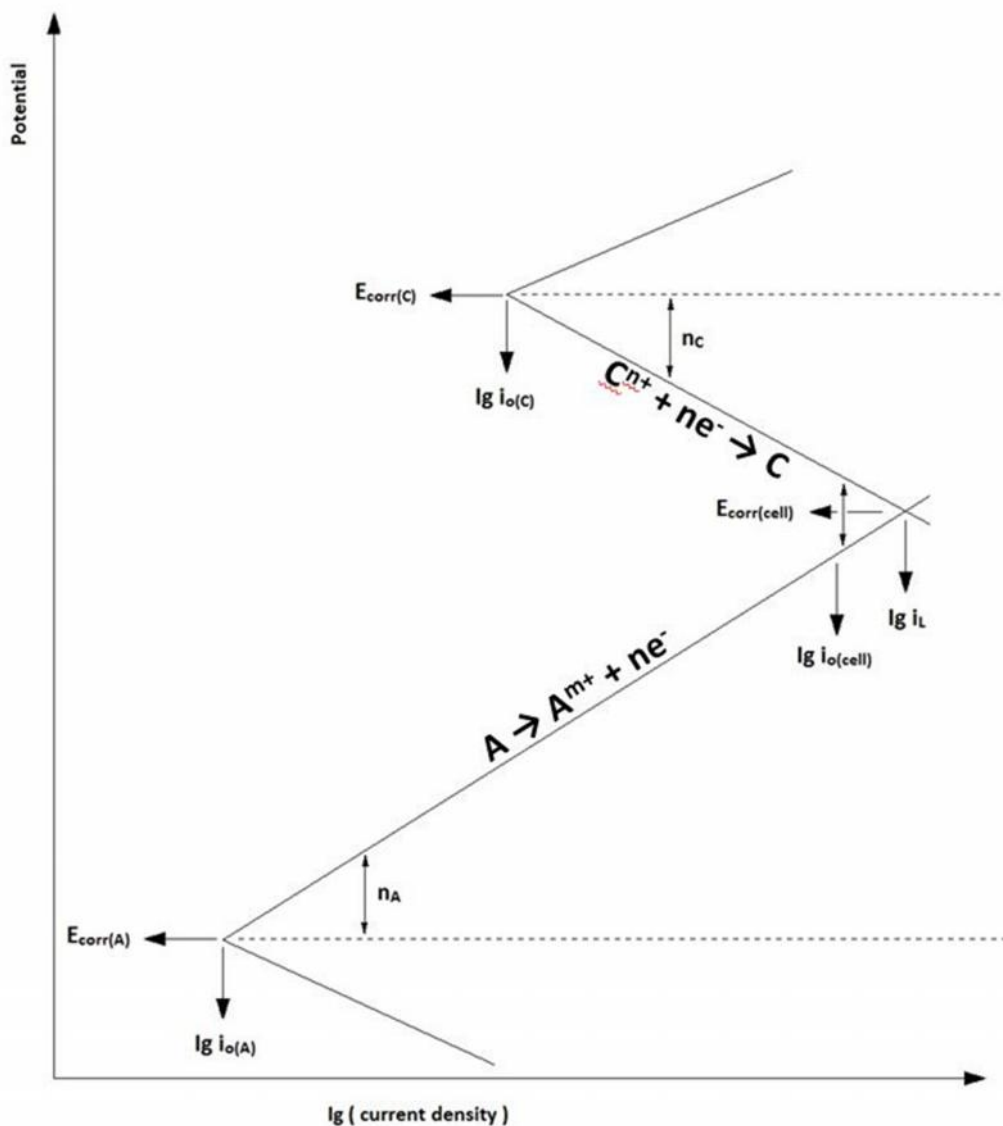


Figure 47 :The individual free corrosion potentials of copper (C) and zinc (A) are changed to a cell potential when the metals are short-circuited. The limiting current density,  $i_L$ , is never achieved because of the finite internal resistance of the cell

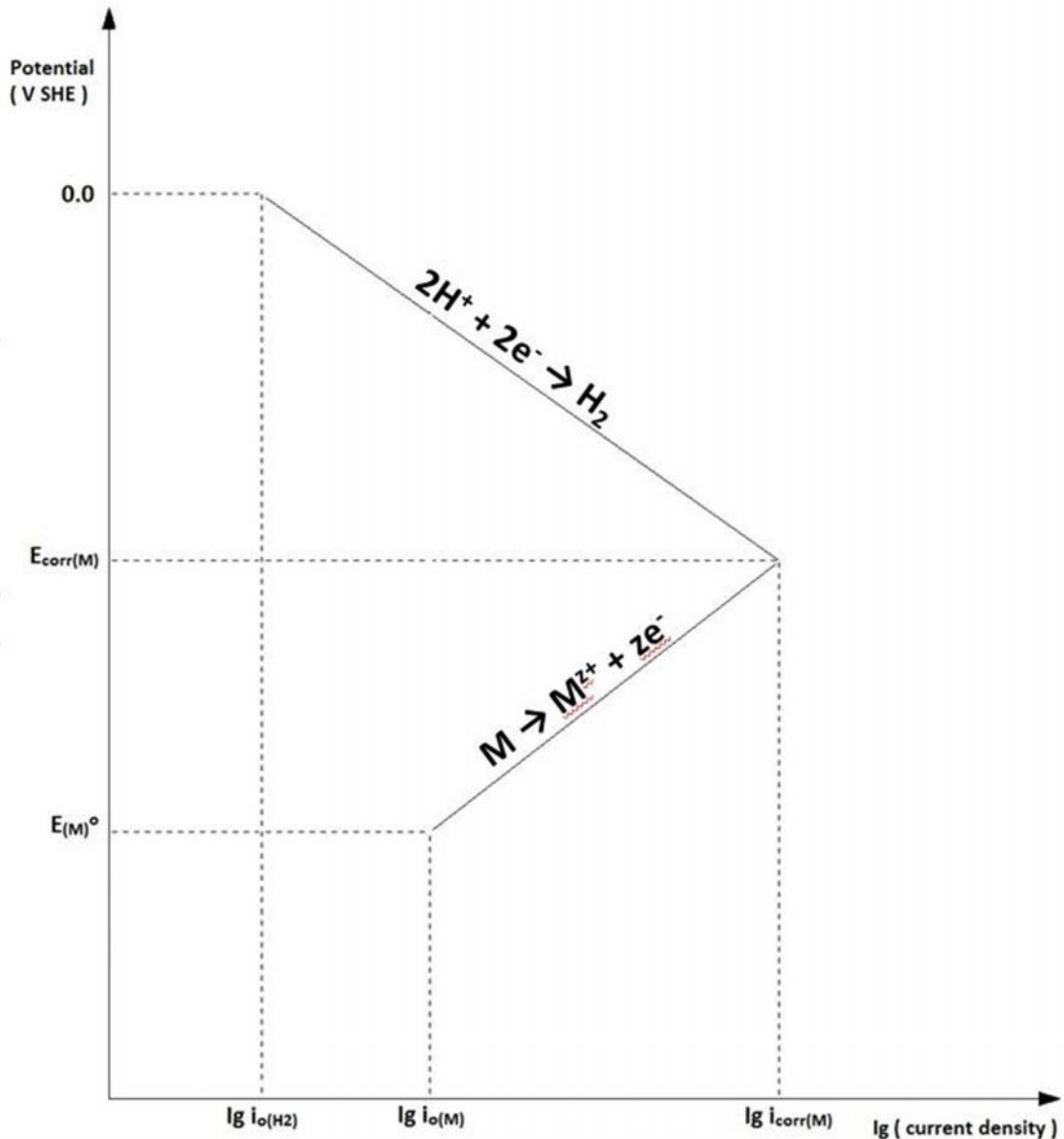


Figure 48 : A metal, M, corroding in an acid solution with the evolution of hydrogen. The microstructure of the metal causes it to act as its own anode and cathode; the cathode reaction is the reduction of hydrogen ions

Figure 49 shows such a diagram using a zinc anode (A) and a copper cathode (C), as we were using in the Daniell cell. First, the equilibrium potentials of the individual metals in their solutions,  $E_{(A)}$  and  $E_{(C)}$ , are recorded at their respective exchange current densities; the cathode has the more positive value. As the zinc corrodes, according to



It is polarized upwards to more positive values by an amount  $n_a$ , the anodic polarisation. At the copper electrode,



causes a cathodic polarisation,  $n_c$ , downwards to more negative values. For completeness it may be desirable to draw both the anodic and cathodic polarisations for each electrode. The slopes of these lines, the anodic and cathodic beta (Tafel) constants, are not necessarily the same. The steady-state current,  $i_{\text{corr}}$ , will be obtained at the potential of intersection,  $E_{\text{corr}}$ , of the anodic polarisation line of the anode and the cathodic polarisation line of the cathode. These parameters, commonly called the **free corrosion current density** and the **free corrosion potential**, are of considerable practical importance because they are most commonly determined in corrosion cell measurements.

*If the potential of the cathode is more positive than for the anode, why do the anode reactions have positive slopes in the diagram? Surely, as the anode corrodes it will become more anodic and the line will have a negative slope.*

When a piece of metal is placed in an electrolyte, metal ions enter the solution and the metal is left with an excess of negative electrons. This is the source of the electrochemical potential. If the metal is now connected to a more cathodic metal (a positive metal), the electrons will flow away from the anode and towards the cathode, so the anode will become less negative and more positive. **Le Chatelier's Principle** says **the system reacts to oppose any change we try to impose upon it**. When a metal corrodes it loses some of its thermodynamic desire for corrosion.

The use of Evans diagrams such as that shown in **Figure 49** is not restricted to simple cases in which the cathode reaction is one of replating metal ions. The well-known dissolution of metals in acids, accompanied by the evolution of hydrogen, is itself a corrosion reaction and can be described by an Evans diagram such as **Figure 50**. The cathode reaction is now represented by Eq:



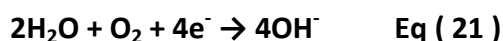
and at the point where the polarisation line intersects the metal dissolution line, the corrosion rate is  $i_{\text{corr(M)}}$ . The value of  $i_{0(\text{H}_2)}$  occurs at **0.0 V SHE**, but at different current densities according to the metal. Obviously, the rate of corrosion of a metal in acid is governed by such factors as

- The anodic polarisation line of the metal
- The exchange current density of hydrogen evolution on the metal

If  $i_{0(H_2)}$  or  $i_{0(M)}$  occurs at higher current densities the metal will corrode much faster; a good example is iron and zinc. In hydrochloric acid under identical conditions iron corrodes much faster than zinc, even though zinc is much more active according to its position in the galvanic series. This is because  $i_{0(H_2)}$  is much greater on iron than on zinc. Explanation by Evans diagram is shown in **Figure 51**. Noble metals such as platinum and palladium have very high values of  $i_{0(H_2)}$  but their greatly positive electrode reduction potentials are responsible for their lack of corrosion.

The hydrogen evolution line for zinc is shown as line a, while the anodic dissolution of zinc is line b. The free corrosion potential and corrosion current density of zinc are shown at the intersection of these two lines. The equivalent lines for iron (corroding independently of the zinc) are shown as a' and b' respectively. The corrosion potential and corrosion current density for the zinc/iron couple occur at the intersection of the cathodic and anodic lines for the couple. To obtain them, it is necessary to sum the two cathodic processes a + a' and the two anodic processes b + b'. These are shown as the dashed diagonal lines in **Figure 51**.

This type of diagram is extremely useful in both explaining and predicting corrosion rates in different environments. This example (in acid solution) was chosen so that the cathodic lines were representative of hydrogen evolution. In neutral or alkaline solutions, the cathode reaction is represented by Eq:



, but is strongly affected by the rate of oxygen diffusion to the metal surface and by stirring. A different environment can considerably alter the plot. In particular, experimental effects can sometimes cause complications. However this should not detract from the usefulness of Evans diagrams is that they combine thermodynamics and kinetics to form a whole picture; the potential axis is the experimentally derived information is now likely to be done with microcomputers instead of Evans plots because microcomputers give rapid access to the component parts of the curves.

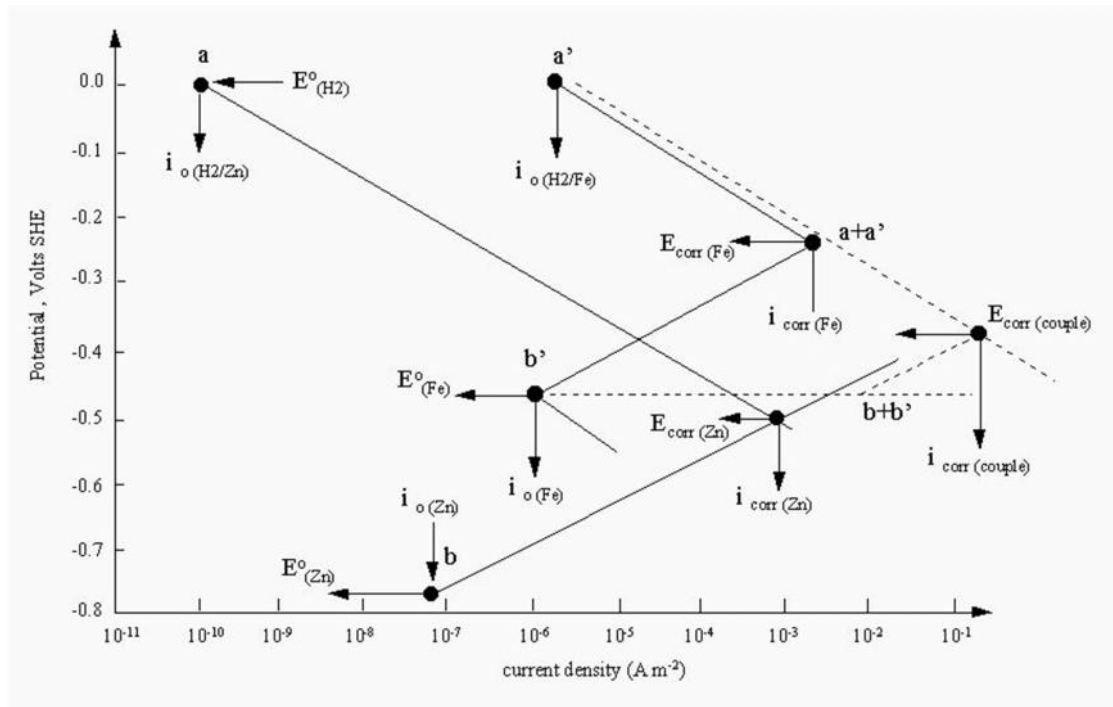


Figure 49 : A mixed potential plot for the bimetallic couple of iron and zinc. The diagram also explains the higher corrosion rate of iron than zinc in hydrochloride acid solution. Despite the more positive reduction potential of iron, the evolution of hydrogen on iron has a high exchange current density



# **EXPERIMENTAL PART**

## 4 Experimental Procedure

### 4.1 Introduction

The objective of this project is to study how super-hydrophobic film effects corrosion behavior of copper. In particular a series of electrochemical experiments took place. The main objective is to prove through some potentiodynamic polarization curves the superiority in corrosion of copper specimens with super-hydrophobic film than these without. For the fully studies of the phenomenon also applied other methods. Thus, for studying the structure of copper was used a metallurgical microscope, a stereo microscope, and a microhardness tester. Also for the detailed study of copper's structure we used a Scanning Electron Microscope (SEM). For a better understanding of super-hydrophobic film we make some extra measurements. We take contact angle measurements with optical tensiometry and 3D images with Atomic Force Microscopy (AFM). The following pages of this section describe the experimental procedure that had been followed step by step, as well as describe the principles of experimental methods.

## 4. 2 Raw Material

Cu substrates were obtained from a commercial wafer fabrication plant. They were two bars of **Electrolytic Tough Pitch Copper (Copper No. C11000)**. The dimension of each bar was:

**L = 14,6 cm**

**B = 3,9 cm**

**T = 0,4 cm**



Figure 50 : Raw material

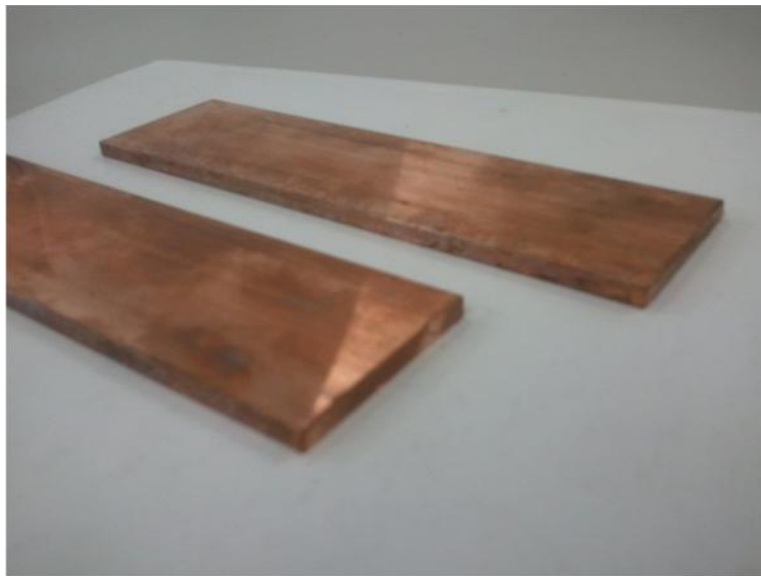


Figure 51 : Raw material

### 4.2.1 Nominal Chemical Composition % by weight

Table 4 : Nominal Chemical Composition % by weight

<i>Copper</i>	<i>Oxygen</i>
99,90	0,04

### 4.2.2 Material Properties

Hard drawn bus bar with high thermal and electrical conductivity. Good resistance and tempering. Not suitable for case hardening.

### 4.2.3 Mechanical Properties

Typical for 1" solid diameter Hard (35%) Temper

Table 5 : Mechanical Properties

<i>Hardness*</i>	Rockwell F Scales	87
<i>Tensile Strength**</i>	KSI	48
<i>Yield Strength**</i>	KSI	44
<i>Elongation**</i>	% in 2 inch	10

\*Hardness conversions are approximate

\*\*Test values are nominal approximations and depend on specimen size and orientation.

### 4.2.4 Physical Properties

Table 6 : Physical Properties

<i>Thermal Conductivity</i>	BTU/ (sq ft-ft-hr-F)	226
<i>Specific Heat</i>	BTU/lb/°F @ 68F	0,092
<i>Thermal Expansion</i>	Per °F from 68 F to 212 F	0,0000094
<i>Density</i>	lb/cu in @ 68 F	0,321 - 0,323
<i>Electrical Conductivity</i>	% IACS @ 68 F	101
<i>Modulus of Elasticity</i>	KSI	17.000

### 4.2.5 Fabrication Properties

Table 7 : Fabrication Properties

<i>Capacity for being cold worked</i>	Excellent
<i>Capacity for being hot formed</i>	Excellent
<i>Hot forgeability rating (forging brass = 100)</i>	65
<i>Hot working temperature</i>	1400 - 1600 F or 750-875 C°
<i>Annealing temperature</i>	700-1200 F or 375-650 C°
<i>Machinability rating (Free Cutting Brass = 100)</i>	20
<i>Suitability for being joined by:</i>	Soldering/Excellent
	Brazing/Good
	Oxyacetylene Welding/Not Recommended
	Gas Shielded Arc Welding/Fair
	Coated Metal Arc Welding/Not Recommended
<i>Resistance Welding</i>	Spot/Not Recommended
	Seam/Not Recommended
	Butt/Good

### 4.3 Cutting off Process

The first step in the materialographic process is usually cutting. The purpose of cutting is to section a representative, yet manageable sample from a large or irregular piece of a given material, or to obtain sections in specific angles, for example cross sections. The bars were cut in sections using the **Struers Discotom 50**. Section dimensions were **2 cm x 1,8 cm**.



Figure 52 : Struers Discotom 50

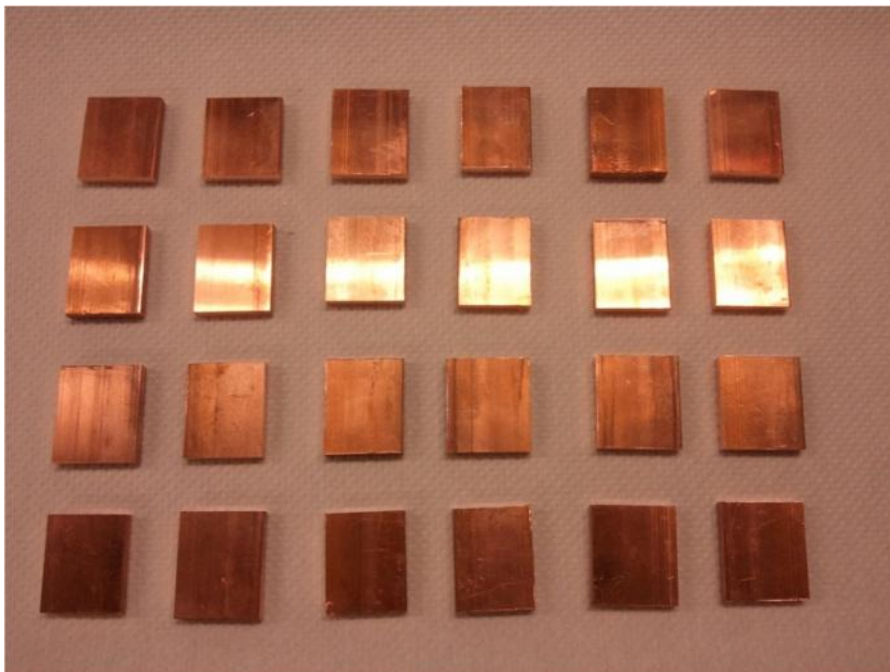


Figure 53 : The copper specimens

## 4.4 Cold Mounting Process

Mounting also allows for a safer, more convenient handling of e.g. small, sharp or irregularly shaped specimens or when the protection of layers is imperative. Cold mounting is especially suited for mounting specimens that are sensitive to heat or pressure. Additionally, cold mounting does not require an investment in a mounting press and is therefore good for infrequent mounting tasks. The resin, a mixture of two or three components, is poured over the specimen after it has been placed in a mounting cup. After curing, the specimen can be taken out of the cup and processed. Samples were painted using the **EpoFix Kit** from Struers before experiment, leaving an exposed area of **20 mm × 18 mm** on the material surface.



Figure 54 : EpoFix Kit

## 4.5 Grinding Process

Grinding is the first stage in mechanical material removal. Proper grinding removes damaged or deformed surface material while introducing as little new deformation as possible, thus preparing the sample surface for polishing. Grinding is divided into two processes: **Plane Grinding (PG)** and **Fine Grinding (FG)**.



Figure 55 : Struers Silicon Carbide Papers

### 4.5.1 Plane Grinding

The grinding process always begins with plane grinding. Plane grinding ensures that the surfaces of all specimens are in the same condition before the preparation continues, and that the surfaces of all specimens in a specimen holder are at exactly the same level.

### 4.5.2 Fine Grinding

Single specimen preparation is usually started with fine grinding. Fine grinding must remove the deformation existing from cutting or plane grinding and produce a surface that is ready for polishing. Choosing the correct fine grinding materials is vitally important to ensure fast and economical preparation.

For the grinding process we followed the guide “*Metallographic preparation of copper and copper alloys*” from Struers. The process given in the table

below:



Figure 56 : Struers LaboForce-5 & LaboForce-3

<b>Mechanical Preparation</b>				
Pure copper and copper alloys with low alloying contents.				
<b>Grinding</b>				
Step	PG	FG 1	FG 2	FG 3
Surface	SiC- Paper	SiC-Paper	SiC-Paper	SiC-Paper
Grit	320	800	1200	4000
Lubricant	Water	Water	Water	Water
rpm	300	300	300	300
Force (N)	150	150	150	150
Time	As needed	1 Min.	1 min.	1 min.

Figure 57 : Metallographic preparation , grinding process guide



The equipment we use for the process was:

- i. **Struers LaboPol – 5**
- ii. **Struers LaboForce – 3**
- iii. **Struers MD-Fuga**
- iv. **Silicon Carbide Papers: 320 grade – 800 grade – 1200 grade – 4000 grade**

## 4.6 Polishing Process

To remove deformations from fine grinding and obtain a surface that is highly reflective, the specimens must be polished before they can be examined under the microscope. Polishing is carried out on cloths of differing resilience with different abrasives. Two processes are available: **Diamond Polishing (DP)** and **Oxide Polishing (OP)**.



Figure 58 : Polishing clothes

For the Polishing process we followed the guide “**Metallographic preparation of copper and copper alloys**” from Struers (**only the Diamond Polishing part**). Diamond Polishing had to be carried out until all deformation and embedded abrasives from grinding had been removed. The process given in the table below:

<b><i>Polishing</i></b>		
<b>Step</b>	<b>DP</b>	<b>OP</b>
<b>Surface</b>	MD-Mol*	OP-Chem
<b>Suspension</b>	DiaPro Mol	OP-S**
<b>rpm</b>	150	150
<b>Force (N)</b>	150	90
<b>Time</b>	3 min.	1-2 min.

Figure 59 : Metallographic preparation , polishing process guide

The equipment we use for the process was:

- i. **Struers LaboPol – 5**
- ii. **Struers LaboForce – 3**
- iii. **Struers MD-Fuga**
- iv. **Struers MD-Mol**
- v. **Struers Dia Pro Mol**

## 4.7 Etching Process [23]

Once The Polished metallographic specimen is properly prepared, the next stage is to reveal the microstructure. When examining the as-polished metallographic specimen in the light microscope, microstructural constituents such as pearlite, ferrite, bainite, and martensite cannot be observed, because the specimen surface is highly polished and these constituents require a difference in the reflectivity or absorption of the light beam

as it is seen by the human eye. The metallurgical microscope operates with a beam of light that is reflected from the specimen surface (the specimen is opaque to light), as opposed to the biological microscope where the beam of light passes through the specimen (the specimen is transparent to light). In the biological specimen, differences in density and transparency of light reveal the microstructure being examined. In fact, many biological specimens are stained to provide density differences to enhance contrast. With an opaque metallographic specimen, only differences in light reflectivity from the specimen surface can reveal the microstructure, that is, the light that is 100% reflected back to the viewer's eye, as in a mirror, will appear differently than the light that is only partially reflected. The full reflection will appear much brighter than the partial reflection. One way to create differences in reflectivity at the surface of the as-polished metallographic



**Figure 61: Annealed electrolytic tough-pitch copper prepared by the contemporary method plus a brief vibratory polish (Klemm's II reagent, 50X, crossed-polarized light with light use of sensitive tint.)**

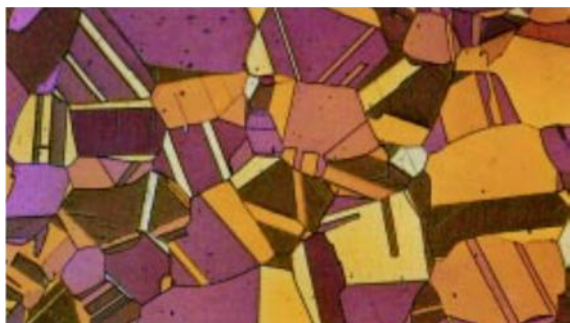


**Figure 60 : This annealed cartridge brass, Cu-30Zn, was prepared using the traditional method, and the process included multiple etch-polish cycles (Klemm's I reagent, 100X).**

specimen is to subject the surface to chemical attack. The constituents in the microstructure are then selectively etched by the chemical attack, that is, selective corrosion takes place. For example, in a specimen with a ferritic microstructure, each neighboring ferrite grain has a different crystal lattice orientation, where each ferrite grain is a single crystal of body-centered cubic iron. Each ferrite grain etches at a different rate, depending on its crystallographic orientation with respect to the polished surface. The different crystallographic planes that are exposed by the chemical attack can reflect light at different angles from the incident beam in the microscope. Also, between the individual ferrite grains there is a grain boundary. These boundaries selectively corrode when exposed to the acid contained in most metallographic etching solutions. The light beam from the microscope is thus reflected from these attacked grains and boundaries at an angle to the incident light beam, thus creating the contrast observed in the eyepiece of the microscope.

The art of revealing microstructure is the most important tool of the metallographer. An experienced metallographer knows how to use this tool, much like an artist knows how to use and mix the different color paints on his palette to express the mood of his painting.

For the Etching process we followed the **ASM Handbook - Vol 09 - Metallography and Microstructures**, Metallography and Microstructures of Copper and Its Alloys, Table 2 Etchants and procedures for microetching of coppers and copper alloys, row 11, as we can see below :

Table 8 : Etchants and Procedures

<i>Composition</i>	<i>Procedure</i>
5 g FeCl <sub>3</sub> , 100 mL ethanol, 5 – 30 mL HCl	Immersion or swabbing for 1 s to several minutes

## 4.8 The Metallurgical Microscope [27]

The metallographer's most important tool is the metallurgical microscope. Every metallographic laboratory has at least one metallurgical microscope for observing microstructures. This microscope is different from the conventional microscope, which uses transmitted light for transparent material, for example, stained biological specimens. Metallographic specimens are opaque to light, and therefore, a metallurgical microscope needs a source of reflected light.

Both kinds of microscopes are commonly called optical microscopes. This term is not used in this book, because it is more appropriate to use the name of the source of the incident "beam" being used to illuminate the specimen. For example, a

controlled beam of light is used in both the metallurgical and biological microscopes. Thus, they are called **light microscopes** or light optical microscopes. If a beam of electrons is employed, the microscope would be called an **electron microscope**, and if a beam of ions is employed, it is called an **ion microscope**. Electron microscopes are valuable tools for the metallographer and are discussed in the next chapter.

When discussing microscopes, one is entering a field of physics called optics, and many terms, concepts, and mathematical expressions are used that are generally unfamiliar to the metallographer. This chapter describes only those items that are necessary for the metallographer to develop a basic understanding of the microscope. Some of the basic terms described in this chapter include resolving power, the virtual image, bright- and dark-field illumination, numerical aperture, focal length, image contrast, depth of field, and spherical and chromatic aberration. For more detailed technical descriptions, there are several references listed at the end of the chapter. The metallographer must obviously know the basics of the microscope in order to use it properly. These are sophisticated scientific instruments, and the metallographer must have the required working knowledge in order to obtain the optimal benefit from the microscope. The modern-day metallographer is very involved with metallographic interpretation and must fine-tune the microscope to obtain the ultimate image for accurate microstructural interpretation. Also, a metallographer may be in the position to recommend or purchase a microscope or metallograph (a dedicated microscope with built-in camera for taking micrographs). A full understanding of the various features of a metallurgical microscope is necessary in order to intelligently procure this type of instrument. These features include such things as apochromatic objectives, hyperplane oculars, vertical illuminators, counting reticles, widefield oculars, polarization filters, field diaphragms, interferometers, and tungsten-halogen lamps. This chapter discusses all these features.

In addition to developing a basic understanding of the metallurgical microscope, the metallographer must also develop a basic understanding of methods to record the microstructural image. The latter part of this chapter is devoted to the metallograph, a metallurgical microscope that is dedicated to micrography that is, recording the microstructure. First, the metallographer must understand the microscope.

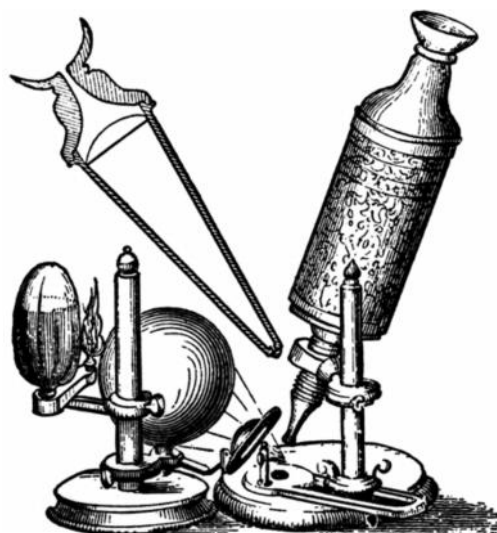


Figure 63 : A sketch of an early 17th century microscope used by Robert Hooke in 1665

### 4.8.1 The Microscope

The term “microscope” is derived from the Greek words *mikros* (small) and *skopein* (to see). The words were combined and given a Latin form by Giovanni Faber, a Roman scientist, in 1625. The microscope is thus an instrument that can see small things. The Dutch eyeglass maker, Zacharias Janssen, has been credited with developing the principles of the compound microscope in 1590. In the mid of 1600, Anthony Van Leewenhoek, a Dutch amateur scientist, was the first to observe microscopic life in pond water and has been called the father of the microscope. He constructed a simple microscope (not a compound microscope) with a power of 270x, which, at the time, was the most powerful microscope ever built. An early example of a compound microscope is seen in Fig. 63. This type of microscope was used by Robert Hooke, an English microscopist, in 1665.



Figure 64 : An upright metallurgical microscope

Although the microscope has been used for over 300 years, it was only in the latter part of the 19th century that the microscope was first used for observing metals. Sir Henry Clifton Sorby, the father of metallography, used the microscope to observe the microstructure of a polished and etched steel specimen.

### 4.8.2 The Basic Metallurgical Microscope

In this book, only the metallurgical microscope is discussed. Examples of this type of microscope are seen in Fig. 64 and 65. There are two types of metallurgical microscopes: the **upright** and **inverted** microscope. In the upright microscope (Fig. 64), the specimen is positioned below the objective, and in the inverted microscope (Figure 65); the specimen is upside down above the objective. Each type of microscope has advantages and disadvantages. We used the inverted metallographic microscope of our lab a **Leica DMICM**.



Figure 65 : The inverted metallurgical microscope of our lab Leica DMICM

## Inverted microscope

- i. Difficult to see the beam of light on the specimen surface
- ii. Leveling of the specimen is not required.
- iii.  $x$ - $y$  movement not limited by stage opening (diameter of hole limits the area of specimen to be seen)
- iv. Polished surface may contact the stage surface (potential for scratches)
- v. Ideal for large specimens
- vi. Usually built with ample weight capacity
- vii. Scribing not possible

### 4.8.3 The Mechanical System

The mechanical system includes those components that are required for moving the specimen beneath or above the light beam and for focusing the image of the microstructure.

*The stage* is a movable flat platform that supports the specimen. Atop view of a typical stage on an upright microscope can be seen in Fig. 66a.

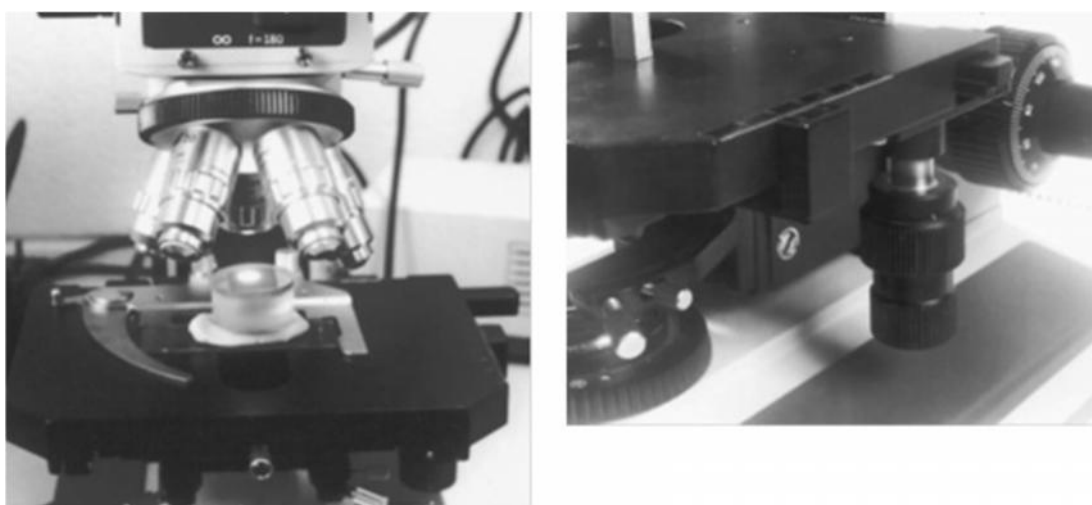


Figure 66 : a) The stage of an upright metallurgical microscope with a mounted specimen directly beneath the incident beam of light b) Coaxial knurled knobs used to move stage in  $x$ - and  $y$ -directions

On the stage, one can see the specimen directly below the objective of the microscope. All stages have mechanical movement in two horizontally perpendicular directions. This allows the metallographer to move the specimen from left to right ( $x$ -movement) and front to back ( $y$ - movement). Coaxial knurled knobs, that is, one knob within the other, are used to make these horizontal adjustments. These knobs can be seen in the center of Fig. 66b. The amount of  $x$ - and  $y$ -movement of the stage

can be measured by graduated scales along the edge of the stage. These scales are shown along the edges of the stage. Some stages also allow rotation of the specimen. This is generally the case for an inverted microscope. Also, as described subsequently, all metallurgical microscope stages have a third, up-and-down z-motion that is used for coarse and fine focus of the specimen. Some metallographers use the scales on the stage to obtain a rough measure of the thickness of certain features in the specimen, such as the thickness of a coating or the length of a crack. The scale is usually calibrated in 0.1 mm divisions. For more accurate measurements, an eyepiece reticle is used. The reticle is a graduated scale within the eyepiece that can be focused along with the image of the microstructure. Reticles are discussed later in this chapter.

*The Coarse- and Fine-Focus Knobs.* On older tube-type microscopes, the coarse- and fine-focus knobs adjusted the barrel of the tube up and down, and the stage was at a fixed vertical position. On modern-day microscopes, the upward and downward movements of the stage are controlled by coaxial knurled knobs easily accessible to the metallographer. In



Figure 67 : Coaxial knurled knobs for fine (small, inside knob) and coarse (large knob) focus. Note the graduated scale on the fine-focus knob, which indicates the amount of vertical (z-axis) movement.

metallurgical microscopes, these are the coarse- and fine-focus knobs similar to those shown in Fig. 67. For coarse focus, the large-diameter knob is used, and for fine focus, the small-diameter knob is used. Most microscopes have sets of knobs on both sides of the microscope stand for both right- and left-handed operators. In Fig. 67, the fine-focus knob has a graduated scale from 0 to 180, with each increment representing a movement of 0.001 mm. The metallographer can use the graduations on the fine-focus knob to measure depth of a feature within a specimen. For example, the depth of a pore can be measured by magnifying the pore so that both its edge and bottom are in the field of view. With the field aperture of the light source fully open, the metallographer first focuses on the edge of the pore and records the graduated location on the barrel of the fine-focus knob. The knob is then moved to focus on the bottom of the pore. By subtracting the location at the bottom of the pore from that at the top of the pore, the depth is determined. Generally, the graduations on the fine-focus barrel are 0.001 to 0.005 mm, depending on the microscope manufacturer.

#### 4.8.4 The Optical System

The optical system consists mainly of an objective (the lens assembly close to the object or specimen) and an eyepiece or ocular (the lens assembly close to the eye). They are called lens assemblies, because each objective and eyepiece contains more than one lens element, that is, compound lenses. Some objectives contain up to 14 different lenses. Older microscopes are constructed with a fixed distance between the objective and the eyepiece, called the mechanical tube length. The tube length is measured from the top of the tube to the last thread of the objective, that is, at the point where the unthreaded portion of the objective meets the microscope or nosepiece. Each microscope manufacturer has a fixed tube length that generally varies between 160 and 250 mm. For this reason, most objectives could not be interchanged between microscopes of different manufacturers. However, more and more manufacturers are developing infinity-corrected objective lenses that depend less on tube length.

#### 4.9 Stereo microscope [27]

The stereo or dissecting microscope is an optical microscope variant designed for low magnification observation of a sample using incident light illumination rather than transillumination. It uses two separate optical paths with two objectives and two eyepieces to provide slightly different viewing angles to the left and right eyes. In this way it produces a three-dimensional visualization of the sample being examined. Stereomicroscopy overlaps macrophotography for recording and examining solid samples with complex surface topography, where a three-dimensional view is essential for analysing the detail.



Figure 68 : Leica MZ6 Stereomicroscope



The stereo microscope is often used to study the surfaces of solid specimens or to carry out close work such as dissection, microsurgery, watch-making, circuit board manufacture or inspection, and fracture surfaces as in fractography and forensic engineering. They are thus widely used in large numbers in manufacturing industry, both for manufacture, inspection and quality control. It tends to make them of lower cost compared with conventional microscopes.

The stereo microscope should not be confused with a compound microscope equipped with double eyepieces and a binoviewer. In such a microscope both eyes see the same image, but the binocular eyepieces provide greater viewing comfort. However, the image in such a microscope is no different from that obtained with a single monocular eyepiece.

We used the Stereo microscope of our lab a **Leica MZ6** to get a **first look** at **flowerlike structure** of the Super-hydrophobic surfaces that had been obtained after the immersion time in the ethanol solution of *n*-tetradecanoic acid.

#### 4.10 The Microhardness Tester [27]

Sometimes, a metallographer needs to know the hardness of the individual constituents in a microstructure. For example, small regions of retained austenite can be identified from the harder martensite matrix in a quenched steel, or the hardness of a thin, carburized or decarburized steel surface can be measured. Another example would be determining the hardness of individual carbides in a tool steel. These measurements cannot be performed by a conventional Brinell, Vickers, or Rockwell hardness tester, because the indentation size far exceeds the dimensions of an individual constituent. In fact, the conventional hardness tester obtains an average or bulk hardness of a particular microstructure. A microhardness tester has to be used for “fine-scale” hardness measurements. A microhardness tester is shown in Fig. 69. A microhardness tester uses loads of 1 kg or less, whereas a conventional hardness



Figure 69 : SHIMADZU HMV of our lab

tester uses higher loads. The indenter is an important feature of the microhardness tester. There are basically two types of indenters: the Vickers indenter, which leaves a diamond-shaped “pyramid” impression, and the Knoop indenter, which leaves an elongated, rhomboid-shaped impression. Examples of the two types of indenters and the shapes of the indentations are shown in Fig. 70. The Vickers (also referred to as diamond pyramid) indentation has diagonals of equal length, whereas the Knoop indentation has one diagonal longer than the other. The depth of the Vickers impression is about  $1/7$  of the diagonal dimension, and the depth of the Knoop impression is about  $1/30$  of the length of the long diagonal. Because the Vickers indentation is deeper than the Knoop indentation, it is less sensitive to surface conditions. Because the Knoop indentation has a longer diagonal than the Vickers indentation, it is less sensitive to measurement errors.

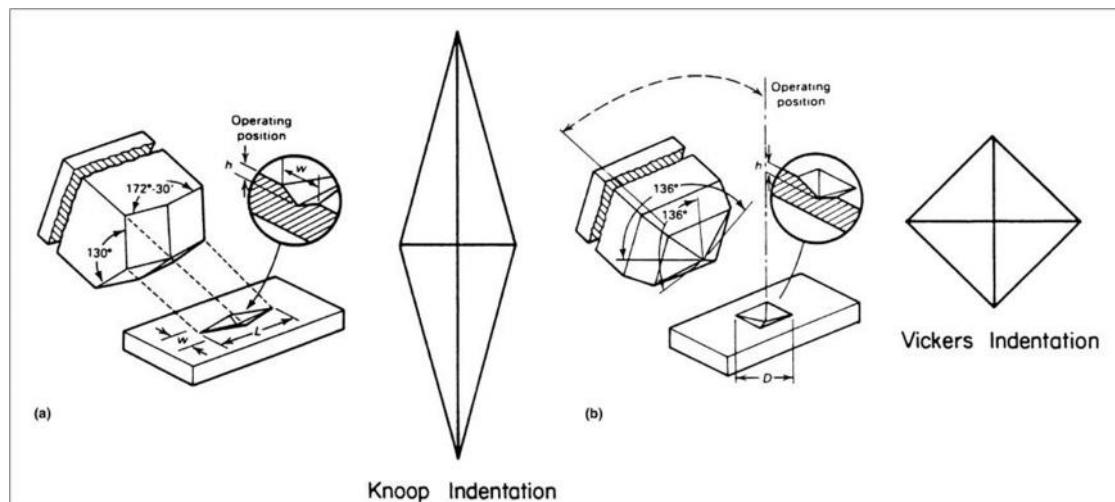


Figure 70 : A comparison between the (a) Knoop and (b) Vickers microhardness indenters

The hardness is determined by measuring the length of the diagonals of the impression. With the Knoop indenter, only the long diagonal is measured, but with the Vickers indenter, both diagonals are measured, and the average diagonal length is used. For both indenters, there are tables that relate impression length to hardness for a fixed load, for example, 10 g. It is important not to place indentations too close to one another or too close to the edge of the specimen. The general rule would be to keep indentations **at least three diagonal lengths apart**.

We used a **SHIMADZU HMV – 2** to measure the microhardness of copper. Indentation measurements were carried out with a **Vickers indenter a 0,2 N load for 20 sec** and a **0,2 N load for 15 sec**.

## 4.11 The Scanning Electron Microscope (SEM) [27]

The most versatile electron microscope is the SEM. A typical SEM is shown in Fig. 76. Thus, the SEM is used to observe and characterize surface features over large (or small) areas of the specimen. The primary electron beam interacts with the specimen surface to produce secondary electrons, backscattered electrons, and x-rays. With detectors mounted just above the specimen, these electrons and x-rays can be collected and analyzed to provide important information about the specimen surface. Subsequently, we look at each interaction.

The backscattered electrons are those electrons that are scattered from the specimen surface and can be collected as the primary beam scans the specimen surface. The collected backscattered electron image of the specimen surface is displayed on a cathode ray tube (CRT) and can be photographed. There is some electron energy loss during the backscattering process. The higher the atomic number of the elements in the sample, the greater the degree of backscattering (less energy loss). This means that elements with higher atomic numbers, such as iron with an atomic number of 26, will appear brighter on the backscattered electron image on the CRT than elements with lower atomic numbers, such as oxygen with an atomic number of only 8. An example of a backscattered electron image of oxide scale penetration into the surface of an AISI/SAE 1045 steel is shown in Fig. 71.

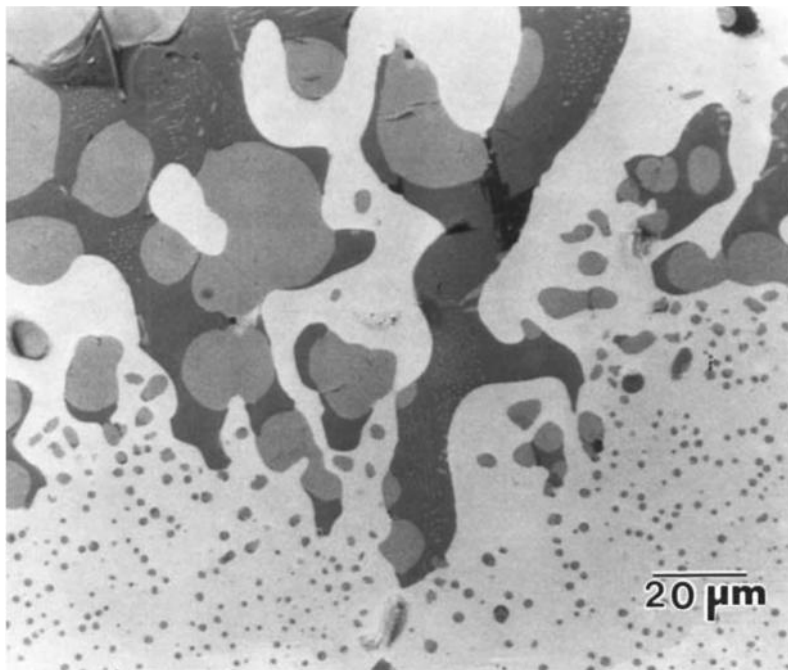
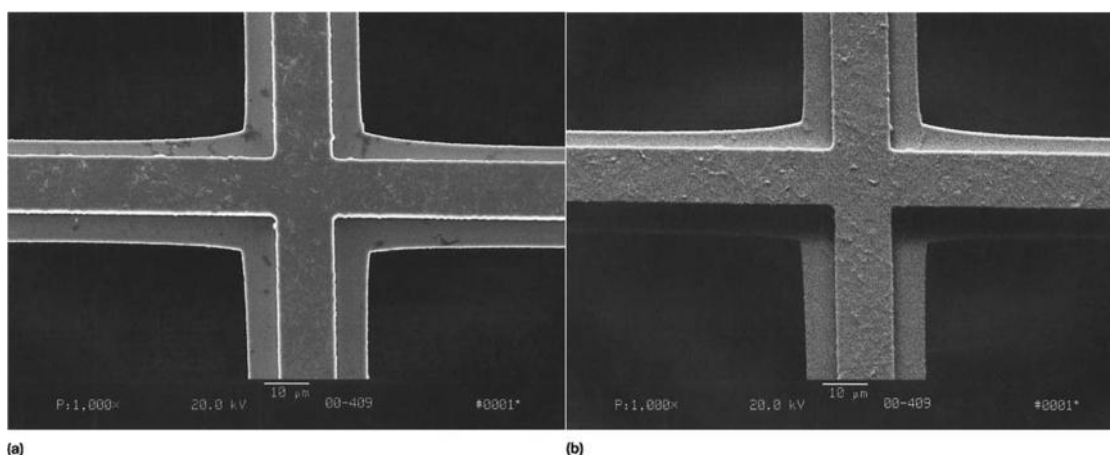


Figure 71 : A SEM backscattered electron micrograph of oxide scale penetration on the surface of an AISI/SAE 1045 steel. The dark-gray appearing constituent is silicon-rich iron oxide (fayalite- $\text{Fe}_2\text{SiO}_4$ ), the medium gray constituent is iron oxide (wustite- $\text{FeO}$ ), and the light gray constituent is steel. The black constituent is a calcium aluminum oxide (Ca aluminates). 540x

The steel appears as the light gray constituent, and the oxide appears as two darker gray constituents. Note that, because of its higher atomic number (i.e., the higher density), the steel appears brighter than the oxide. Thus, backscattered electrons are useful in giving what is called “atomic number contrast” in a microstructure.

Secondary electrons, on the other hand, are the result of the interaction of primary (beam) electrons with those electrons contained within the atoms in the sample. The primary electrons can actually knock the loosely held orbital electrons from atoms. These displaced electrons are called secondary electrons. The secondary electrons have much lower energy than the backscattered electrons described previously. This means that secondary electrons are only detected from the surface and near-surface regions of the specimen, because those from deeper regions are easily absorbed by the sample. Thus, secondary electrons yield a secondary electron image on the cathode ray tube that reveals surface topography and produces an image with enhanced depth of field. It is this depth of field that makes the SEM one of the most useful of all electron microscopes. Note the tremendous depth of field that is obtained. This capability is what makes the SEM a popular instrument for studying surface features. The remarkable advantage is that the images can be obtained at magnifications varying from 10 to 30,000x. As an example, a small copper support grid for viewing surface replicas and thin foils is examined in the SEM. The grid viewed in the SEM shows a secondary electron image at 1000x in Fig. 72a and a backscattered electron image in Fig. 72b. The grid openings are produced by a punching process. Another SEM secondary electron image of a different type of copper grid made by an electrolytic process is shown at the bottom of Fig. 73 (also at 1000x). The rougher surface details of the image of this grid show that it was manufactured by a different process.

X-rays are also emitted from the sample, because of the interaction of the primary and backscattered electrons with the inner shell electrons of atoms in the sample.



**Figure 72 : A copper grid made by the punching process, as seen in the scanning electron microscope. (a) Secondary electron image (760x) and (b) backscattered electron image**

The primary/backscattered electrons have sufficient energy to knock inner shell electrons (the shell closest to the atom nucleus) out of orbit. When an electron is knocked out of a particular inner electron shell, an x-ray is emitted when an electron (from an electron shell further out from the nucleus) moves into its place. These x-rays have a characteristic energy (and wavelength) for the particular atomic species present. Because of

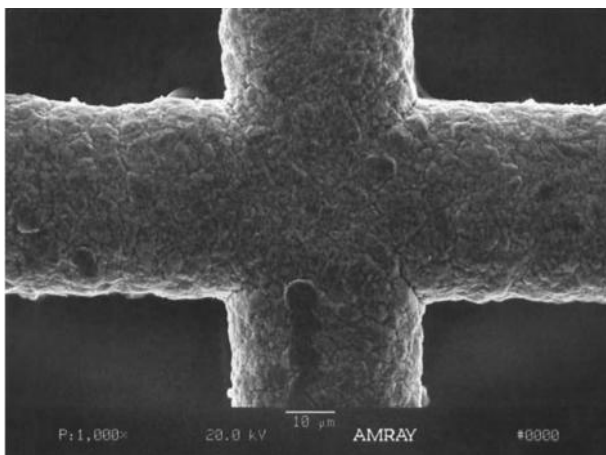


Figure 73 : A copper grid made by an electrolytic process, as seen in the scanning electron microscope. Secondary electron image.750x

this, they are called characteristic x-rays. This means that every x-ray that is collected has an energy and wavelength that is unique to the particular element present in the sample. The importance of collecting these x-rays is that compositional information can be thus obtained. Generally, in a SEM, only the x-ray energy is analyzed. The technique is called energy dispersive spectroscopy, or EDS. An example of an EDS analysis is shown in Fig. 75 where a nonmetallic inclusion in a fractured specimen, shown in Fig. 74, is analyzed to determine beam on the nonmetallic inclusion itself and collecting the x-rays emitted, the elements contained within the inclusion can be determined. The energy spectrum of the x-rays collected from the inclusion is shown in Fig. 75. The intensity, or number of x-rays, is plotted on the vertical axis, and the x-ray energy is plotted on the horizontal axis. In this particular case, the peaks in the energy spectrum indicate that calcium, aluminum, and sulfur are present (there are traces of manganese, silicon, and potassium; the iron is from the specimen itself). This analysis indicates the elements present but does not reveal the distribution of elements within the inclusion.

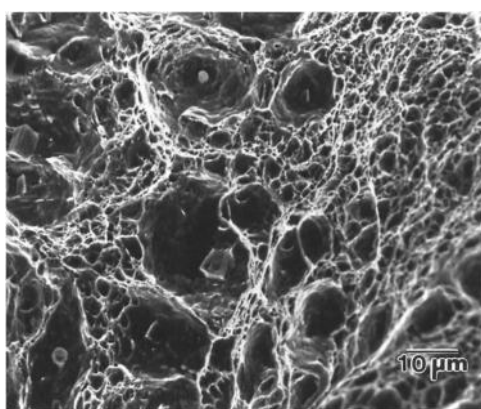


Figure 74 : A SEM secondary electron micrograph of a fractured steel bar. Inclusions can be seen in many of the voids. 1000x

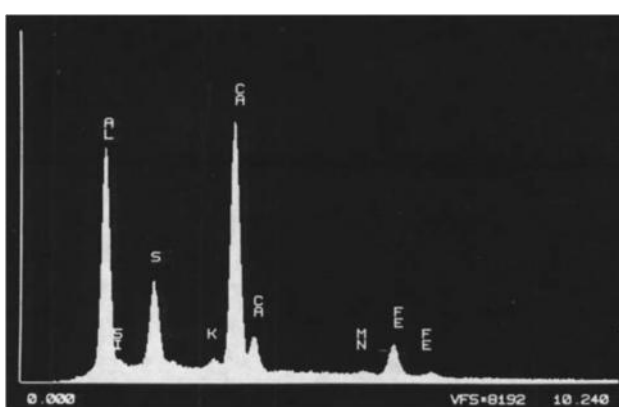


Figure 75 : An EDS spectrum of the elements contained in the nonmetallic inclusion. This EDS spectrum was photographed from the cathode ray tube of the EDS unit.

We used a **JEOL JSM-6390 Scanning Electron Microscope**, with Resolution: 3.0 nm(30kV), Accelerating voltage: 0.5 to 30 kV, Magnification: x5 to 300,000, Filament: Pre-centered W hairpin filament (with continuous auto bias), Objective lens: Super conical lens, Objective lens apertures: Three position, controllable in X/Y directions. With SEM we succeeded to study the **flowerlike structure** of the Super-hydrophobic surfaces in a very close range.



Figure 61 : JEOL JSM-6390 Scanning Electron Microscope

## 4.12 Optical Tensiometry Contact Angle Measurements

Analysis of the shape of a drop of test liquid placed on a solid is the basis for optical tensiometry (goniometry). The basic elements of an optical tensiometer (also called contact angle meter) include light source, sample stage, lens and image capture. Contact angle can be assessed directly by measuring the angle formed between the solid and the tangent to the drop surface.

The production of drops with advanced and receded edges involves one of two strategies. Drops can be made to have advanced edges by addition of liquid. Receded edges may be produced by allowing sufficient evaporation or by withdrawing liquid from the drop. Alternately, both advanced and receded edges are produced when the stage on which the solid is held is tilted to the point of incipient motion. Using an instrument with high speed image capture capabilities shapes of drops in motion may be analyzed.

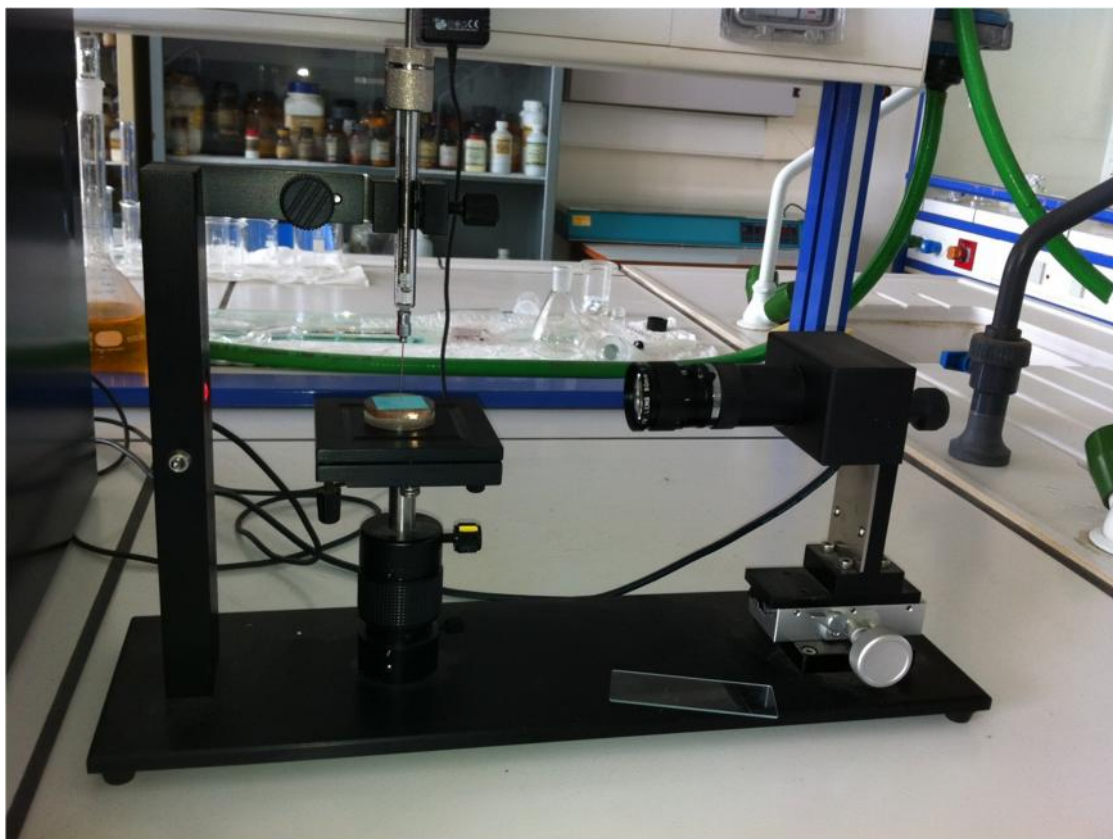


Figure 62 : The experimental setup we used in Dimokritos research center

## 4.13 Electrochemical Measurements [3] [4] [24] [25]

### 4.13.1 Three Electrode Cells

The three-electrode cell is the standard laboratory apparatus for the quantitative investigation of the corrosion properties of materials. It is a refined version of the basic wet corrosion cell and a typical example is illustrated in Fig. 79. It can be used in many different types of corrosion experiments. For our electrochemical measurements we used the three-electrode cell of our lab in Fig.78. First we shall examine the components in more detail.



Figure 638 : The three-electrode cell of our lab

#### 4.13.1.1 The working electrode

**The working electrode** is the name given to the electrode being investigated. It is useful, though not essential, the electrode is designed to have a surface area of  $100 \text{ mm}^2$  ( $1 \text{ cm}^2$ ), current measurements can then be more readily converted into current densities, which should be used in calculations. We use the term 'working electrode' rather than 'anode' because we are not limited to investigations of anodic behaviour alone; cathodic behaviour can also be examined.

Electrical connection must be made to the specimen, and this can be done with solder or spot weld on the reverse side before mounting. After mounting, specimens are often ground and polished, as for metallographic examination. If this technique is used, the surface will be activated, in other words, passive films may have been either removed entirely or just changed from the as-received condition. This should always be borne in mind. Obviously, if the original passive film is part of the corrosion investigation, no pretreatment should be used. In fact, **this is the biggest single reason for discrepancies between lab and field data**. Surfaces in real engineering systems are most often as received from manufacture and are not similar to specimens prepared for metallography.



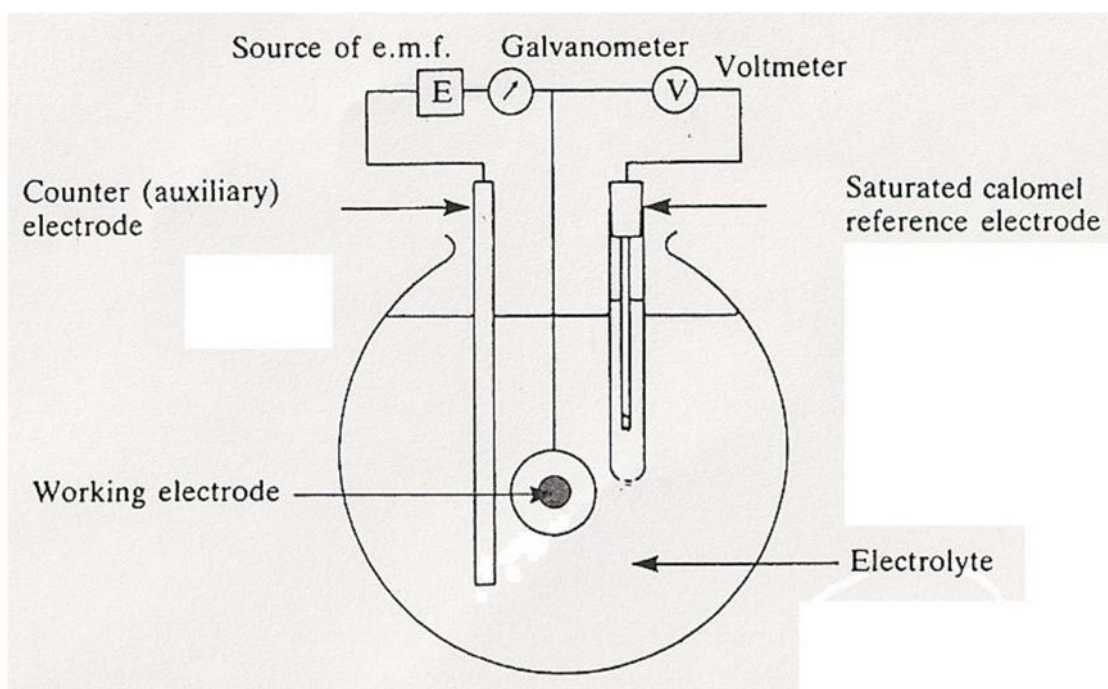


Figure 7964 : The three-electrode cell

#### 4.13.1.2 The Counter Electrode

**The counter (auxiliary) electrode:** is the name given to the second electrode. The counter electrode is present specifically to carry the current created in the circuit by the investigation, it is not required for measurements of potential. Usually, a carbon rod is used, but it can be any material that will not introduce contaminating ions into the electrolyte. Platinum or gold can also be used with success, especially if space is at a premium, when smaller electrodes can be used, titanium is also suitable. In our experimental setup the counter electrode is made of platinum.

#### 4.13.1.3 The Reference electrode

**The reference electrode:** is present to provide a very stable datum against which the potential of the working electrode can be measured. It cannot itself carry any more than the most negligible current. If it did, it would participate in the cell reactions and its potential would no longer be constant, hence the requirement for the counter electrode. **By far the most convenient reference electrode to use in such an experiment is a saturated calomel electrode (SCE).**

The external circuit can be varied considerably. The essential components are a current-measuring device, a potential-measuring device and a source of potential. The **current-measuring device** should be capable of reading microAmps, at least. The

**potential-measuring device** should draw no current during the act of measurement, traditionally potentiometers have been used for this purpose. The modern digital meter, however, can have an impedance of the order of gigohms, and may be used with as good an accuracy as a potentiometer.

#### 4.13.1.4 The Source of Potential

**The source of potential** 'drive' the working electrode to produce the desired cell reactions. Typical potentiostats are readily available commercially and have been used extensively by corrosion scientists. Potentiostats apply predetermined potentials to the working electrode so that measurement of the cell current can be made. This is done by altering the current at the counter electrode to maintain the set value of working-to-reference potential. A simple constant voltage source is not suitable. We used a VersaSTAT 4 Fig. 80



Figure 80 : VersaSTAT 4

The three electrodes are placed in a suitable glass vessel of capacity about 1 liter containing the chosen electrolyte Fig. 78

#### 4.13.1.5 The Electrolyte

**Electrolyte** is a fundamental part of the whole corrosion process. It is extremely important to consider the conductivity of the electrolyte, since by carrying the ionic current, it plays such an important role in corrosion reactions. The use of a reference electrode is to enable the potential of a working electrode to be measured and it should be placed as close to the electrode surface as possible. This is because the measured potential will always include the potential difference across the electrolyte occupying the space between the working electrode surface and the reference electrode. Most corrosion measurements involve the use of direct currents, so Ohm's Law applies and the potential difference across the electrolyte can be estimated, i.e.  $V=IR$ . Not surprisingly,

this potential is often referred to as the **Ohmic** or ***IR* drop**, and may be large if either the current or the resistance of the electrolyte is large. It is usually preferable to make the *IR* drop as small as possible, otherwise its contribution to the overall cell potential may be difficult to quantify. When using a high conductivity electrolyte, such as 3.5% sodium chloride solution or sea-water, the effect will be small, so the experimental apparatus described in Fig. 79 is adequate for most investigations. If more dilute solutions are necessary for the experiments then it is essential to use a more sophisticated reference electrode measurement. This is achieved by means of a device called a **Luggin capillary** Fig. 81

The traditional Luggin design utilises a glass capillary with a very fine tip placed as close to the metal surface as is practical. The capillary leads away from the reaction vessel to a separate small receptacle containing an SCE and filled with saturated potassium chloride solution. The tube which carries the electrolyte between the reference and test electrodes is known as the **salt bridge**.

The biggest problem with such an arrangement is from contamination of the low conductivity electrolyte by diffusion of the saturated potassium chloride. A better method is to use the equipment of Fig. 32 in which a special Vycor tip considerably reduces the leakage rates and the *IR* drop through the tip.

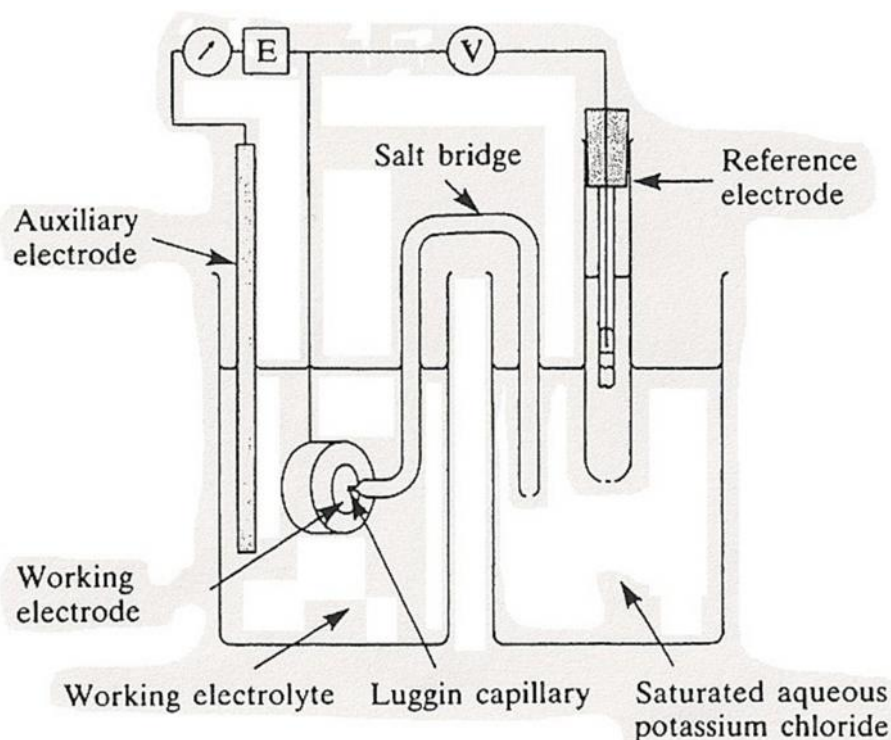


Figure 81 : Simple capillary made from glass tube salt bridge

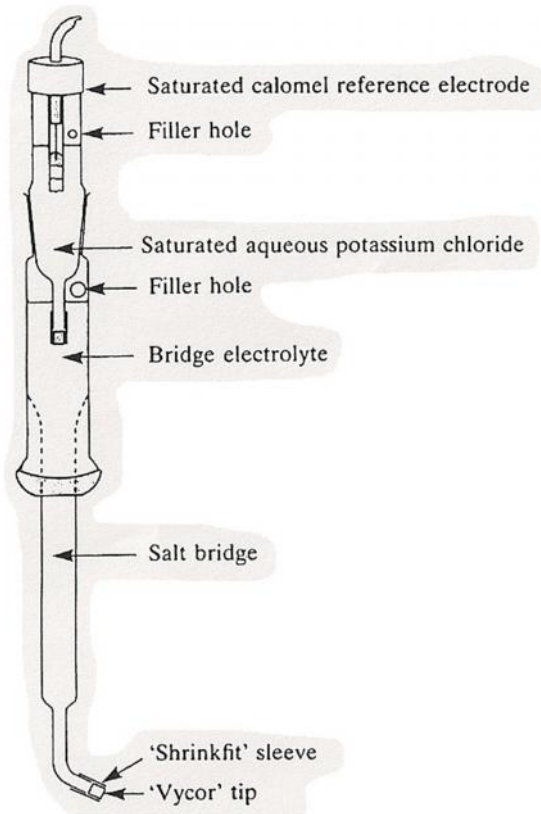


Figure 82 : Specialist design incorporating ball-and-socket ground glass joint

### Experiment

If we set up the equipment that described in Fig. 79 using **pure copper** of measured exposed surface area as a working electrode, and a solution of **3.5% sodium chloride** as an electrolyte. Adjust the potentiostat to read **-0.400 V**. Scan through the potentials to **+0.400 V** and take measurements of current at 0.010 V (10 mV) intervals. Allow the cell to settle at each value of potential for one minute before moving on to the next. Observe the surface of the specimen and note any changes that occur. Compile a table of applied potential (V) and current density ( $A\ m^{-2}$ ), treating all current values as positive. **Plot a graph of  $E$  as ordinate and  $\lg i$  as abscissa.**

#### 4.13.2 $E/\log(i)$ Plots

The  $E/\lg i$  plot, or **potentiodynamic polarisation curve**, is one of the most common methods of examining the corrosion behaviour of materials. It has become

common practice in  $E/\lg i$  plots for all current densities to be treated as positive. This is really just a convenience for it reduces the size of the graphs and gives a much clearer indication of the value of potential when the current density changes from negative to positive. The portion of the graph for which you measured negative currents that is from  $-0.400$  V to about  $-0.240$  V, represents the copper behaving as a cathode. From  $-0.240$  V to more positive values of potential, the copper is behaving as an anode and it is during this part of the scan that you will have observed visible changes to the specimen because of the numerous reactions which occurred as the copper corroded. At potentials in the region of  $-0.050$  to  $-0.080$  V, a marked reduction in the corrosion current is observed. This represents partial passivation of the metal because of the presence of the corrosion products, in this case quite small, as evidenced by the relatively small reduction in current.

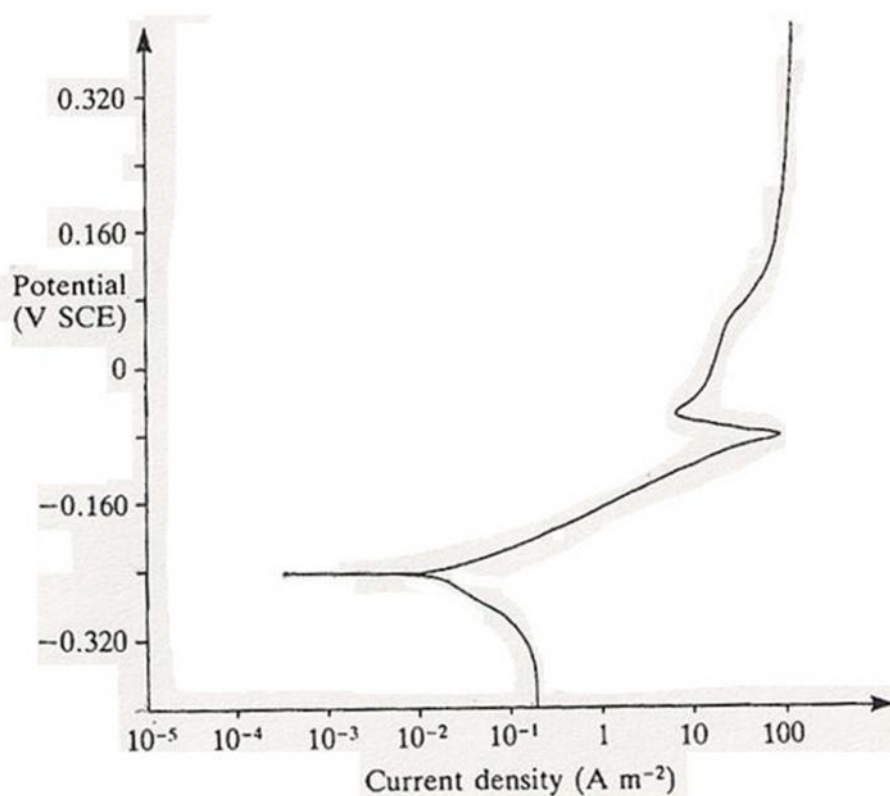


Figure 65 : Potentiodynamic scan for copper in 3.5 % sodium chloride solution

### *The significance of the changeover from negative to positive currents*

In practical terms it represents the state the metal assumes under freely corroding conditions. The value of potential is commonly called the **free corrosion potential** and the symbol used is  $E_{\text{corr}}$ . In your experiment you should have, measured  $E_{\text{corr}}$  at about  $-0.24$  V SCE. At this potential the specimen could be described as being in a steady-state condition, equivalent to the condition it would have achieved with the potentiostat

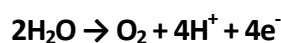
switched off. Remember that the purpose of the instrument is to perturb the potential of the with the potentiostat rest potential. In practice, equilibrium conditions are impossible to achieve, the metal surface acts as an assembly of many tiny anodes and cathodes, and corrosion occurs at a rate given by the theoretical anode current density,  $i_a$ . At the free corrosion potential  $i_a$  is replaced by  $i_{corr}$ , **the corrosion current density**. This is the simplest way of quantifying the actual corrosion rate under freely corroding conditions, and it emphasises the importance of carrying out polarisation scans and Tafel plots of the data obtained.

### *The corrosion rate*

Corrosion rate is always equivalent to  $i_a$  at the prevailing potential for a metal dissolution reaction. When only a single reversible metal redox reaction is being considered and is at equilibrium,  $i_0 = i_a = i_c$ . When more than one redox reaction occurs, as in this case, there is a separate exchange current density for each redox process, and the corrosion rate is now symbolised by  $i_{corr}$  (still equal to  $i_a$  for the metal dissolution). There is no theoretical method for calculating  $i_0$ . One way is to perform  $E/\lg i$  measurements very carefully for each metal, both anodically and cathodically polarised under conditions in which the free corrosion potential is a result of only the metal redox pair of reactions.

*When the copper is in the region of potential from -0.24 to -0.40 V, it is acting as a cathode in the aqueous corrosion cell. What is the anode and what corrodes in this cell at these potentials?*

The auxiliary electrode, in this case the carbon rod, becomes the anode. There is no corrosion, because the auxiliary electrode is chosen so that it will not contaminate the solution with ions which are not part of the investigation. Other electron-producing reactions must take place at the electrode surface if the electrons required by the copper cathode are to be produced. A common reaction in the electrolyte is the generation of oxygen gas by the oxidation of water:



Another possibility, again in the chloride-containing electrolyte, is the generation of chlorine gas:



## 4.14 The Atomic force microscopy (AFM)

The Atomic Force Microscope was developed to overcome a basic drawback with STM - that it can only image conducting or semiconducting surfaces. The AFM, however, has the advantage of imaging almost any type of surface, including polymers, ceramics, composites, glass, and biological samples.

Binnig, Quate, and Gerber invented the Atomic Force Microscope in 1985. Their original AFM consisted of a diamond shard attached to a strip of gold foil. The diamond tip contacted the surface directly, with the interatomic van der Waals forces providing the interaction mechanism. Detection of the cantilever's vertical movement was done with a second tip - an STM placed above the cantilever.

### 4.14.1 AFM Probe Deflection

Today, most AFMs use a laser beam deflection system, introduced by Meyer and Amer, where a laser is reflected from the back of the reflective AFM lever and onto a position-sensitive detector. AFM tips and cantilevers are microfabricated from Si or Si<sub>3</sub>N<sub>4</sub>. Typical tip radius is from a few to 10s of nm. Beam deflection system, using a laser and photodetector to measure the beam position.

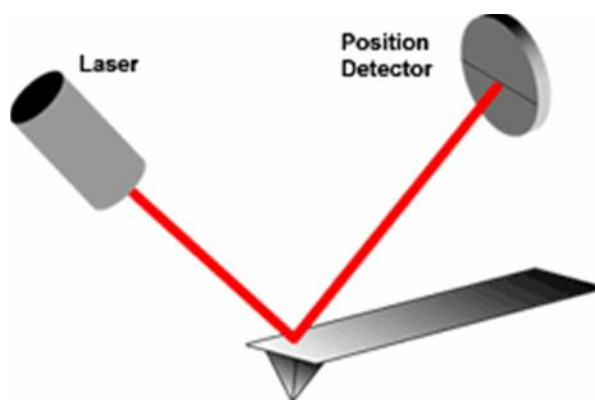


Figure 664 : Probe Deflection

### 4.14.2 Measuring Forces

Because the atomic force microscope relies on the forces between the tip and sample, knowing these forces is important for proper imaging. The force is not measured directly, but calculated by measuring the deflection of the lever, and knowing the stiffness of the cantilever. Hook's law gives  $\mathbf{F} = -kz$ , where  $\mathbf{F}$  is the force,  $k$  is the stiffness of the lever, and  $z$  is the distance the lever is bent.

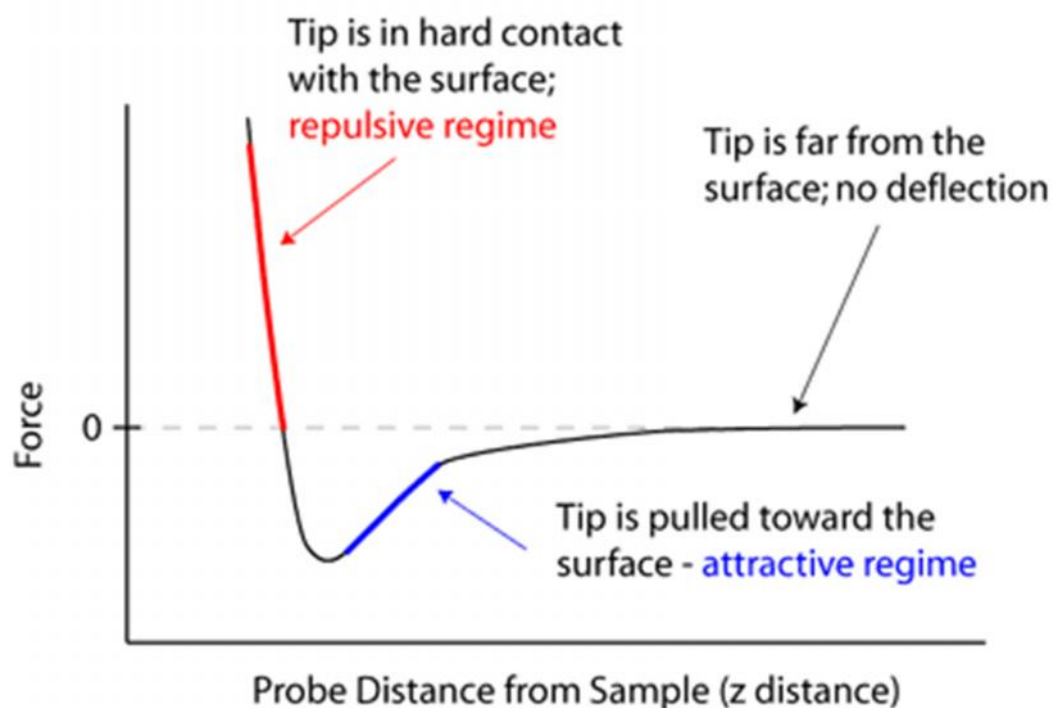


Figure 85 : Force-Probe Distance from Sample

### 4.14.3 AFM Modes of Operation

Because of AFM's versatility, it has been applied to a large number of research topics. The Atomic Force Microscope has also gone through many modifications for specific application requirements.

#### 4.14.3.1 Contact Mode

The first and foremost mode of operation, contact mode is widely used. We also used this mode to the specimens with the Super-hydrophobic surfaces. As the tip is raster-scanned across the surface, it is deflected as it moves over the surface corrugation. In constant force mode, the tip is constantly adjusted to maintain a constant deflection, and therefore constant height above the surface. It is this adjustment that is displayed as data. However, the ability to track the surface in this manner is limited by the feedback circuit. Sometimes the tip is allowed to scan without this adjustment, and one measures only the deflection. This is useful for small, high-speed atomic resolution scans, and is known as variable-deflection mode.

Because the tip is in hard contact with the surface, the stiffness of the lever needs to be less than the effective spring constant holding atoms together, which is



on the order of 1 - 10 nN/nm. Most contact mode levers have a spring constant of < 1N/m.

#### 4.14.3.2 Lateral Force Microscopy

LFM measures frictional forces on a surface. By measuring the “twist” of the cantilever, rather than merely its deflection, one can qualitatively determine areas of higher and lower friction.

#### 4.14.3.3 Noncontact mode

Noncontact mode belongs to a family of AC modes, which refers to the use of an oscillating cantilever. A stiff cantilever is oscillated in the attractive regime, meaning that the tip is quite close to the sample, but not touching it (hence, “noncontact”). The forces between the tip and sample are quite low, on the order of pN (10<sup>-12</sup> N). The detection scheme is based on measuring changes to the resonant frequency or amplitude of the cantilever.

#### 4.14.3.4 Dynamic Force / Intermittant-contact / “tapping mode” AFM

Commonly referred to as “tapping mode” it is also referred to as intermittent-contact or the more general term Dynamic Force Mode (DFM). A stiff cantilever is oscillated closer to the sample than in noncontact mode. Part of the oscillation extends into the repulsive regime, so the tip intermittently touches or “taps” the surface. Very stiff cantilevers are typically used, as tips can get “stuck” in the water contamination layer.

The advantage of tapping the surface is improved lateral resolution on soft samples. Lateral forces such as drag, common in contact mode, are virtually eliminated. For poorly adsorbed specimens on a substrate surface the advantage is clearly seen.

#### 4.14.3.5 Force Modulation

Force modulation refers to a method used to probe properties of materials through sample/tip interactions. The tip (or sample) is oscillated at a high frequency and pushed into the repulsive regime. The slope of the force-distance curve is measured which is correlated to the sample's elasticity. The data can be acquired along with topography, which allows comparison of both height and material properties.

#### 4.14.3.6 Phase Imaging

In Phase mode imaging, the phase shift of the oscillating cantilever relative to the driving signal is measured. This phase shift can be correlated with specific material properties that effect the tip/sample interaction. The phase shift can be used to differentiate areas on a sample with such differing properties as friction, adhesion, and viscoelasticity. The techniques is used simultaneously with DFM mode, so topography can be measured as well.

### 4.15 Preparation of Super-hydrophobic Surfaces

The front surface of the copper specimens was polished using silicon carbide papers from 400 to 1500 grade, then degreased with acetone, washed with distilled water, dried. Cu substrates were etched in 7M HNO<sub>3</sub> for 30 s to remove surface oxides. The etching provided a fresh and active surface. The etched substrates were rapidly rinsed with deionized water followed by pure ethanol. They were subsequently immersed in an ethanol solution of *n*-tetradecanoic acid 0.06M at room temperature for 10 days. The immersed Cu substrates were rinsed with deionized water and ethanol thoroughly, and then dried in air.



Figure 86 : Myristic acid & pure Ethanol

## 5 Results and Discussion [5] [6] [7] [8] [9] [10] [11] [12] [29]

### 5.1 Introduction

In this section given all the results that had been taken from the study of electrolytic tough pitch copper substrates and the study of the Super-hydrophobic specimens of electrolytic tough pitch copper. That results concern the metallographic study, the microhardness measurements, the contact angle measurements, the scanning electron microscope (SEM) measurements, the atomic force microscopy (AFM), and the electrochemical measurements. We are also going to discuss all that results so we can derive some useful conclusions from this work.

### 5.2 Metallographic Study

In the following pages the microstructure photos of Electrolytic Tough Pitch Copper (Copper No. C11000), are presented (Figs 87-97). The copper substrates after the cutting, mounting, grinding, and polishing process, are etched with 5 g  $\text{FeCl}_3$ , in 100 mL ethanol, with addition of 5 – 30 mL HCl as we had described in Section 2. We can observe that there are equiaxed grains, containing twinned areas (Figs. 91-97) and some “dark dots” areas representing  $\text{Cu}_2\text{O}$  oxides, caused by oxygen penetration (Figs. 91-97).

Crystal twinning occurs when two separate crystals share some of the same crystal lattice points in a symmetrical manner. The result is an intergrowth of two separate crystals in a variety of specific configurations. A twin boundary or composition surface separates the two crystals. Crystallographers classify twinned crystals by a number of twin laws. These twin laws are specific to the crystal system. The type of twinning can be a diagnostic tool in mineral identification.

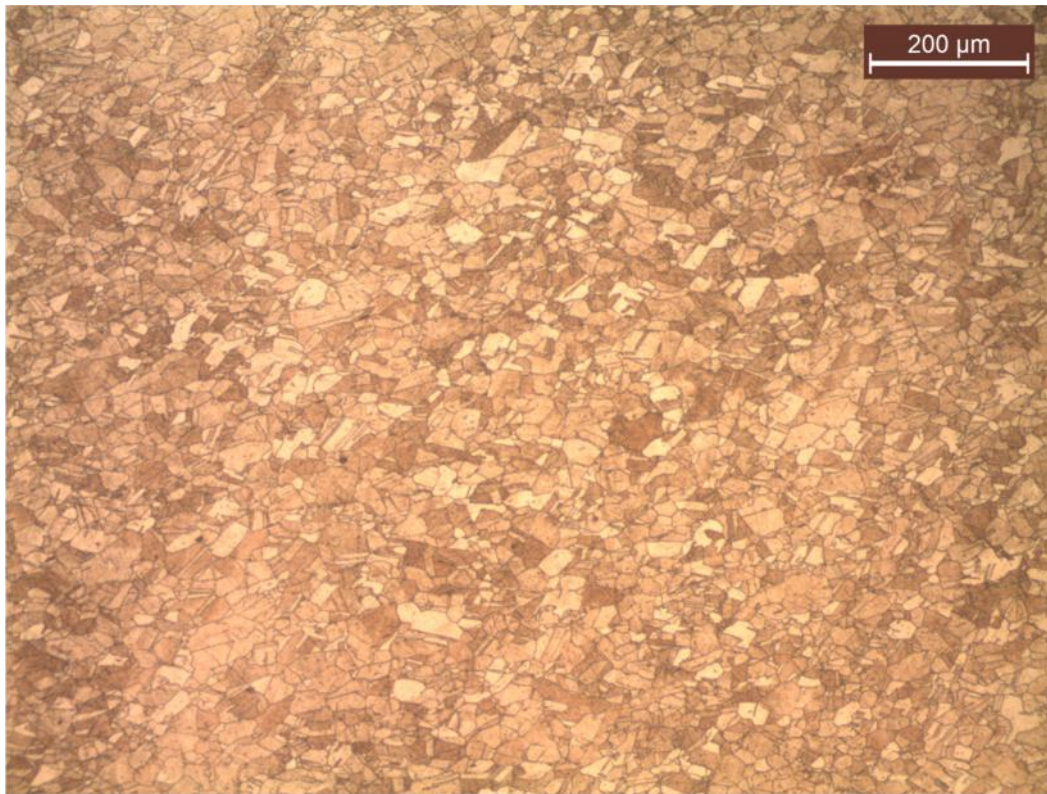


Figure 87 : Microstructure of electrolytic Tough Pitch Copper x10

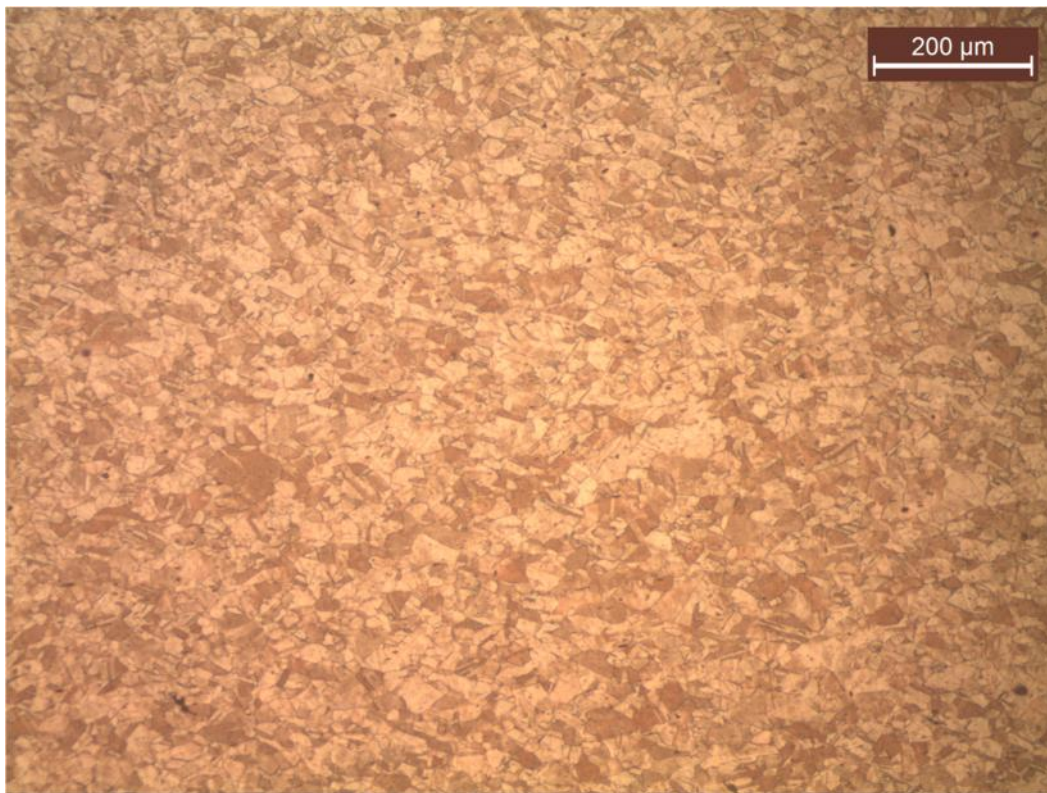


Figure 88 : Microstructure of electrolytic Tough Pitch Copper x10

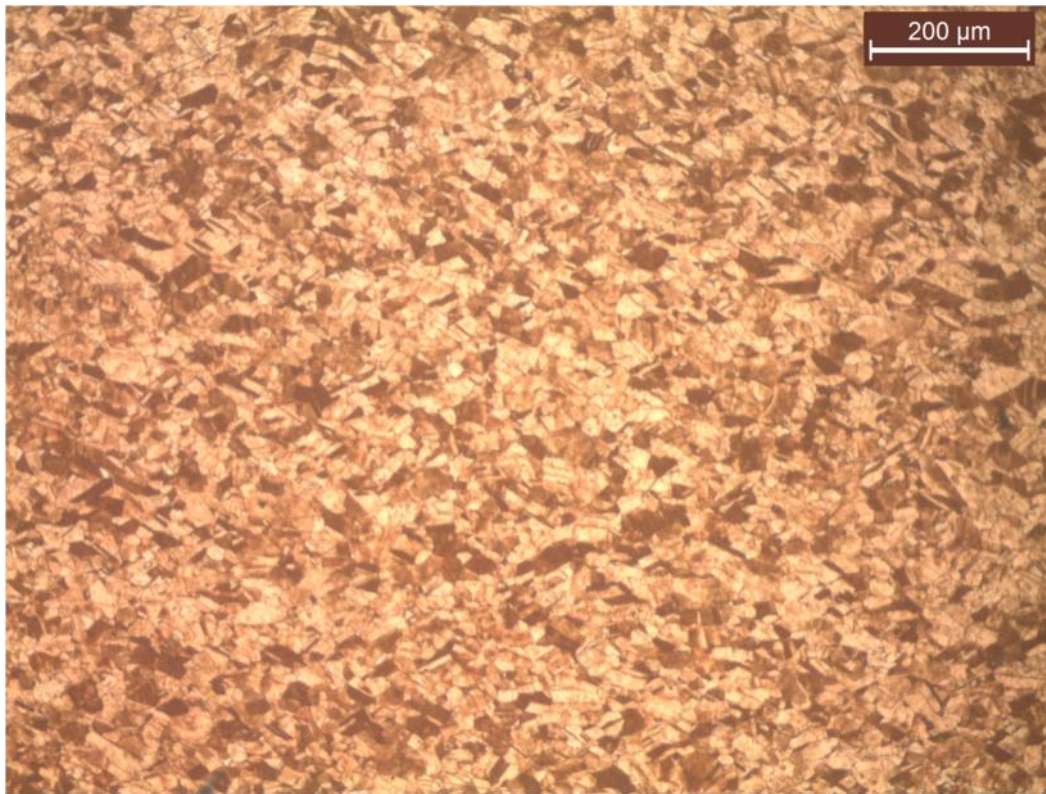


Figure 89 : Microstructure of electrolytic Tough Pitch Copper x10

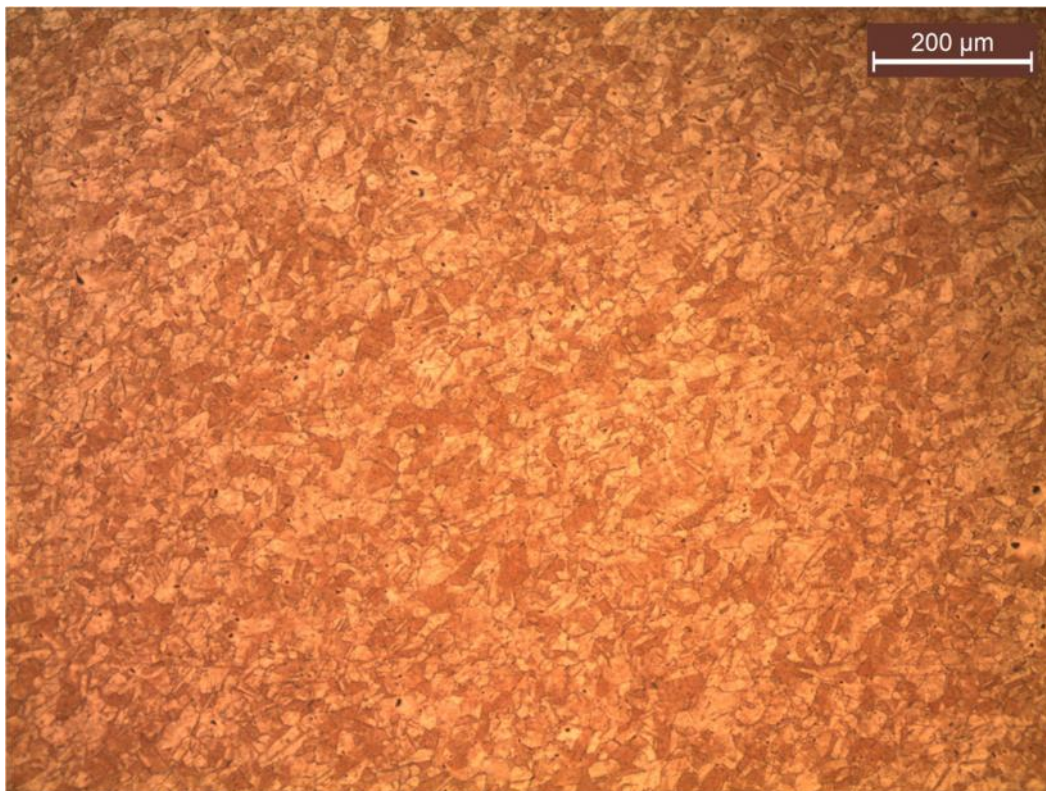


Figure 90 : Microstructure of electrolytic Tough Pitch Copper

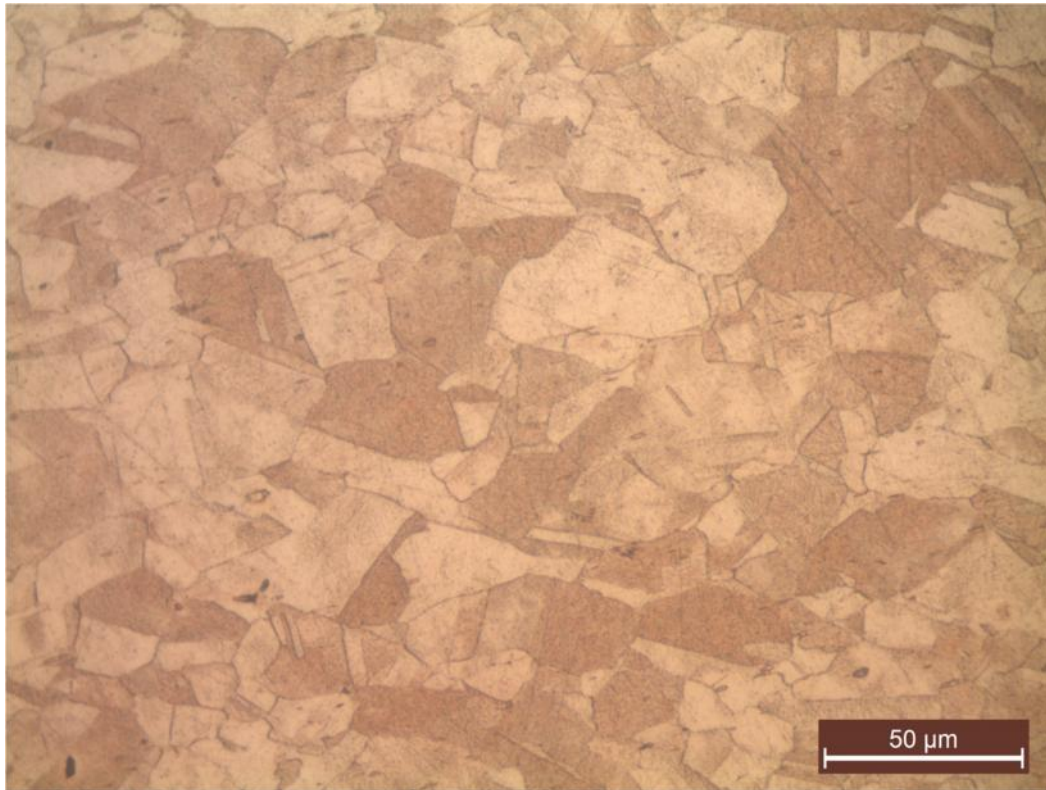


Figure 91 : Microstructure of electrolytic Tough Pitch Copper, large, equiaxed, twinned grains, dark dots are Cu<sub>2</sub>O caused by oxygen penetration

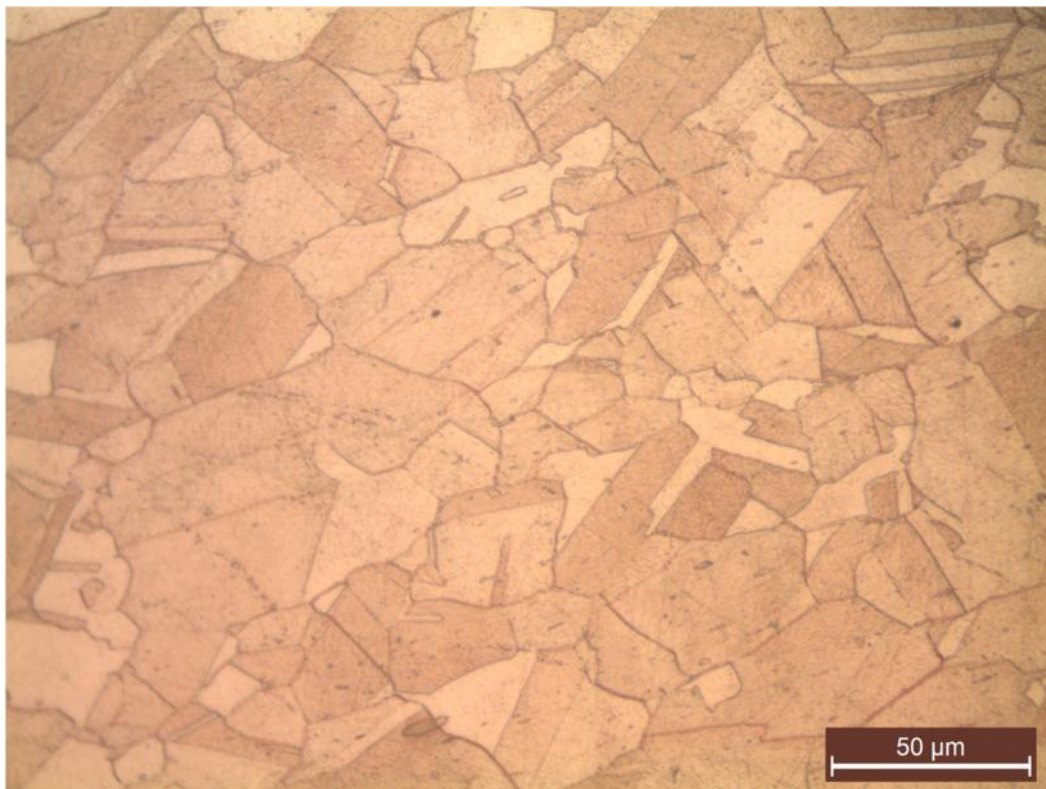


Figure 92 : Microstructure of electrolytic Tough Pitch Copper Large, equiaxed, twinned grains, dark dots are Cu<sub>2</sub>O caused by oxygen penetration

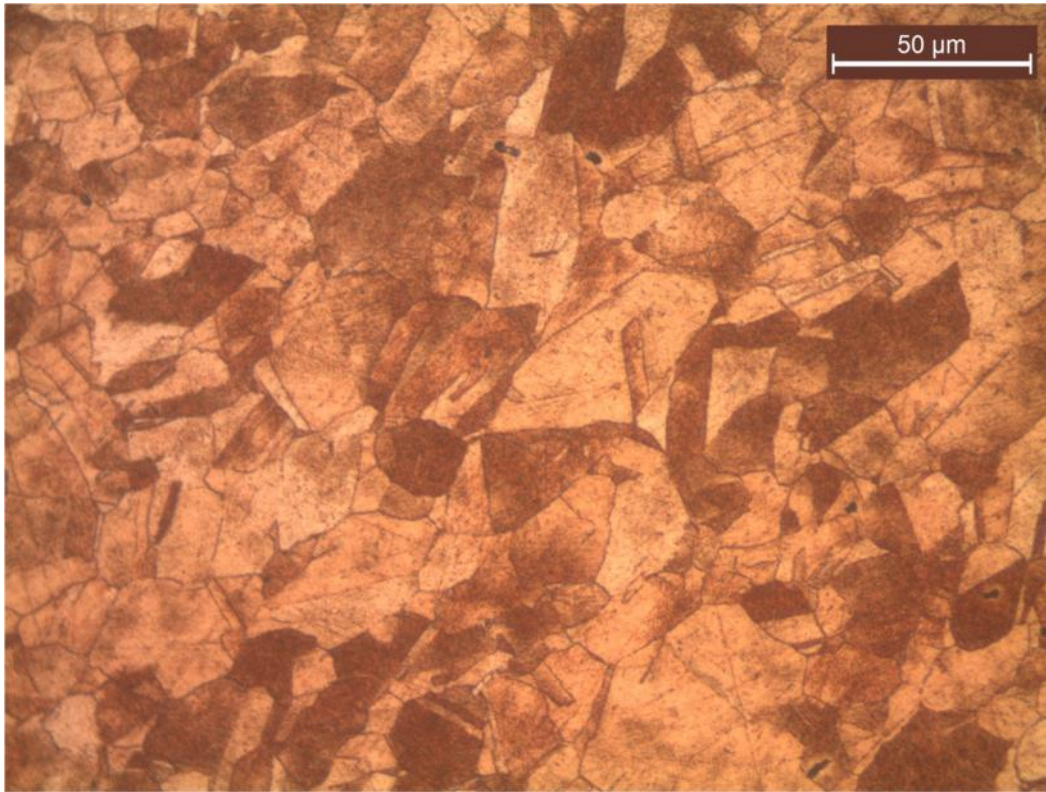


Figure 93 : Microstructure of electrolytic Tough Pitch Copper Large, equiaxed, twinned grains, dark dots are  $\text{Cu}_2\text{O}$  caused by oxygen penetration

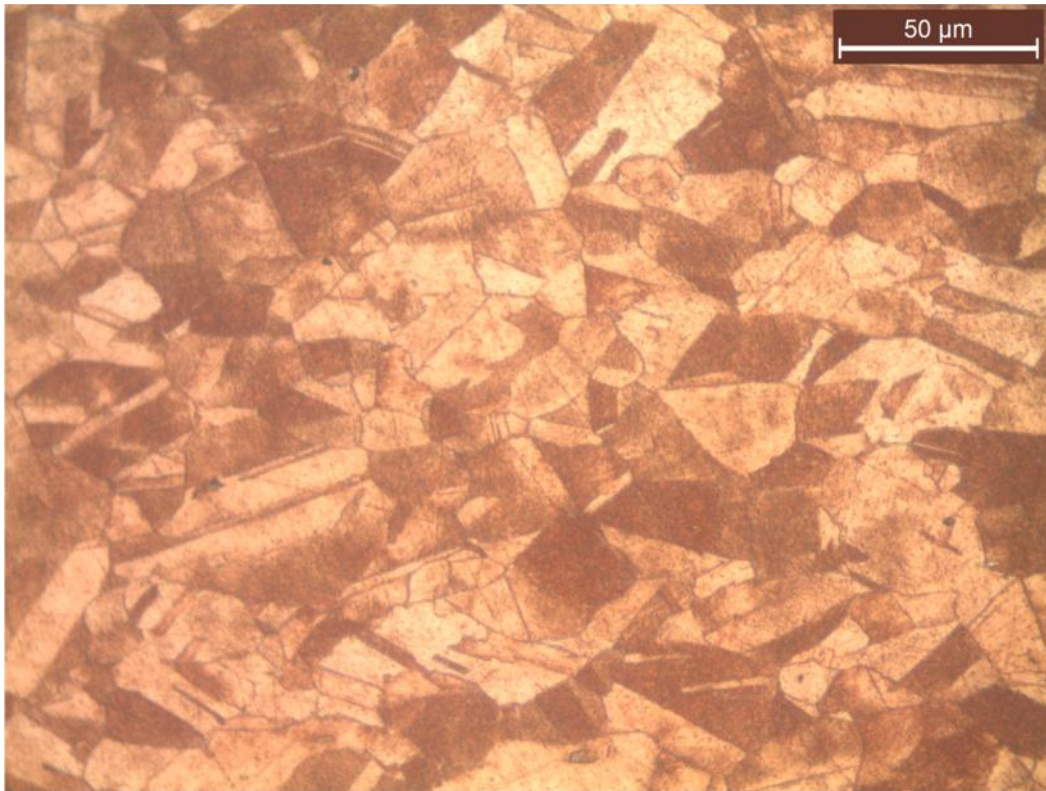


Figure 94 : Microstructure of electrolytic Tough Pitch Copper Large, equiaxed, twinned grains, dark dots are  $\text{Cu}_2\text{O}$  caused by oxygen penetration

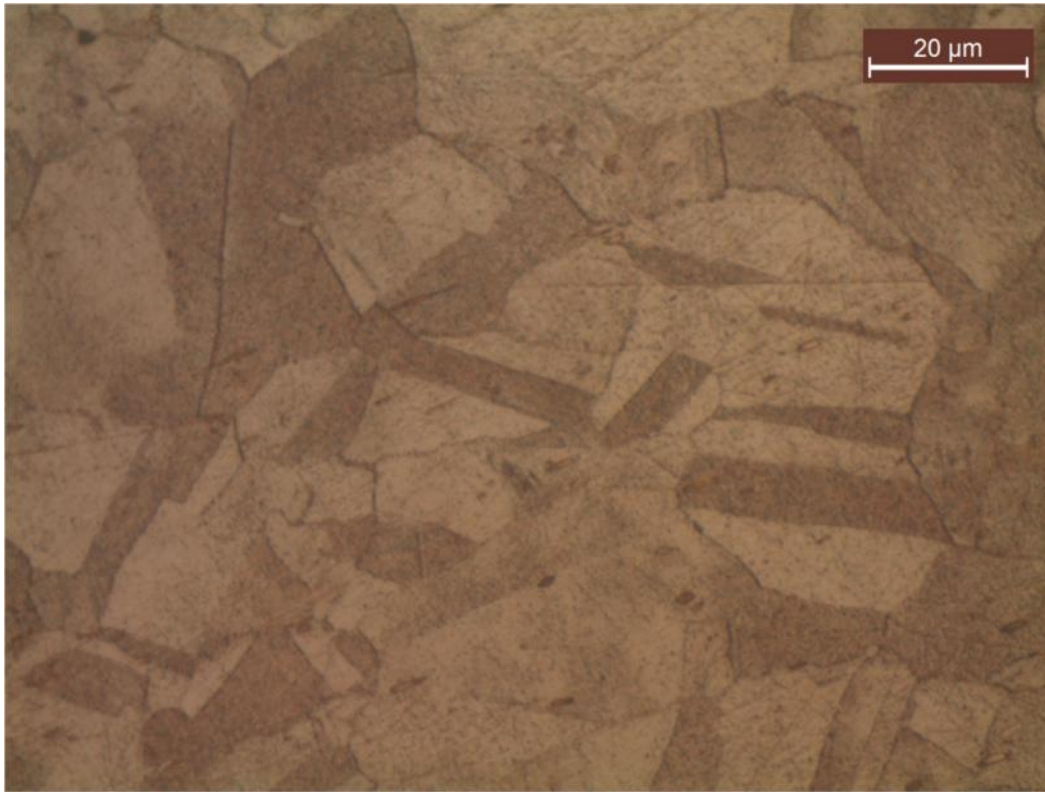


Figure 95 : Microstructure of electrolytic Tough Pitch Copper, large, equiaxed, grains containing twinned areas, dark dots are Cu<sub>2</sub>O caused by oxygen penetration

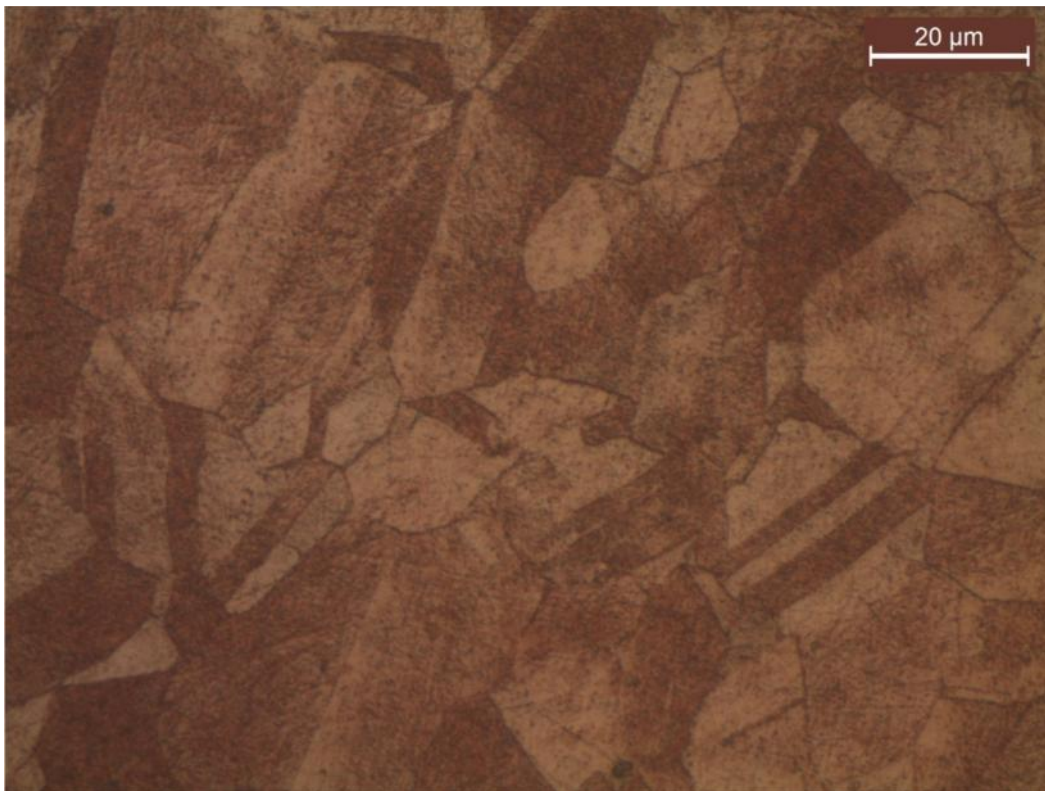


Figure 96 : Microstructure of electrolytic Tough Pitch Copper, large, equiaxed, grains containing twinned areas, dark dots are Cu<sub>2</sub>O caused by oxygen penetration



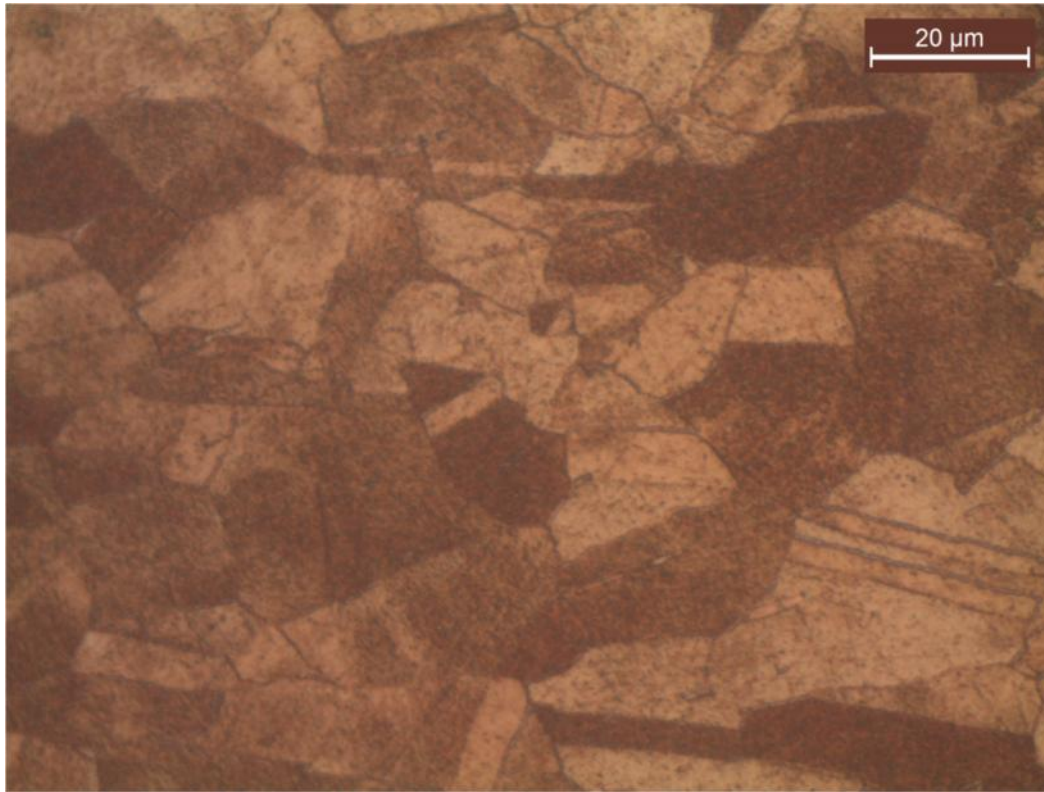


Figure 97 : Microstructure of electrolytic Tough Pitch Copper, large, equiaxed, grains containing twinned areas, dark dots are Cu<sub>2</sub>O caused by oxygen penetration

### 5.3 Microhardness Measurements

The microhardness measurements preceded the cutting, mounting, grinding, polishing, and etching process. The specimens went through two different microhardness measurements. In each experiment we diversified the load and the time magnitudes. In the first twenty measurements we used a **0,3 N load for 15 sec** (Fig.98) and in the next twenty we used a **0,2 N load for 20 sec**. As we can see from the microstructure photos below, the second attempt with a 0,2 N load for 20 sec had better results, since the mark of the intender was more accurate and sharp. So we consider as more accurate microhardness results for our electrolytic tough pitch copper, the results from the second experiment (Fig.99). The microhardness measurements and the microstructure photos are listed in below. The mean value for a 0,2 N load for 20 sec, is 94,1, which is in accordance with the literature.

Table 9. Microhardness measurements

HV 0,3 – 15sec	HV 0,2 – 20sec
98,7	93,5
99,2	93,3
99,0	95,3
100,8	95,0
101,7	97,7
96,0	96,6
97,9	94,0
95,3	94,7
100,6	94,2
96,9	93,7
95,7	95,1
101,2	91,8
97,9	92,7
98,6	94,7
100,8	88,2
96,4	94,1
101,5	95,4
95,2	93,4
98,8	95,3
92,8	94,5
98,7	93,5
99,2	93,3
<b>Average ( 98,2 )</b>	<b>Average ( 94,1 )</b>

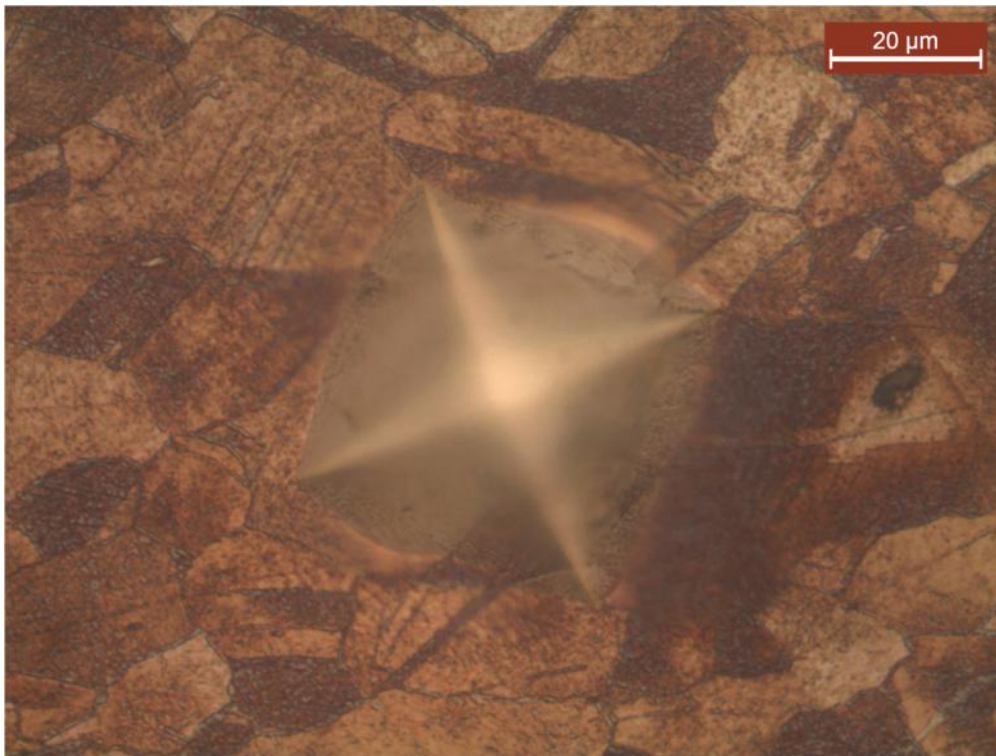


Figure 98 : Microhardness measurements with 0,3 N load for 15 sec

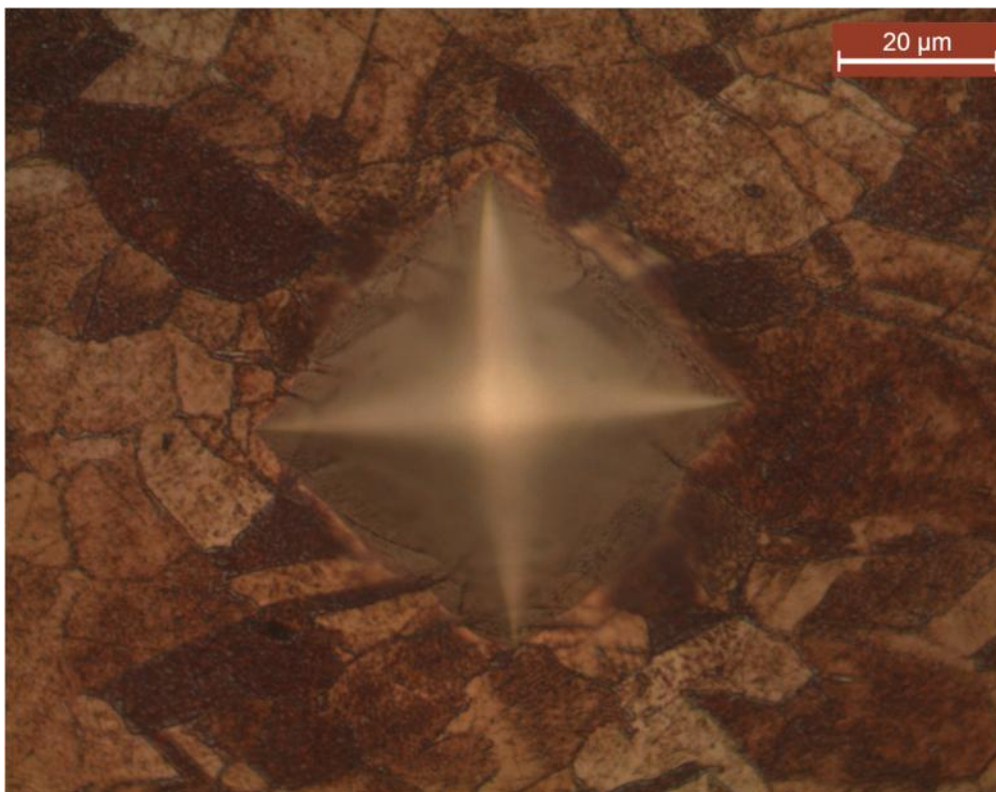


Figure 99 : Microhardness measurements x100 with 0,2 N load for 20 sec

## 5.4 Contact Angle Measurements

Below are presented the Contact Angle measurements. We measured three different specimens. One copper specimen with Super-hydrophobic treatment (SHT), one clean copper specimen (P), polished using silicon carbide papers up to 1500 grade, and one copper specimen where the Super-hydrophobic treatment had been manually removed (RSHT). The measurement on the treated specimen, were very difficult to obtain, since the droplets did not stand still on the surface and roll off the surface immediately. We had to create droplets, bigger than usual and also to reduce the distance between the stage and the needle. The results of the measurements are presented in Table 2. It is obvious that the difference between the treated and the clean surface is quite important large, more than two time. The measurements obtained for SHT are typical, and in accordance to the literature for super-hydrophobic treatments. When the coating was removed, the measured contact is still high, more than 100, implying that may be there is another layer, which still provides hydrophobic properties to the surface.

Table 10. Contact Angle Measurements

	<b>Left Contact Angle</b>	<b>Right Contact Angle</b>	<b>Mean Contact Angle</b>
<b>Super-hydrophobic treatment (SHT)</b>	161,1	160,3	<b>160,7</b>
<b>Polished ( 400-1500) (P)</b>	62,37	59,33	<b>60,85</b>
<b>Removed Super-hydrophobic treatment (RSHT)</b>	101,84	102,64	<b>102,24</b>

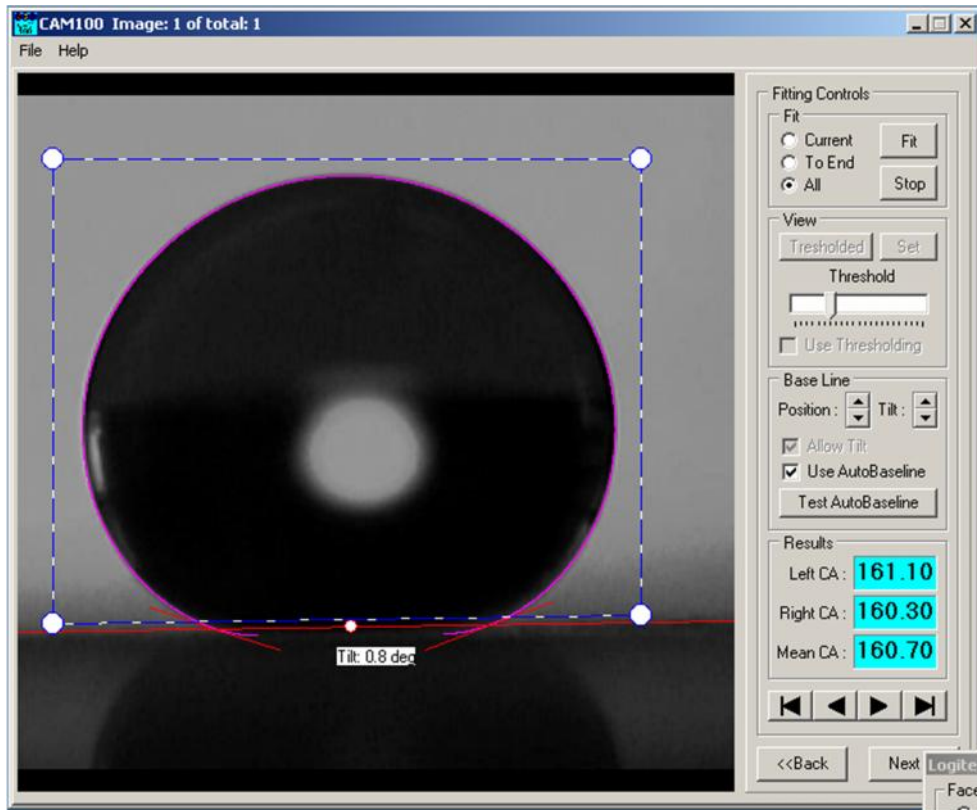


Figure 100 : Copper specimen with Super-hydrophobic treatment

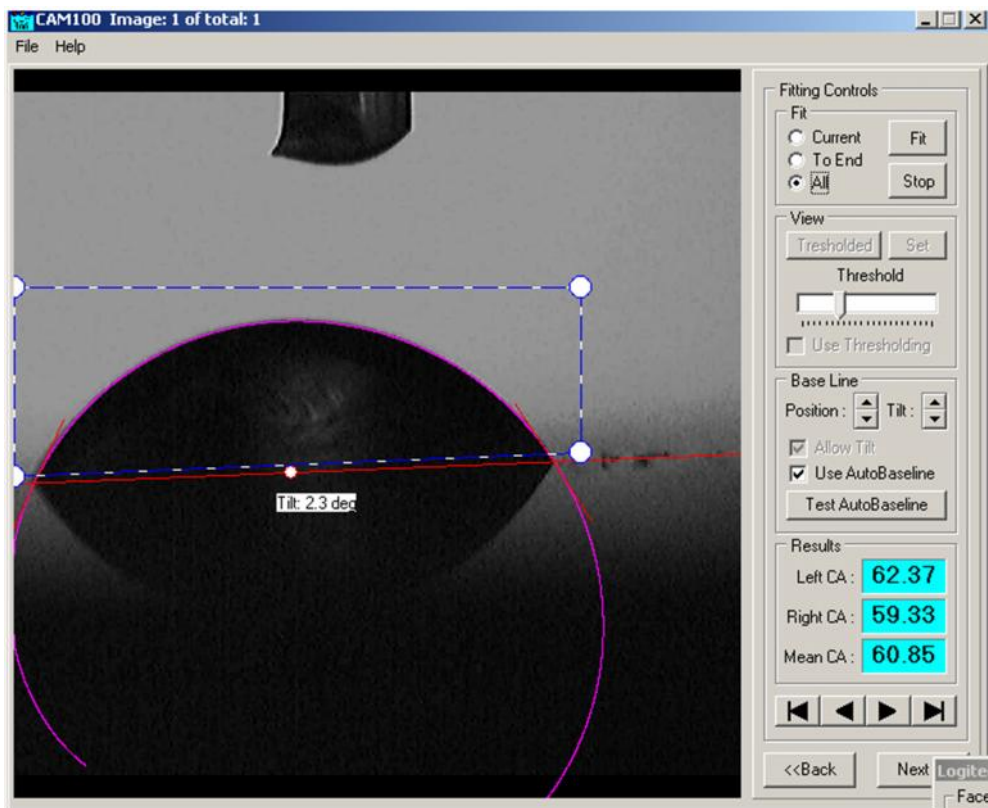


Figure 101 : Copper specimen polished ( 400 to 1500 )

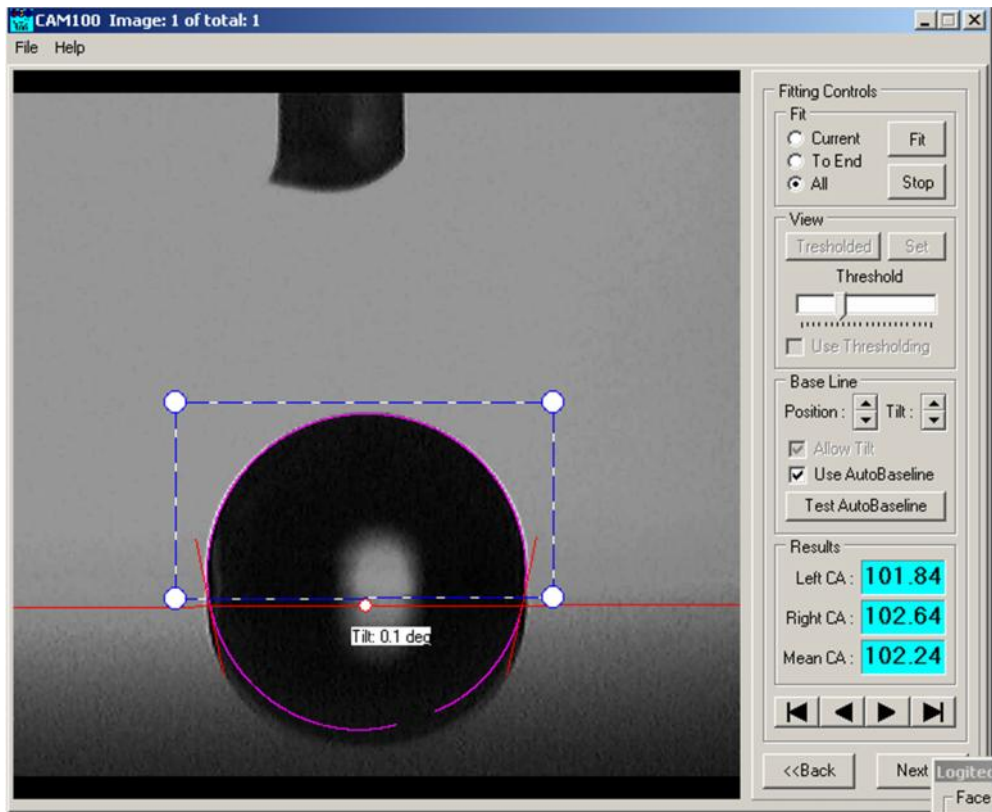


Figure 102 : Copper specimen with removed Super-hydrophobic coating

## 5.5 Atomic Force Microscopy

In order to evaluate the profile of the treated surface we tried to apply Atomic Force Microscopy. After the mounting and grinding (400 – 1500) process, the specimens were chemically modified in an ethanol solution of *n*-tetradecanoic acid 0.06M at room temperature for 10 days, in order to form a Super-hydrophobic film on the fresh copper surface, as we had described in Section 2. The new surface was observed with an Atomic Force Microscope. The AFM images of the specimens' surface morphology are shown in Figs. 103-104. It can be seen that the Cu surface becomes quite rough and develops “*mountain-like*” structure. The “*Mountain ridges*” with a middle height of 150 nm are homogeneously distributed over the whole sample surface. The **two-tier scale of microscopic** ( as we observe the “*flowerlike structure*” in the Stereo microscope and SEM images ), and **nanoscopic** ( as we see the AFM image) roughness is typical for the Lotus leaf, showing Super-hydrophobic properties, and it is undisputed that a topography like this one is advantageous for the superhydrophobic effect. We can also see a cross-section of the “*mountain-like*” structure in Fig.105.

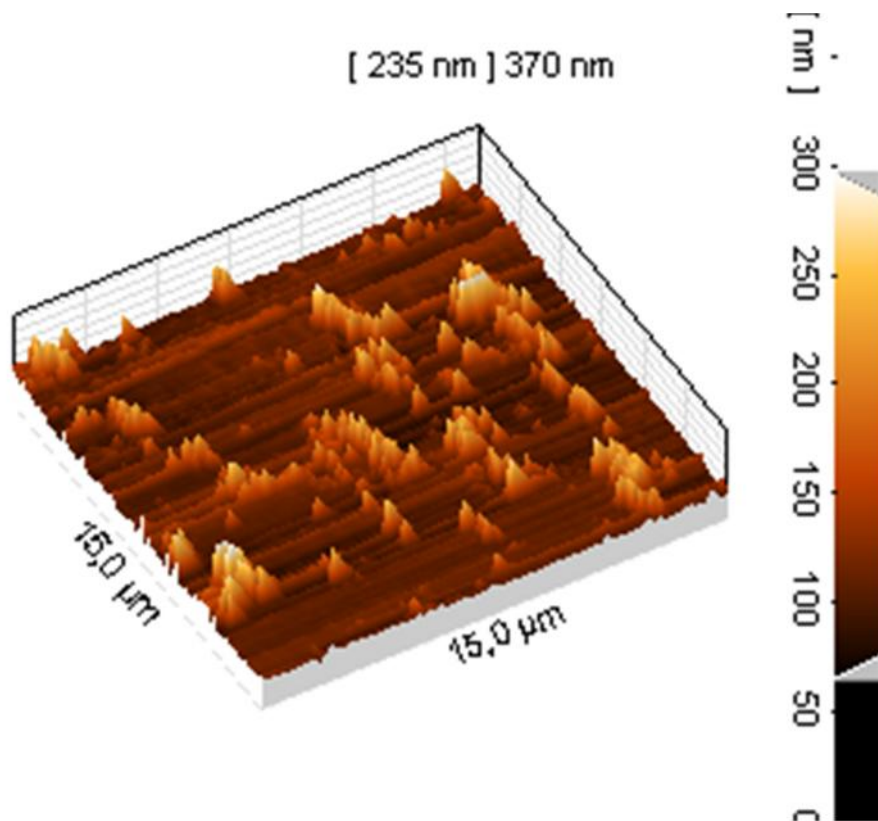


Figure 103 : A 3D image, of the “*mountain-like*” structure, of Super-hydrophobic film on the fresh copper surface

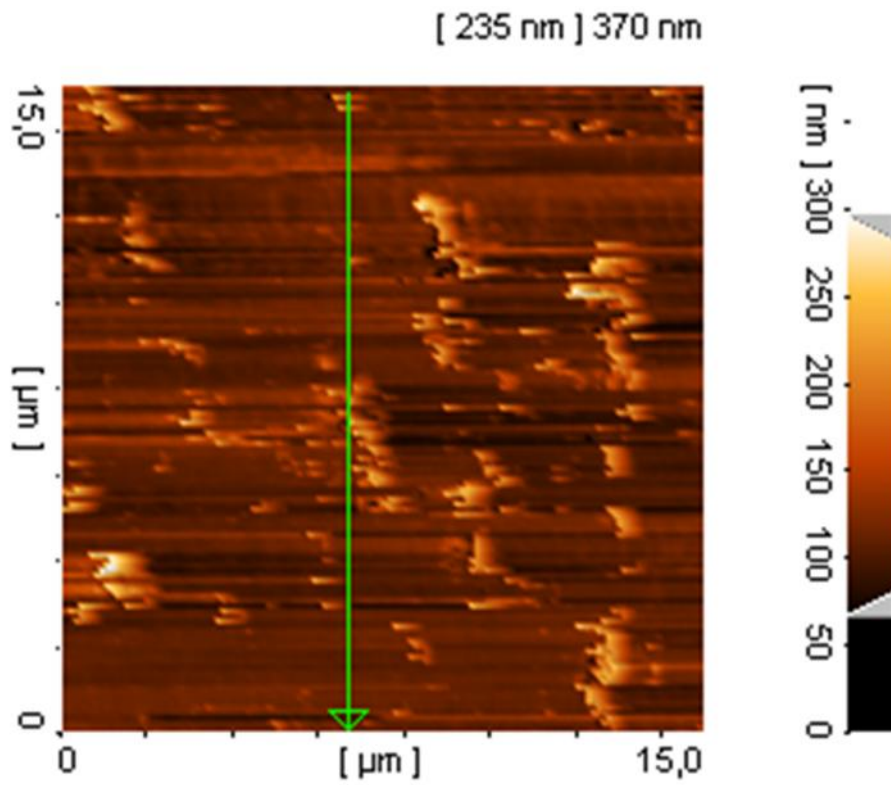


Figure 104 : A panoramic image of the “mountain-like”



Figure 105 : A cross-section of the Super-hydrophobic film on copper surface



## 5.6 Scanning Electron Microscopy

In order to observe the clean and the treated surface we employed Scanning Electron Microscopy. After the mounting and grinding (up to 1500 SiC) process, the specimens were chemically modified in an ethanol solution of *n*-tetradecanoic acid 0.06M at room temperature for 10 days, in order to form a Super-hydrophobic film on the fresh copper surface, as we had described in Section 2. The “*flowerlike structure*” of the surface were revealed in the SEM observations (Figs 106-108). We can also observe some mountain (red circles) and valley areas in Fig. 108. Combined with the results of the AFM images we can tell that the structure of the *n*-tetradecanoic layer is a hierarchical structure (micro roughness covered with nano roughness). That hierarchical structure was not only necessary to have high contact angle but also essential for the stability of the composite interface (water-solid and water- air).

Pure copper surface is presented in figs (110-112). We tried to obtain images also of the cross section of the treated surface. We tried to cut the treated specimens in very low speed using diamond cutter mini-tom. Images of the cross section of specimens are presented in images 113-114. It seems like the treatment is destroyed and is difficult to obtain a clear image of both substrate and treatment.

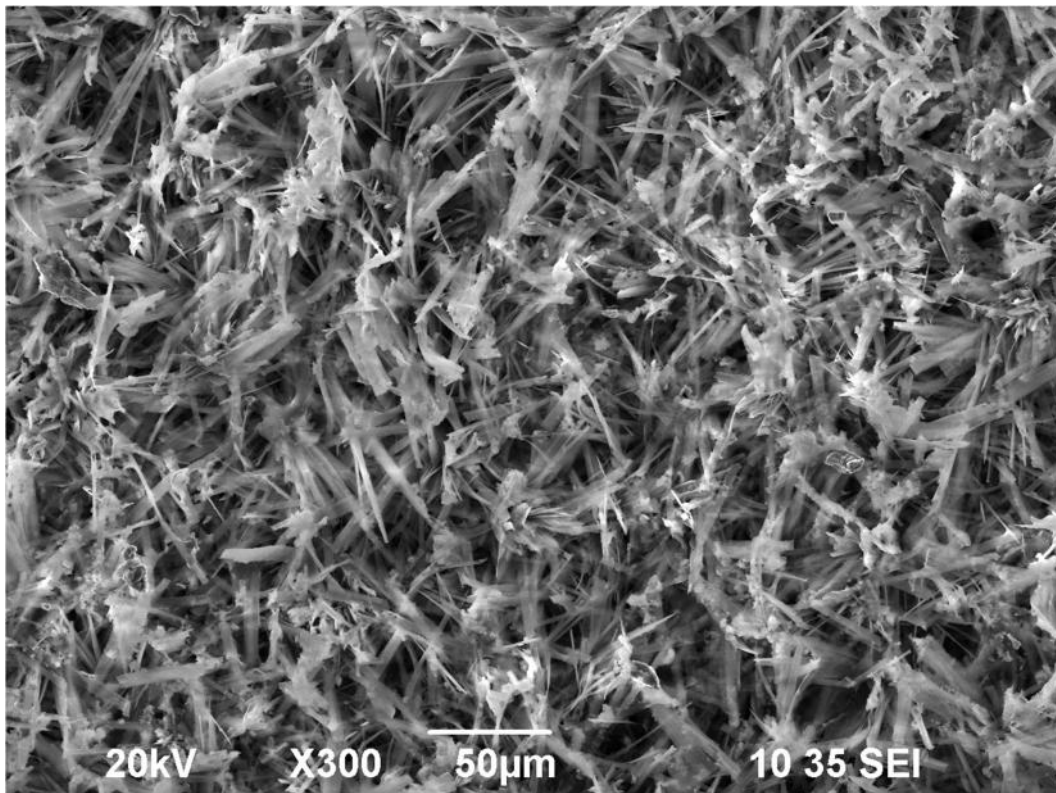


Figure 106 : Flowerlike structure on the chemically modified copper surface, SEM image x300

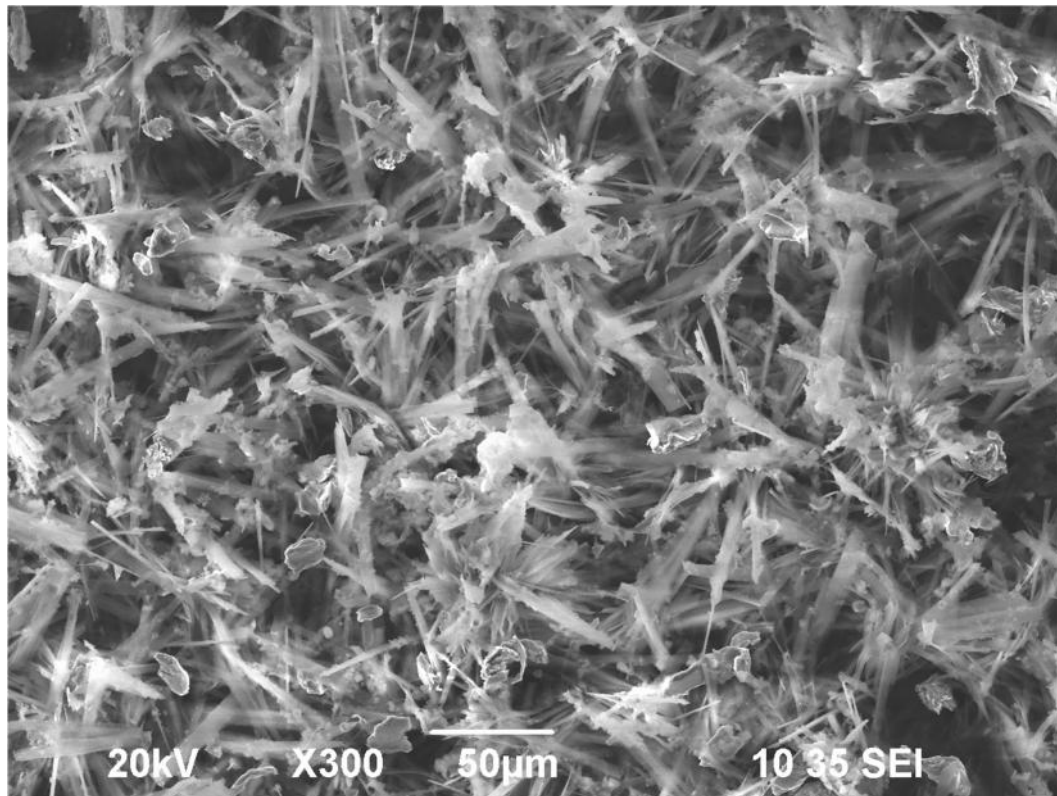


Figure 107 : Flowerlike structure on the chemically modified copper surface, SEM image x300

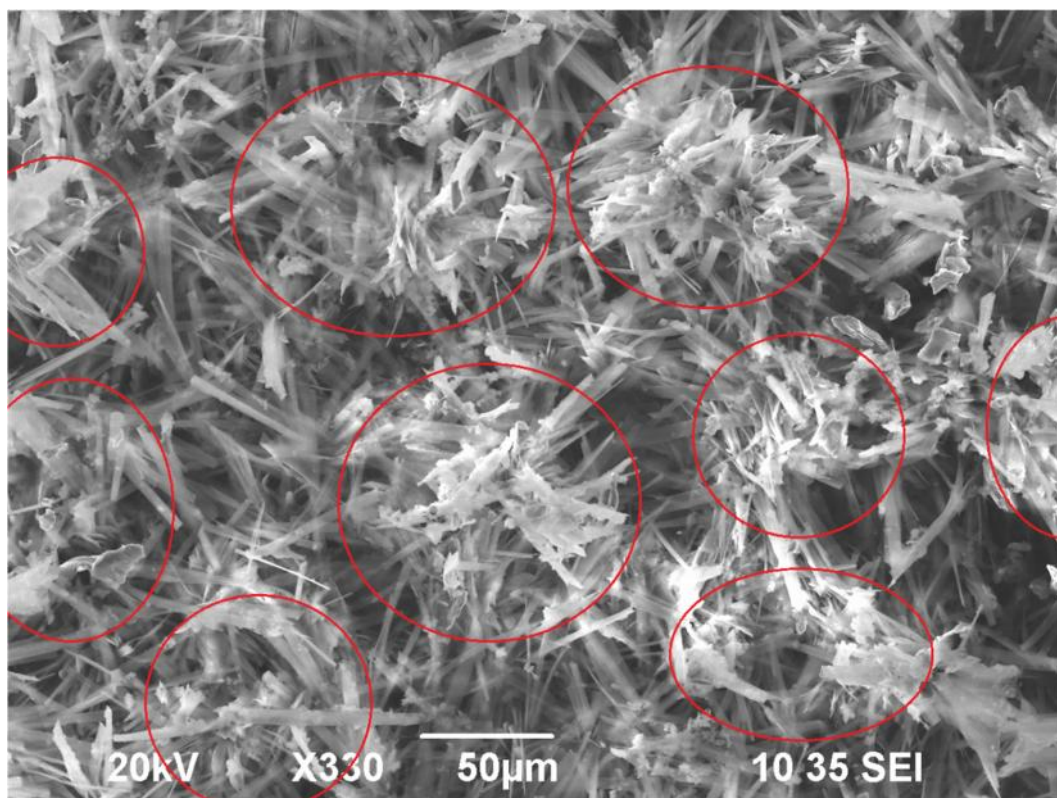


Figure 108 : Mountain and valley areas, SEM image x330

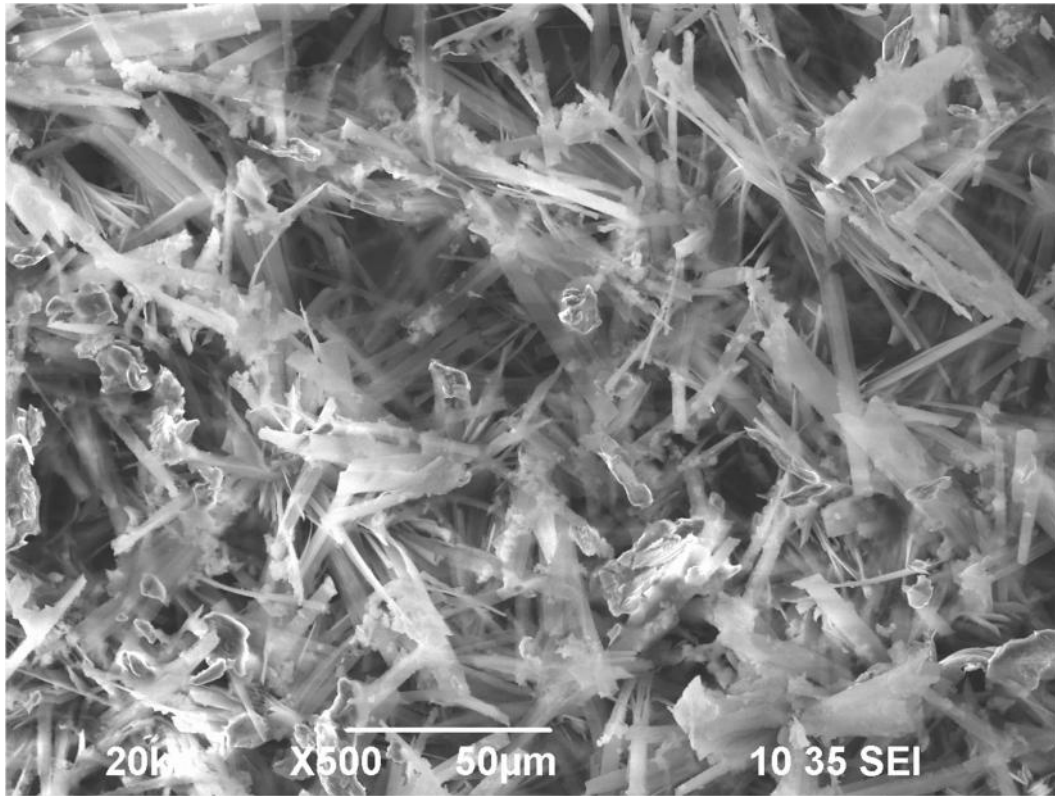


Figure 109 : : Flowerlike structure on the chemically modified copper surface, SEM image x500

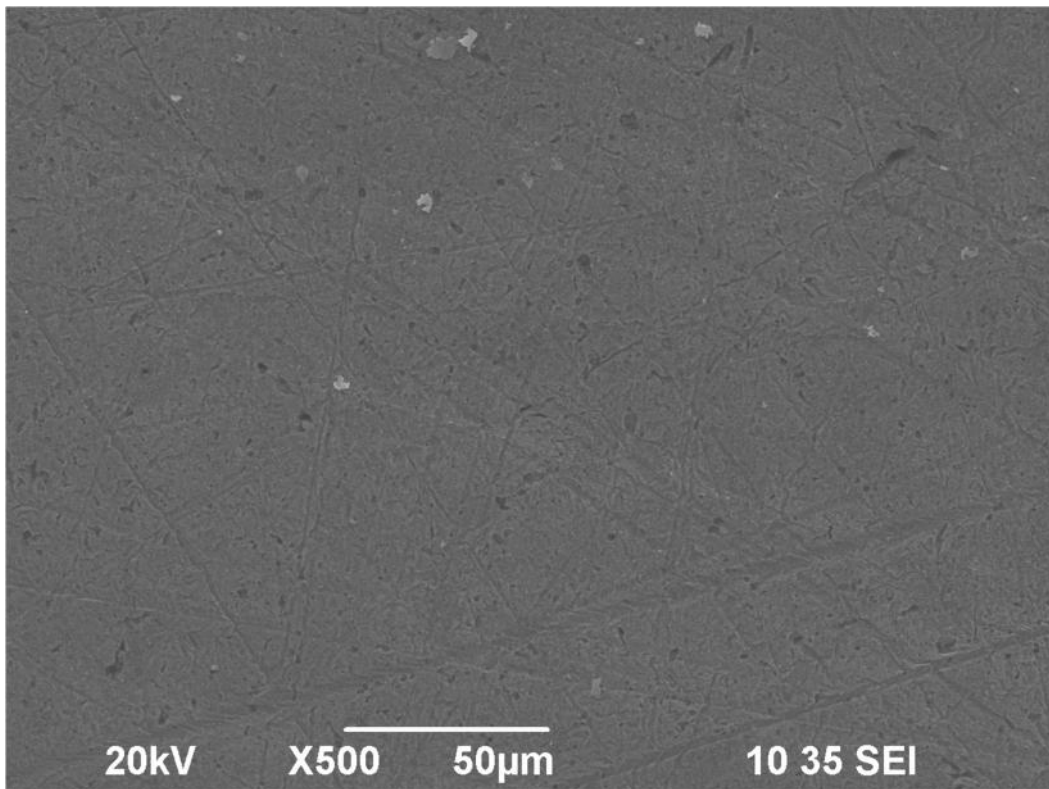


Figure 110 : Pure electrolytic tough pitch copper surface, SEM image x500

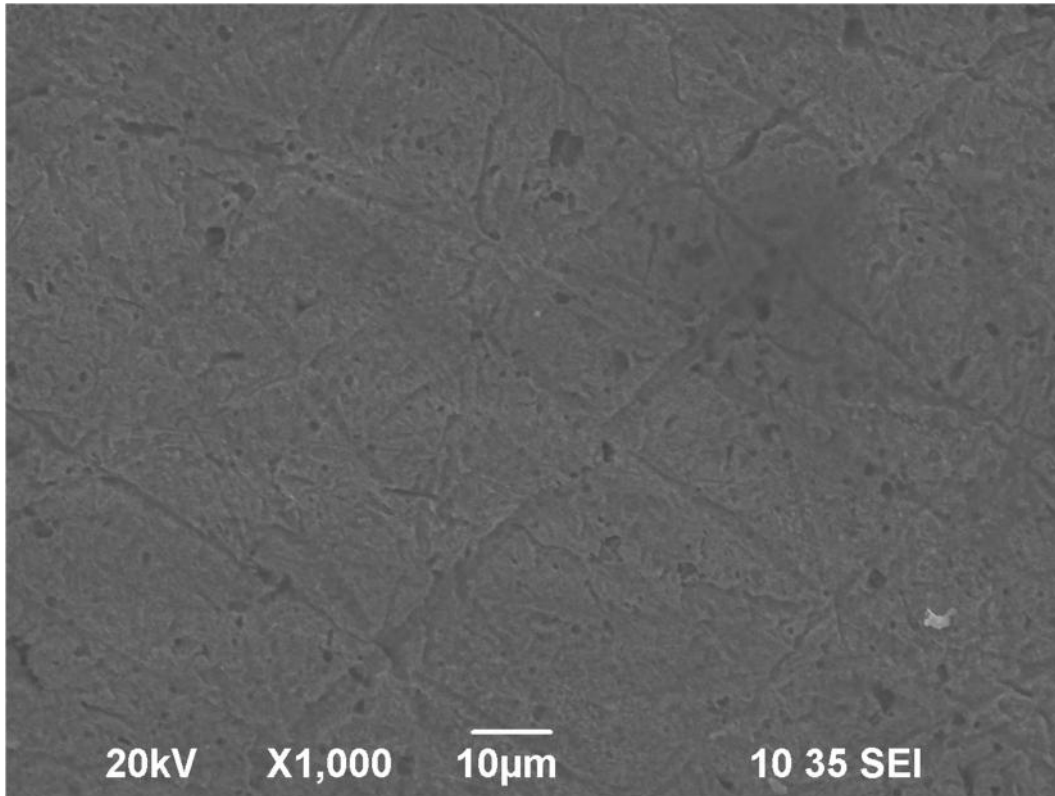


Figure 111 : Pure electrolytic tough pitch copper surface, SEM image x1000

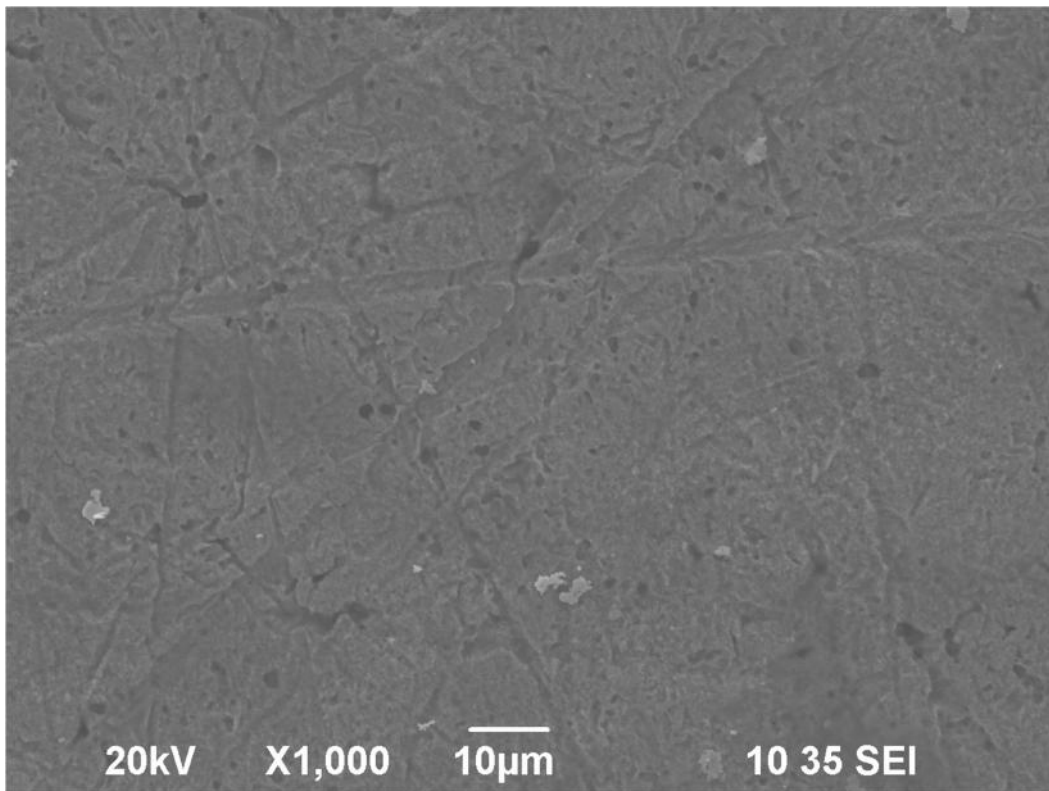


Figure 112 : Pure electrolytic tough pitch copper surface, SEM image x1000

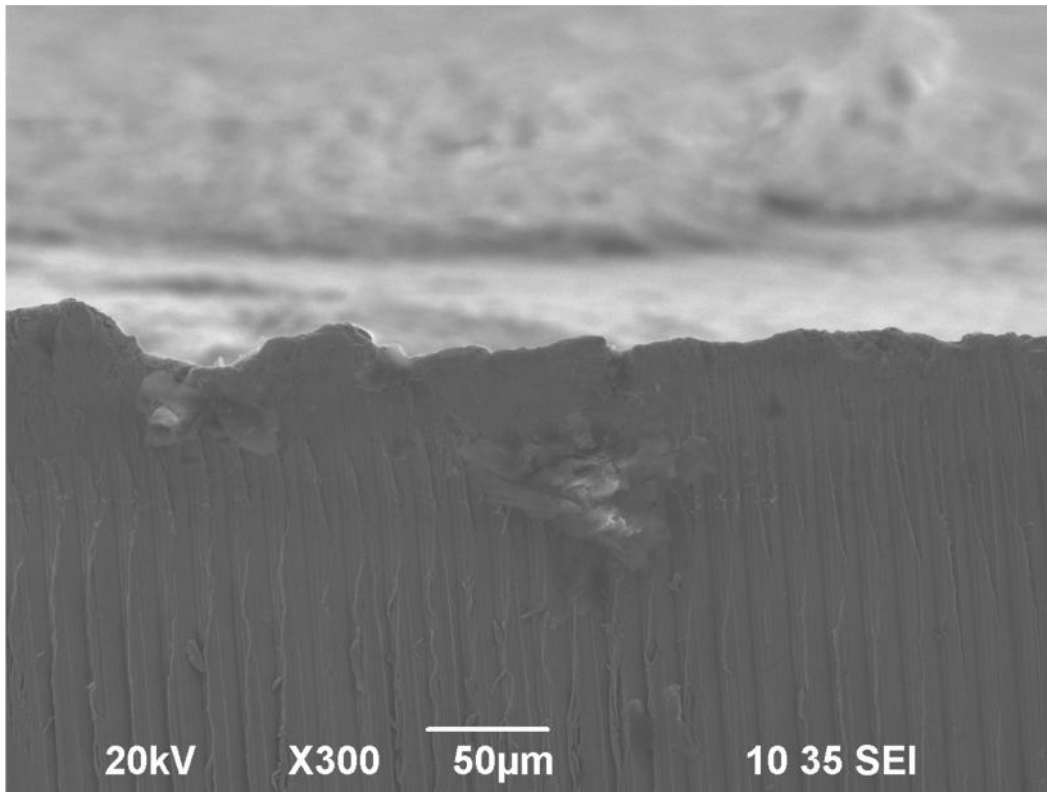


Figure 113 : Cross-section of a chemically modified specimen

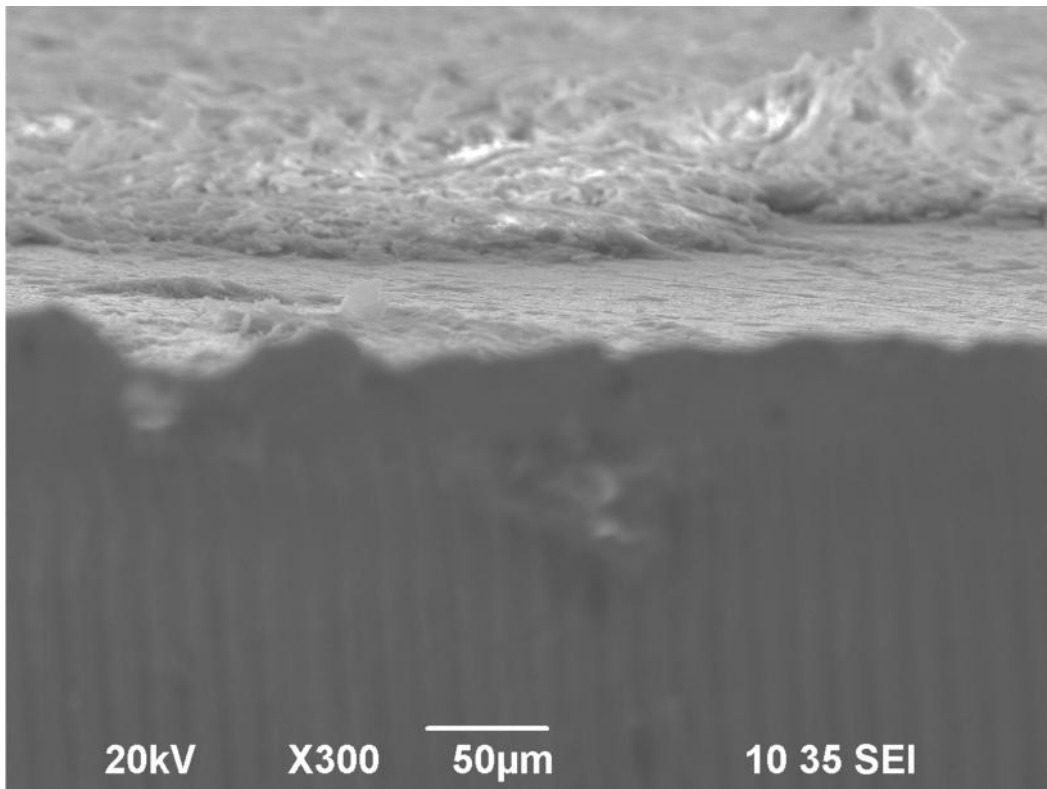


Figure 114 : Cross-section of a chemically modified specimen

## 5.7 Electrochemical Experiments

We conducted two sets of electrochemical measurements. One set with **Open Circuit** measurements, which were followed by **Potentiodynamic polarization** measurements. The open circuit measurements were applied mainly to obtain a stable potential for the Potentiodynamic Polarization measurements.

The working cell was a standard three-electrode cell having a Pt net as a counter electrode and Saturated Calomel Electrode (SCE) as reference electrode. Working solutions prepared at room temperature were 3.5% NaCl (0.6M, pH~6-7). We studied two different types of specimens:

- the **pure electrolytic tough pitch copper** substrates and
- the chemically modified substrates with the **Super-hydrophobic film**.

For the first substrate category the results of electrochemical measurements were taken after the mounting and grinding (up to 1500 SiC) process. For the second substrate category the specimens mounted, grinded (up to 1500 SiC), and immersed in an ethanol solution of *n*-tetradecanoic acid 0.06M at room temperature for 10 days.

### 5.7.1 Open Circuit Experiments

In the **Open Circuit** set we run eight (8) experiments, each had 40000 sec duration. The Average Potential calculated after the first 10000 seconds, for better stabilization of potential. The measurements of the experiments are presented in Table 11. The average potential of treated surface is -0.2578 V, while for the clean, untreated copper surface the mean value comes up to -0.2482 V (excluding the value of experiment C -0.1011V). The open circuit value for copper -0.2482 V, is in accordance to the literature ~240mV, and the results do not prove any important difference for the thermodynamics susceptibility to corrosion. The curves for open circuit experiments are presented in Figs 116-125.

Trying to explain the phenomenon that takes place when the clean copper specimen is immersed into the NaCl 3.5% solution we can observe the following. When the copper specimen is immersed in the NaCl solution  $\text{Cu}_2\text{Cl}$  is formed, strongly adhered to the surface. The reaction :



According to the literature the standard potential for reaction (1) is  $E_0=0.520\text{V}$ , vs NHE, thus the free energy  $\Delta G$ , for reaction (1) can be calculated from Faraday law:

$$\Delta G_1 = -n_1 * F * E_1^0 = -(1) * 96500 * 0.520 = -50180 \text{ J/mol}$$

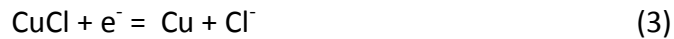
For the reaction :



The  $K_{sp}$  value for the reaction (2) is equal to :

$$\Delta G_2^0 = -R \cdot T \cdot \ln(K_{sp}) = -8.314 \cdot 298 \cdot \ln(1.72 \times 10^{-7}) = 38590 \text{ J/mol}$$

From the reactions (1) and (2), we have reaction (3):



The reaction (3) is the total reaction that takes place in the system and for this we want to calculate the potential  $E$ , thus :

$$\Delta G_3^0 = \Delta G_1^0 + \Delta G_2^0 = -11590 \text{ J/mol}$$

$$\Delta G_3^0 = -n_3 \cdot F \cdot E_3^0 \Rightarrow E_3^0 = -\Delta G_3^0 / n_3 \cdot F \Rightarrow \underline{E_3^0 = -0.120 \text{ V vs NHE}}$$

The above value for the potential  $E_3^0$  is versus to Hydrogen Electrode, and for the Saturated Calomel Electrode, we use:

$$E_3^0 = -0.120 \text{ V} - 0.244 \text{ V} \Rightarrow \underline{E_3^0 = -0.364 \text{ V vs SCE}}$$

Moreover, the above value of  $E_3^0$ , refers to standard conditions, thus for activity of  $(\text{Cl}^-) = 1$ . From the Nernst equation we can calculate the value of  $E_3$  for the laboratory conditions 3.5% NaCl, 0.6M :

$$E_3 = E_3^0 + \frac{RT}{nF} \ln\left(\frac{[\text{CuCl}]}{[\text{Cl}^-] \cdot [\text{Cu}]}\right) \quad (4)$$

$$E_3 = E_3^0 + \frac{RT}{nF} \ln\left(\frac{1}{[\text{Cl}^-]}\right) \quad (5)$$

$$E_3 = -0.363 \text{ V vs SCE} \quad (6)$$

Thus the calculated is  $E_3 = -0.363 \text{ V vs SCE}$ , while the experimental value is  $E_3 = -0,2578 \text{ V vs SCE}$ . This small difference can be attributed in several parameters, the most important of them is the solubility of oxygen into the solution. The potential of oxygen reaction drags the potential into more positive values.

Table 11 : Open circuit measurements

<b>Open Circuit Experiments</b>			
<b>Name of Experiment</b>	<b>Type of Specimens</b>	<b>Average Potential (V)</b>	<b>Average Potential per Type of Specimen (V)</b>
Peirama_A	Chemically modified P.E.T.Copper	-0,2485	-0,2115
Peirama_B	Chemically modified P.E.T.Copper	-0,2368	
Peirama_C	Chemically modified P.E.T.Copper	-0,1011	
Peirama_D	Chemically modified P.E.T.Copper	-0,2594	
Peirama_E	Pure Electrolytic Tough Pitch Copper	-0,2694	-0,2578
Peirama_F	Pure Electrolytic Tough Pitch Copper	-0,2577	
Peirama_G	Pure Electrolytic Tough Pitch Copper	-0,2591	
Peirama_H	Pure Electrolytic Tough Pitch Copper	-0,2449	

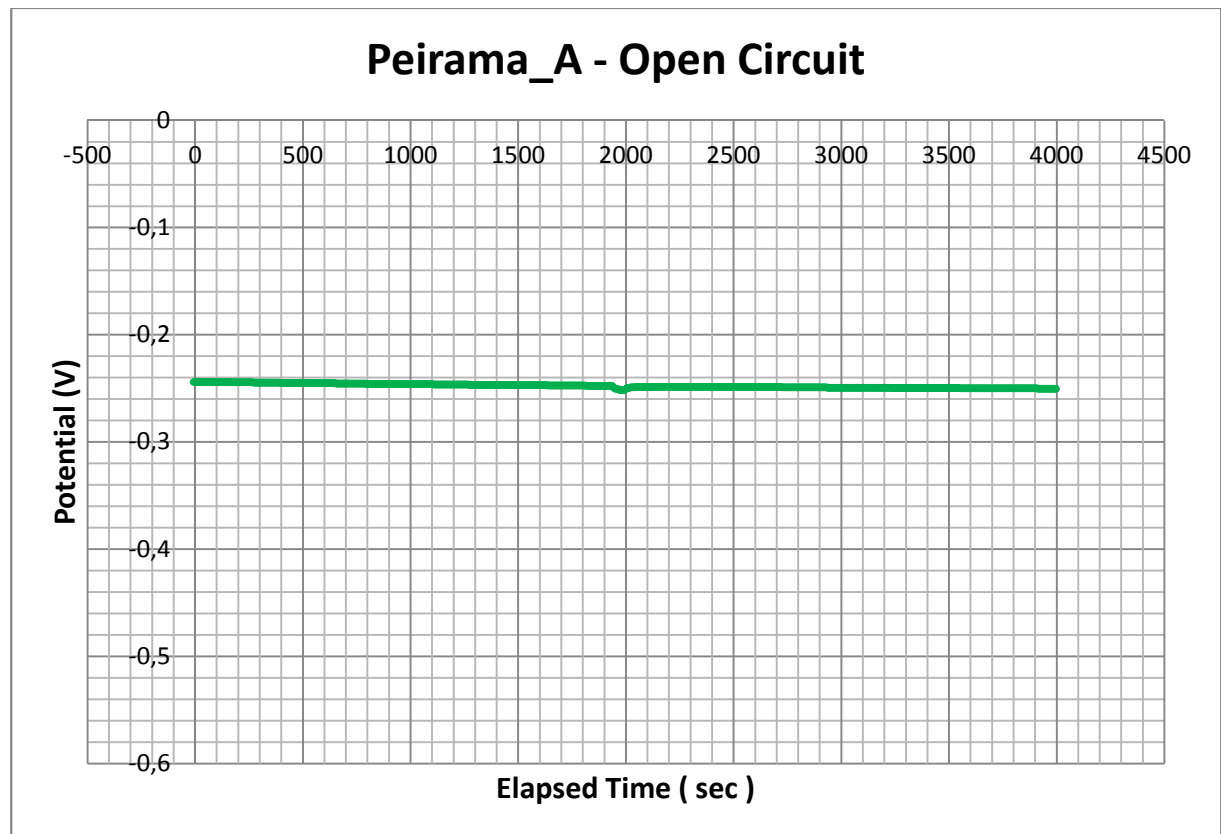


Figure 115 : Peirama\_A – Treated surface- Open Circuit Curve



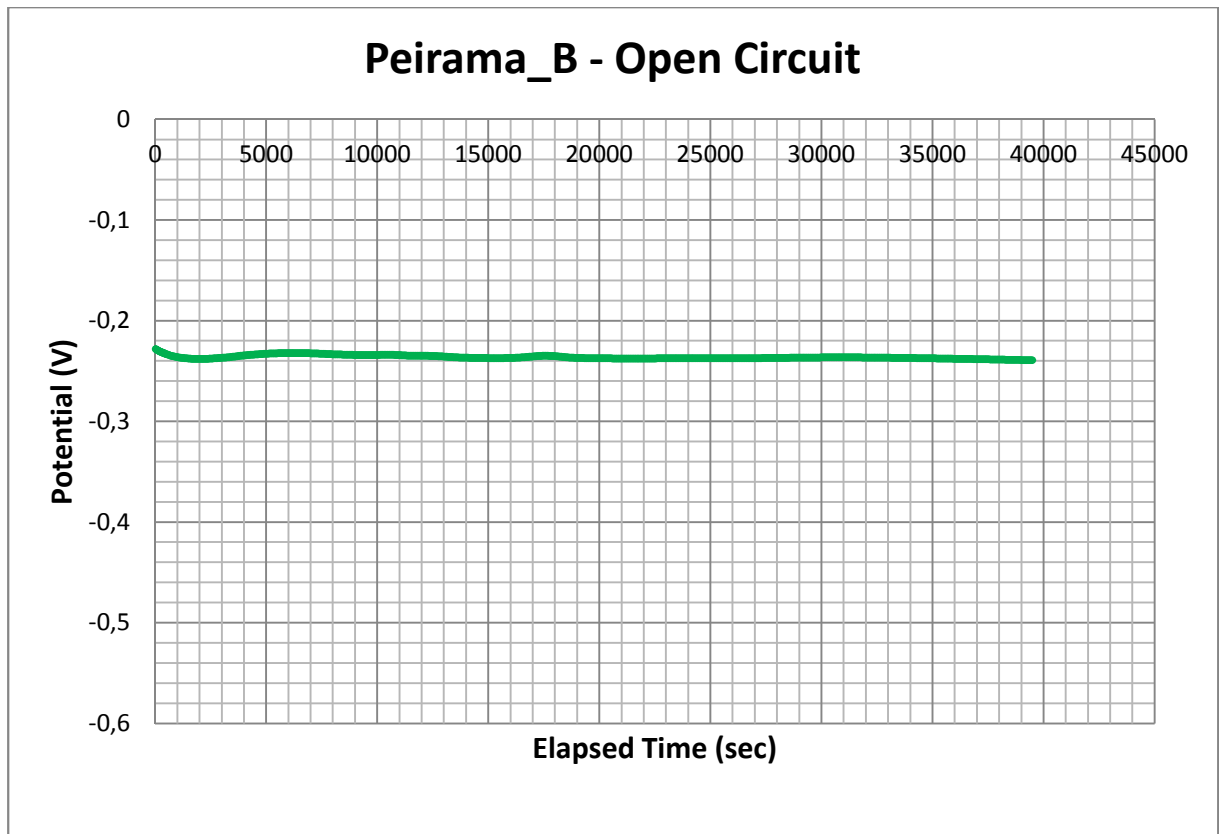


Figure 116 : Peirama\_B- Treated surface - Open Circuit Curve

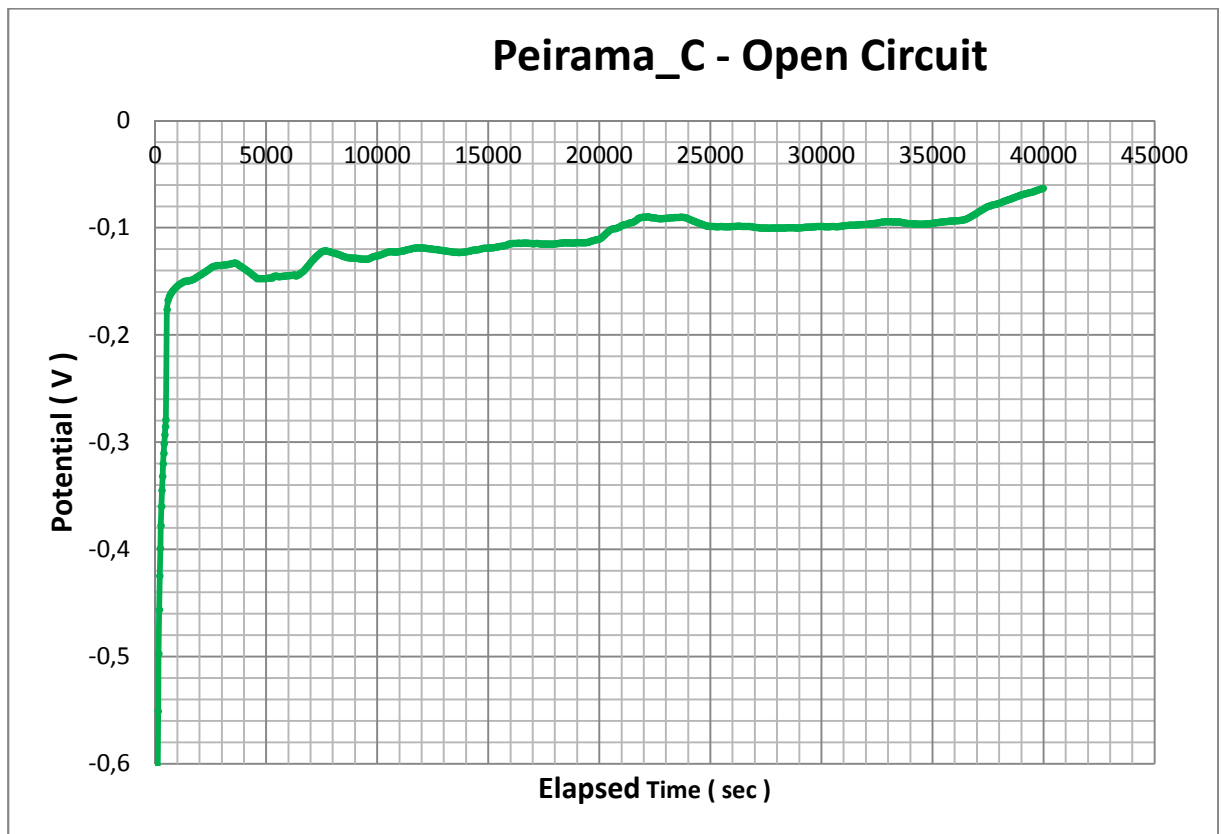


Figure 117 : Peirama\_C - Treated surface - Open Circuit Curve

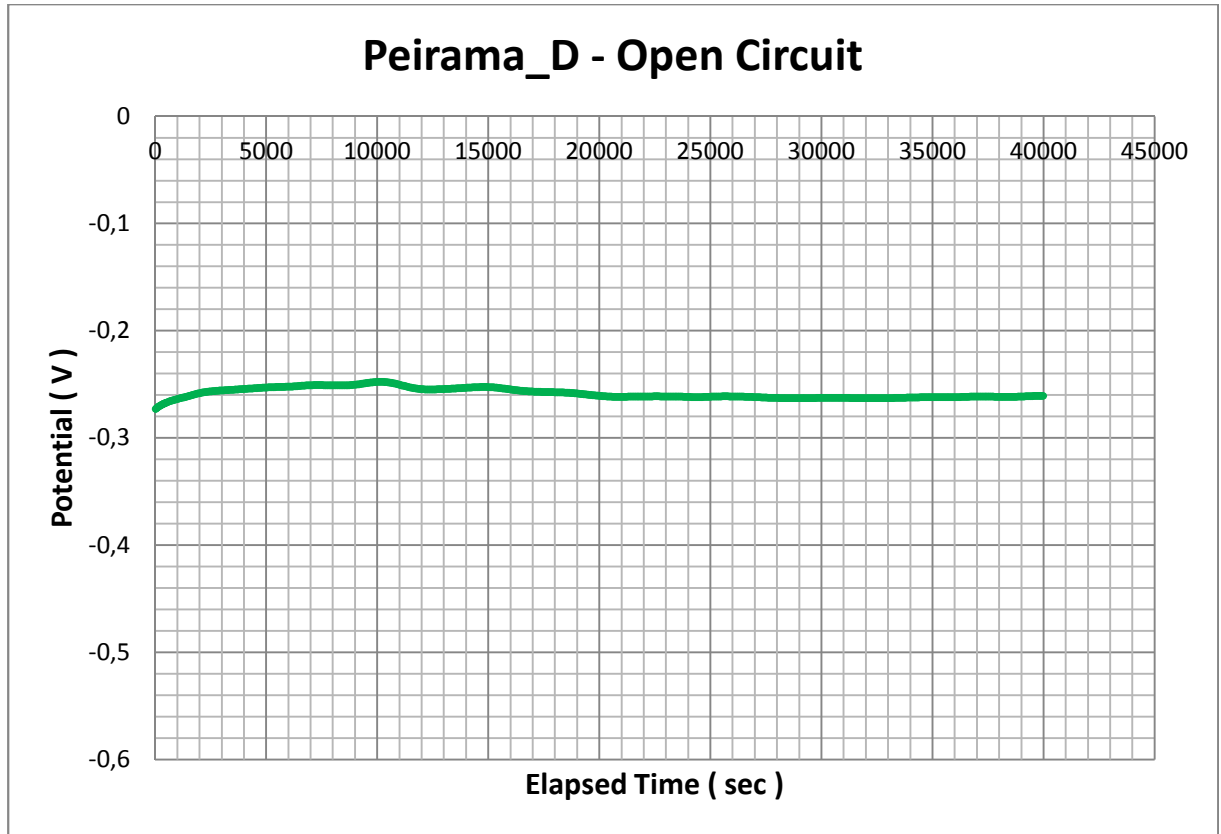


Figure 118 : Peirama\_D- Treated surface - Open Circuit Curve

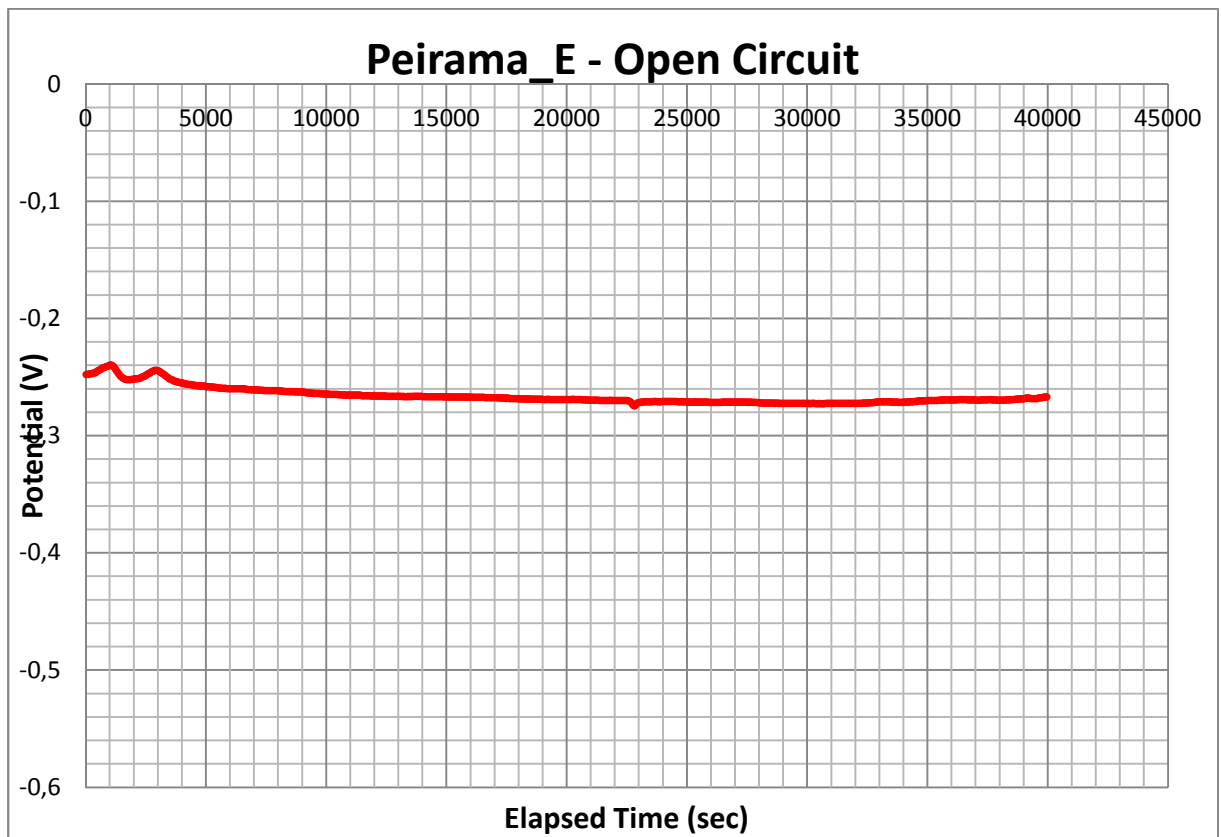


Figure 119 : Peirama\_E –Bare copper surface- Open Circuit Curve

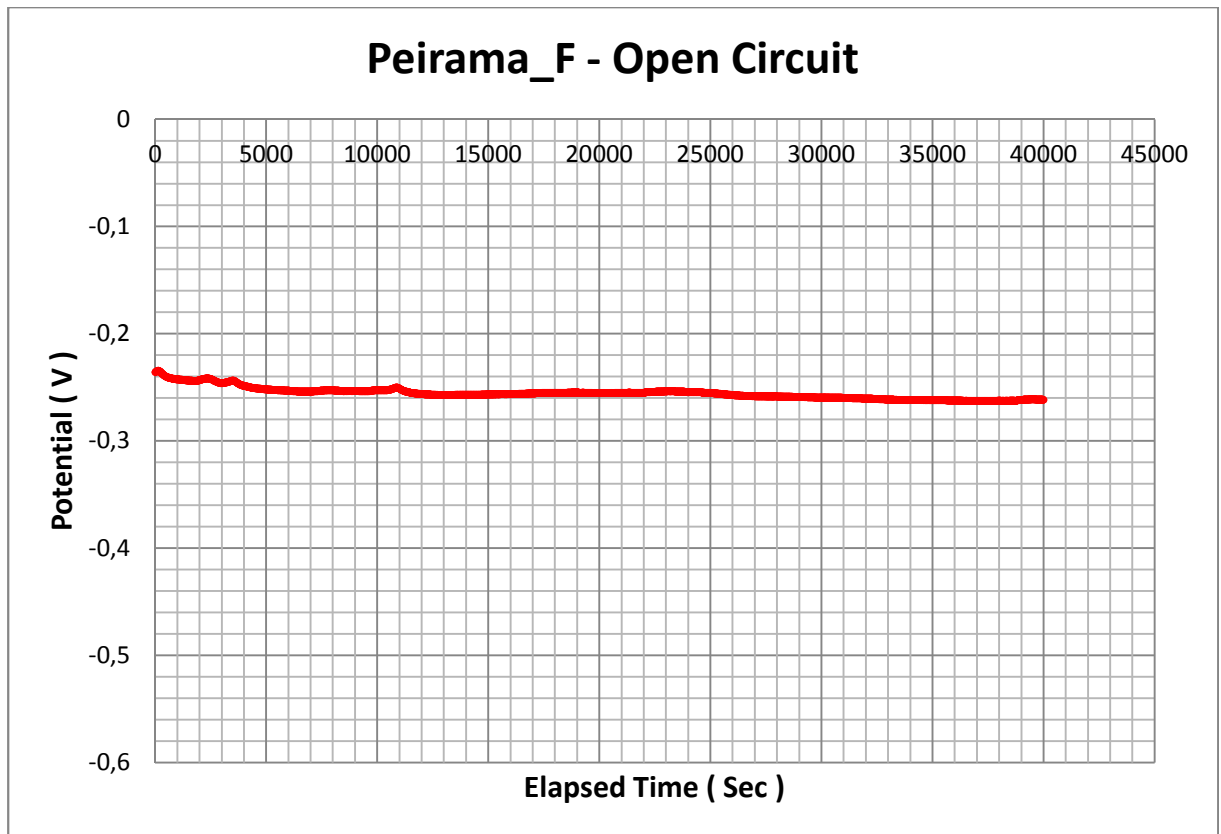


Figure 120 : Peirama\_F - Bare copper surface- Open Circuit Curve

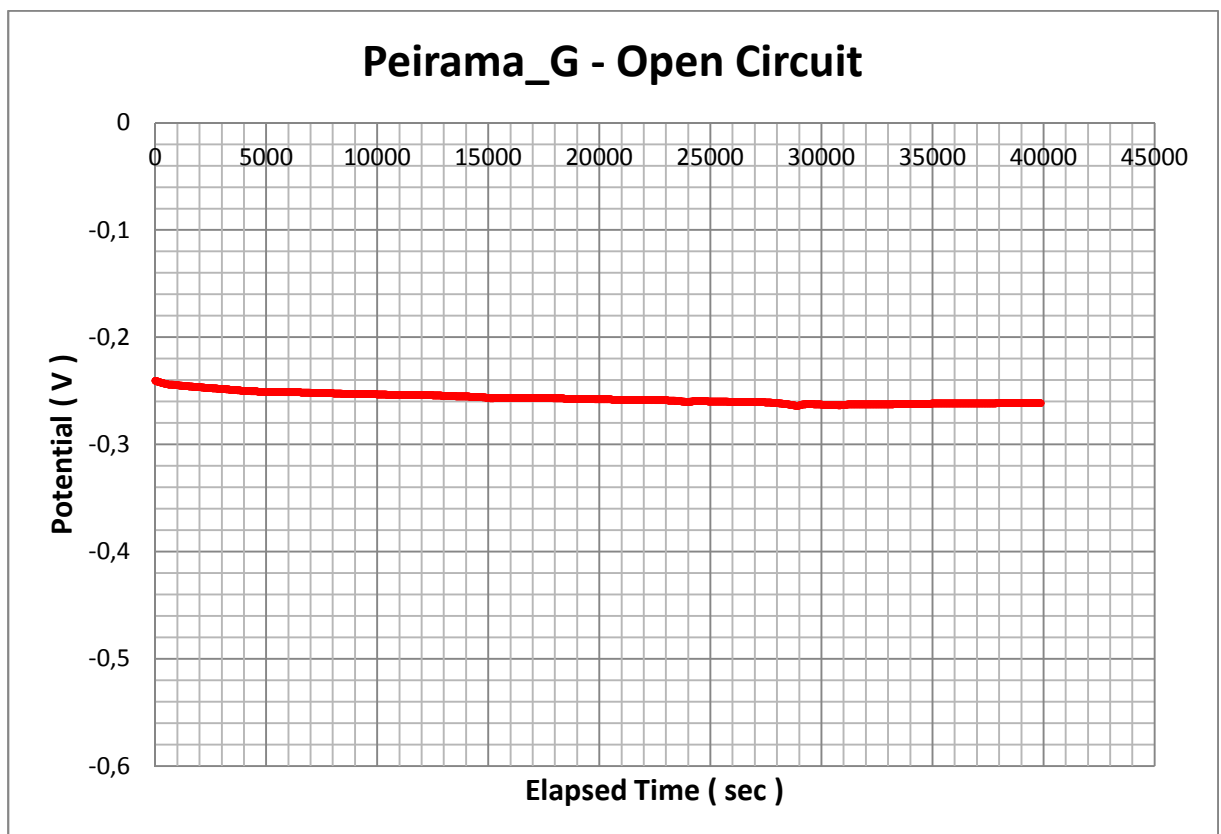


Figure 121 : Peirama\_G - Bare copper surface- Open Circuit Curve

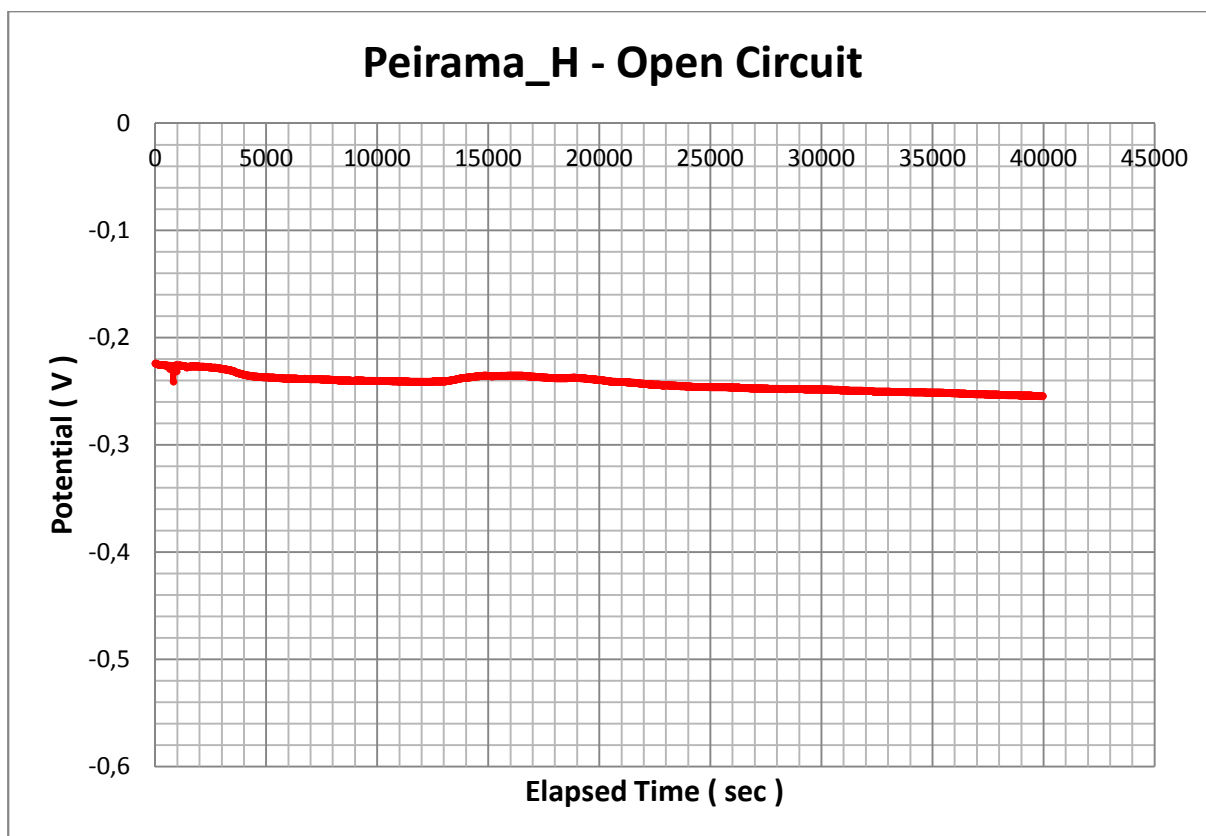


Figure 122 : Peirama\_H - Bare copper surface- Open Circuit Curve

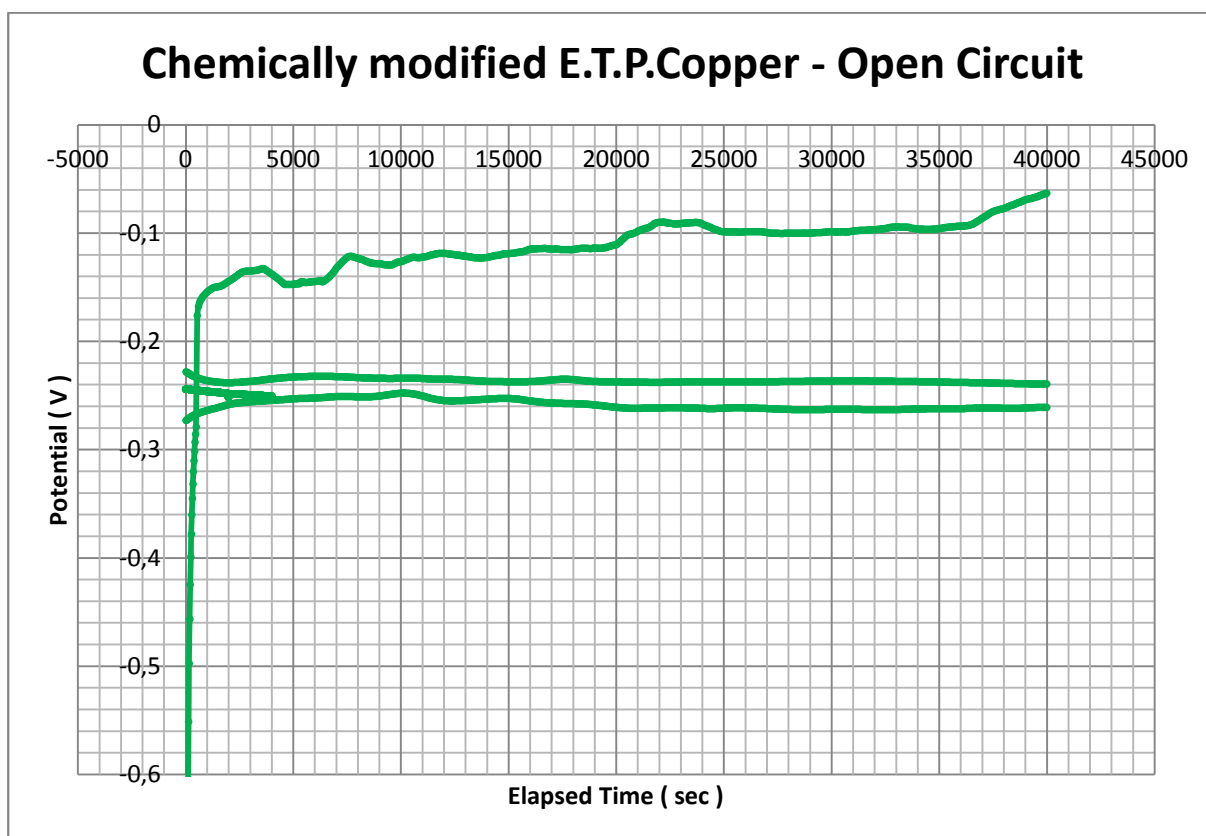


Figure 123 : Chemically modified E.T.P.Copper - Open Circuit Curves

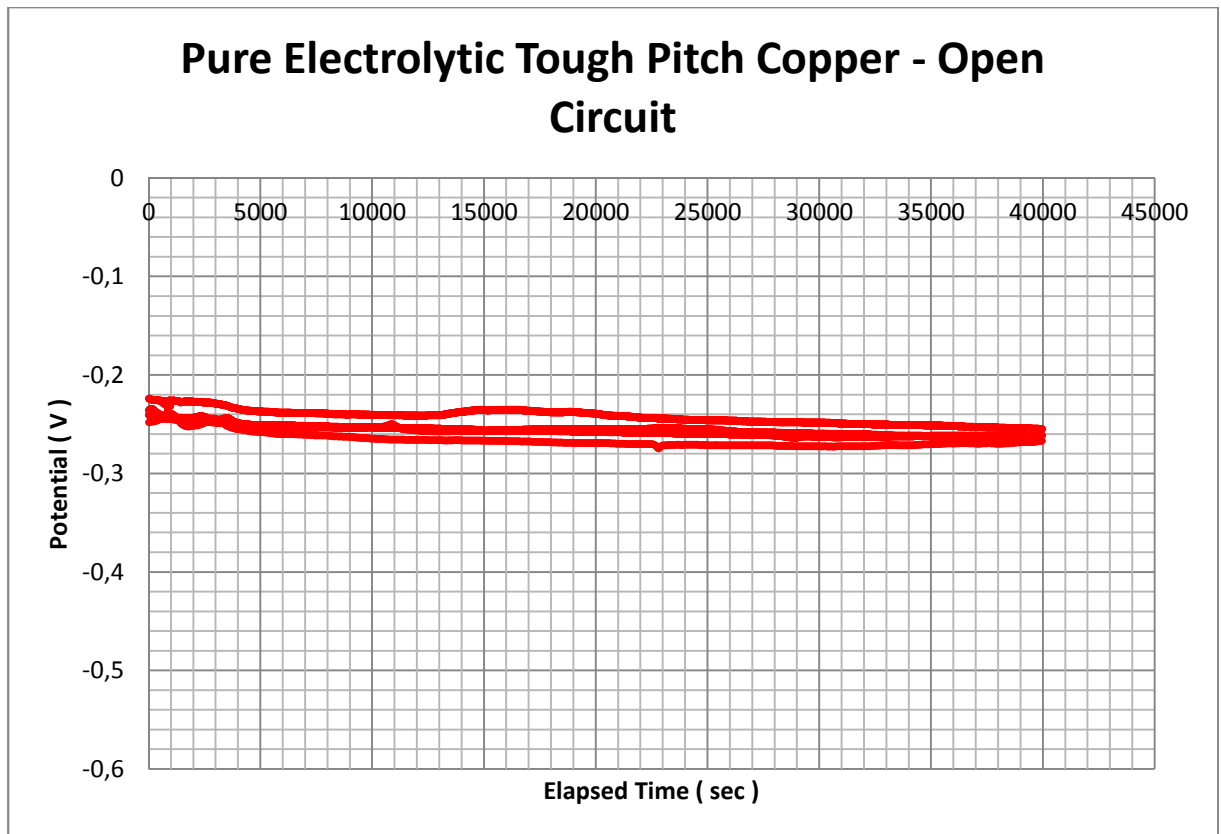


Figure 124 : Pure Electrolytic Tough Pitch Copper - Open Circuit Curves

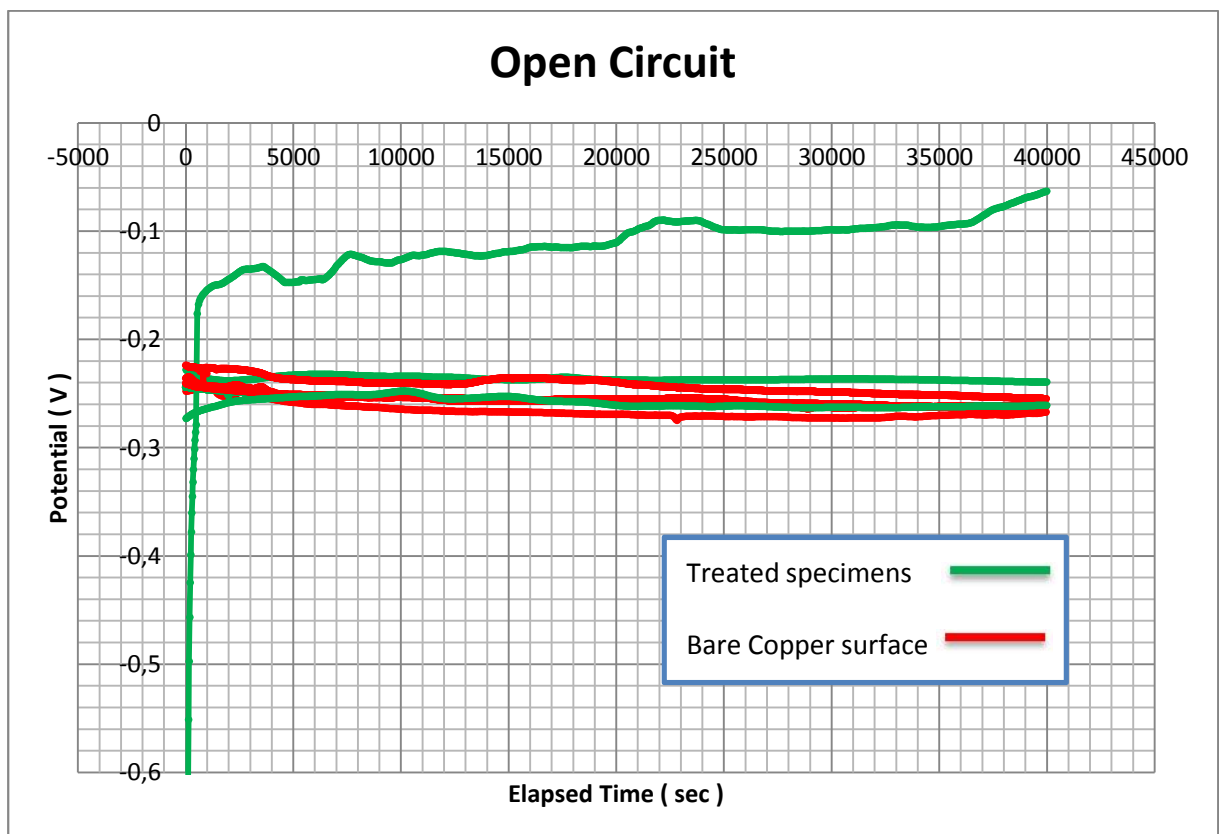


Figure 125 : Open Circuit Curves for Treated and Bare Copper Surface

### 5.7.2. Potentiodynamic Experiments

In the Potentiodynamic polarization set of experiments, six (6) electrochemical experiments were conducted: three for pure copper surface and three for treated copper surfaces. A range of potential from -0,8Volts to +0,6 Volts, was applied, with scan ratio of 2 mV/sec. The curves obtained are presented in the following Figures 128-136. The potentiodynamic experiments preceded the open circuit experiments.

According to the literature, after the open circuit experiment, when cathodic current is applied the previously formed  $\text{Cu}_2\text{Cl}$ , is destroyed, by the  $\text{Cl}^-$  ions of the NaCl solution (chemical reaction).



In aerated  $\text{Cl}^-$  solution the cathodic reaction is either water and/or the oxygen reduction according to:



Moreover, according to the Emf series, for solutions of  $\text{pH} \sim 7$ , the value of  $E^\circ$  for the above reaction is  $E^\circ = +0.82\text{V}$  vs NHE, thus this reaction is present in the voltage range of our experiments.

Oxygen reduction is the main cathodic reaction in aerated solution, which is responsible for the high cathodic, corrosion and anodic currents.

The anodic dissolution of copper can be represented in all solutions as follows:



Anodic currents in 3% NaCl alone display three distinct regions: a Tafel region at lower over-potentials extending to the peak current density  $i_{\text{peak}}$ , a region of decreasing currents until a minimum  $i_{\text{min}}$  is reached, and a region of sudden increase in current density leading to a limiting value  $i_{\text{lim}}$ . The anodic curves start with the dissolution of copper to form the cuprous ion equation (3) leading to an increase in

the current to the maximum values  $i_{peak}$ . Then CuCl is formed on the copper surface equation (4), resulting in a decrease in the current to  $i_{min}$ , which then goes into the solution due to the formation of  $CuCl_2^-$  equation (5), upon further potential increase, causing the current to increase again to  $i_{lim}$ . Copper is probably further oxidized to Cu(II) at higher potentials. The values for  $i_{peak}$ ,  $i_{min}$  and  $i_{lim}$  are presented in the Table 12 and in Figure 130.

Table 12 : Parameters obtained from potentiodynamic curves

Experiment	$i_{peak}$ ( $\mu A/cm^2$ )	$i_{min}$ ( $\mu A/cm^2$ )	$i_{lim}$ ( $\mu A/cm^2$ )
Peirama_A	25107	1888	5819
Peirama_B	7468	1607	3094
Peirama_D	17813	1631	2879
Peirama_F	7420	563	8604
Peirama_G	122435	54545	223650
Peirama_H	14869	1669	6912

From the Potentiodynamic curves the following results (Table 13) were obtained, after applying Tafel fit for region of +250mV vs  $E_{corr}$  :

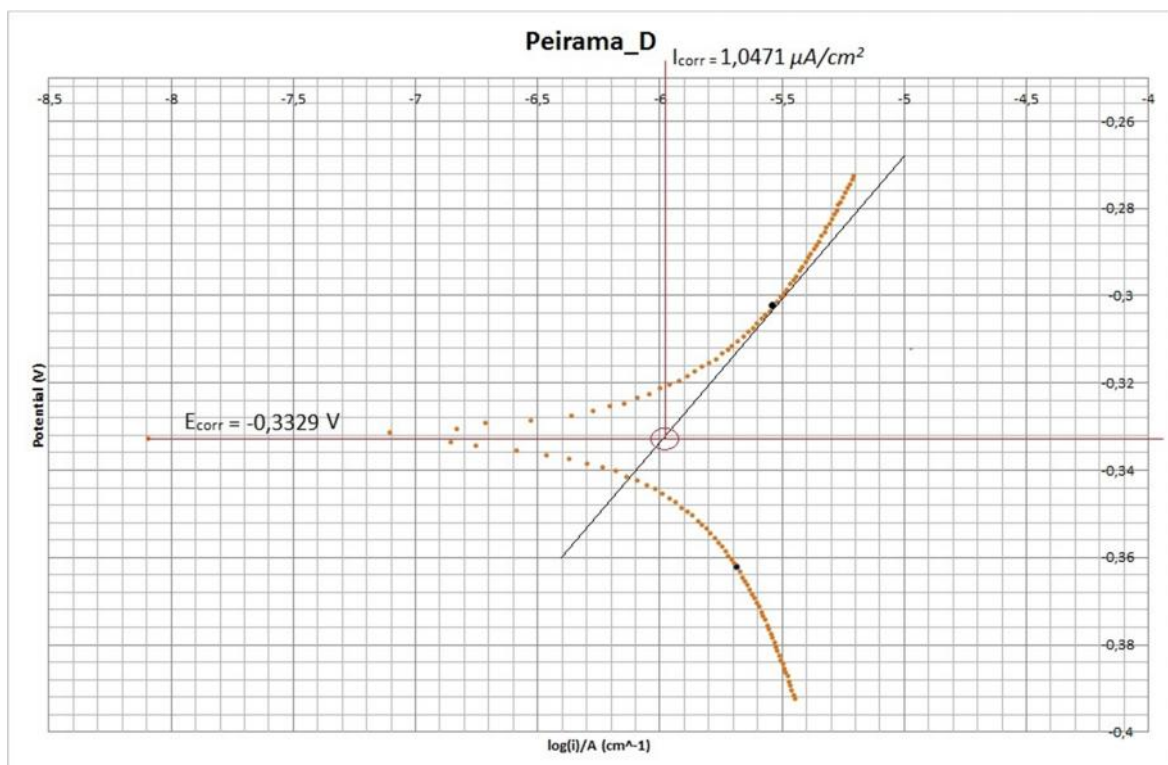


Figure 126 : Tafel fit for the anodic part of the potentiodynamic curves

Table 13 : Values for  $I_{corr}$  and Corrosion Rate for Tafel fit of Potentiodynamic curves

Experiment	$I_{corr}$ ( $\mu A/cm^2$ )	Corrosion rate (mpy)
Peirama_A	1,5488	0,7172
Peirama_B	1,8624	0,8625
Peirama_D	1,0471	0,4849
Peirama_F	3,9811	1,8436
Peirama_G	4,3652	2,0215
Peirama_H	7,9983	3,7039

For the Tafel fit, it must be noted that only the anodic part of the curves was elaborated. The Corrosion Rate values were calculated from the following equation:

$$Corrosion\ Rate = \frac{0,13 * (EW) * I_{corr}}{d}$$

Where Corrosion Rate in mpy, EW accounts for equivalent weight (g),  $I_{corr}$  in  $\mu A/cm^2$  and d is for density ( $gr/cm^3$ ).

From the above values we can safely conclude that the treated specimens (A,B and D) present superior behavior against corrosion, comparing to the bare surface of the copper.

In order to compare the corrosion behavior of treated and bare copper surface, we calculated the Polarization Resistance  $R_p$  values, from the elaboration of potentiodynamic experimental curves. The  $R_p$  values were calculated from the linear anodic and cathodic parts of the curves (approximately  $\pm 25mV$  vs  $E_{corr}$ ), considering Tafel behavior for these regions (Fig127). The  $R_p$  accounts for the slope of the linear anodic and cathodic part of the potentiodynamic curve,  $\pm 25mV$  vs  $E_{corr}$ .

Table 14 : Polarization Resistance ( $R_p$ ) values

Experiment	$R_p$ ( $\Omega$ )
Peirama_A	6607,8000
Peirama_B	6105,5000
Peirama_D	11796,0000
Peirama_F	2857,5000
Peirama_G	218,0200
Peirama_H	1233,3000



The values for  $R_p$  are calculated from the equation:

$$I_{corr} = \frac{\beta_a \beta_c}{2.3R_p(\beta_a + \beta_c)}$$

Where,  $\beta_a$  and  $\beta_c$  are the beta anodic and beta cathodic. From the above equation it can be easily derived that  $I_{corr}$  and  $R_p$  are inversely proportional. Thus, the results in Table 14 in accordance with the results of Table 13.

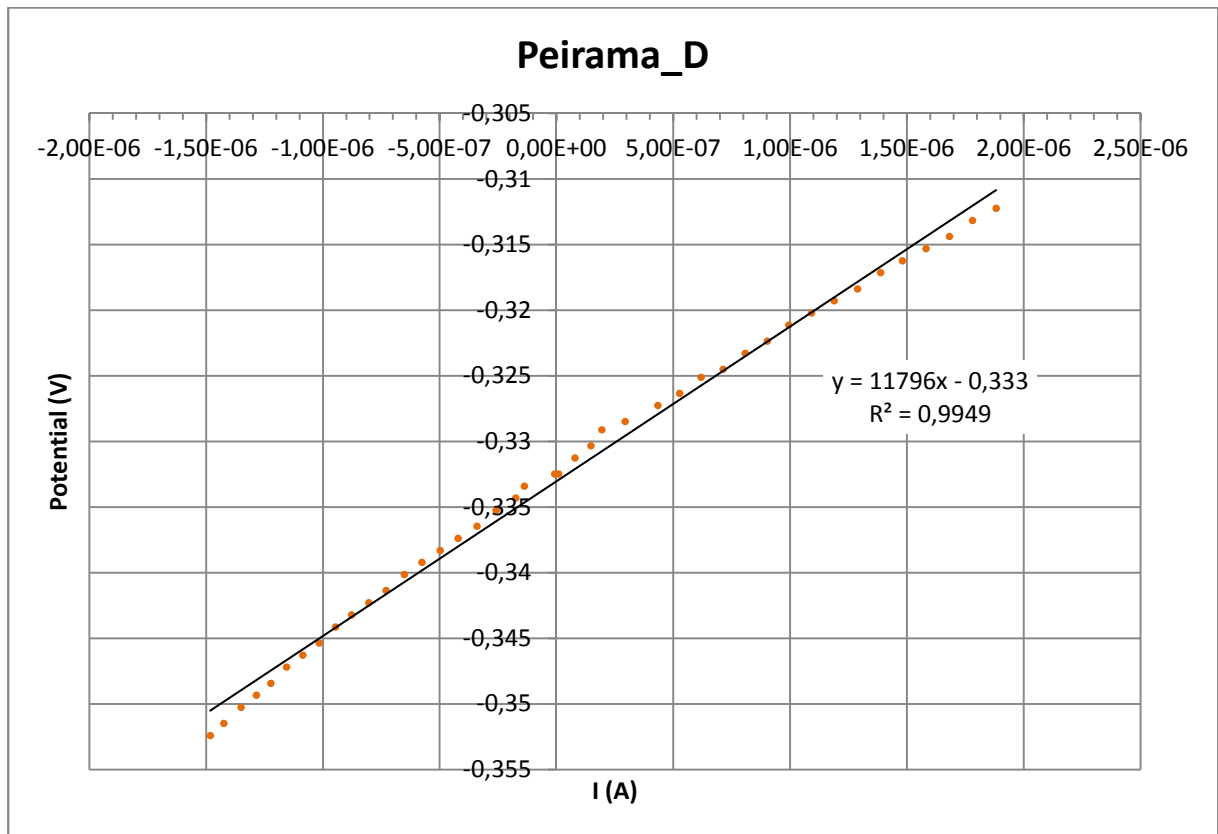


Figure 127:  $R_p$  value for linear anodic and cathodic curve

From the above values we can safely conclude that the treated specimens (A,B and D) present superior behavior against corrosion, comparing to the bare surface of the copper.

Table 15 : E<sub>corr</sub> values for each experiment and mean E<sub>corr</sub> values for treated and untreated Specimens

<b>Potentiodynamic Experiments</b>				
<b>Name of Experiment</b>	<b>Type of Specimens</b>	<b>Extreme log(i)/A (cm<sup>-1</sup>)</b>	<b>Potential (V) for Extreme log(i)/A</b>	<b>Average Potential for Extreme log(i)/A per Type of Specimen (V)</b>
Peirama_A	Chemically modified E.T.P.Copper	-7,1808	-0,2763	-0,2946
Peirama_B	Chemically modified E.T.P.Copper	-7,4511	-0,2751	
Peirama_D	Chemically modified E.T.P.Copper	-8,0983	-0,3325	
Peirama_F	Pure Electrolytic Tough Pitch Copper	-5,5580	-0,3355	-0,3527
Peirama_G	Pure Electrolytic Tough Pitch Copper	-4,4050	-0,3614	
Peirama_H	Pure Electrolytic Tough Pitch Copper	-5,1810	-0,3613	

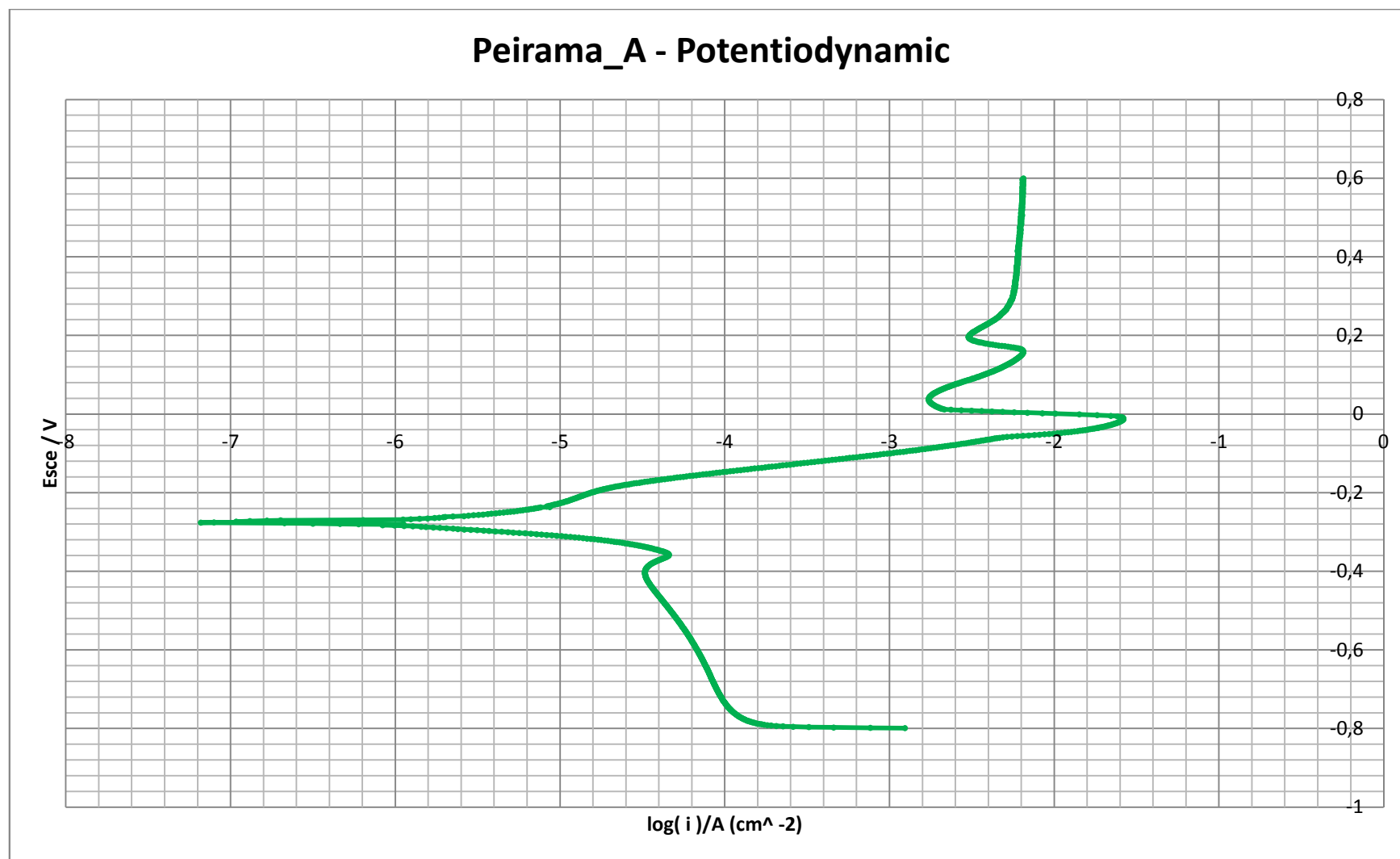


Figure 128 : Peirama\_A –Treated surface- Potentiodynamic Curve

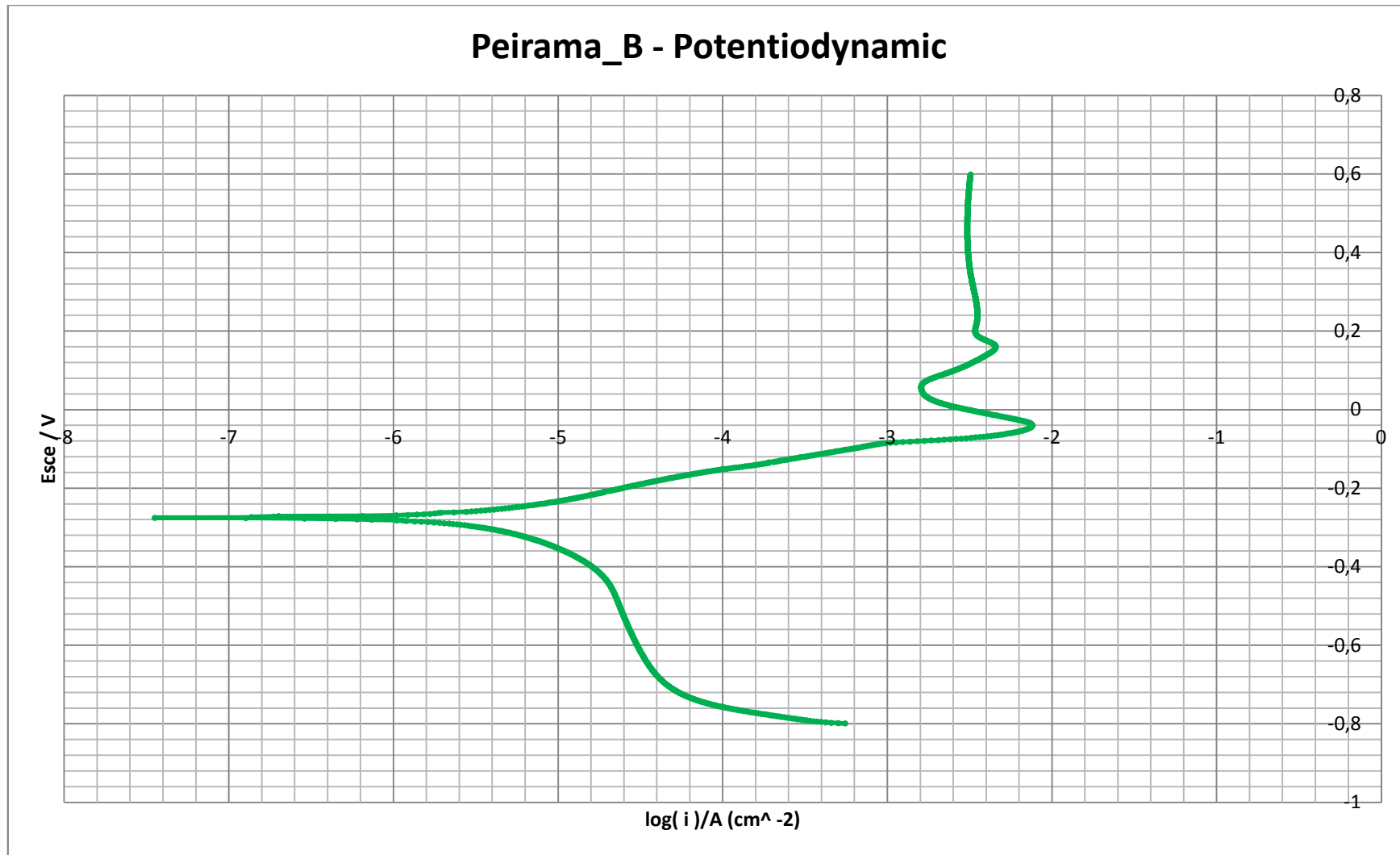


Figure 129 : Peirama\_B – Treated surface- Potentiodynamic Curve

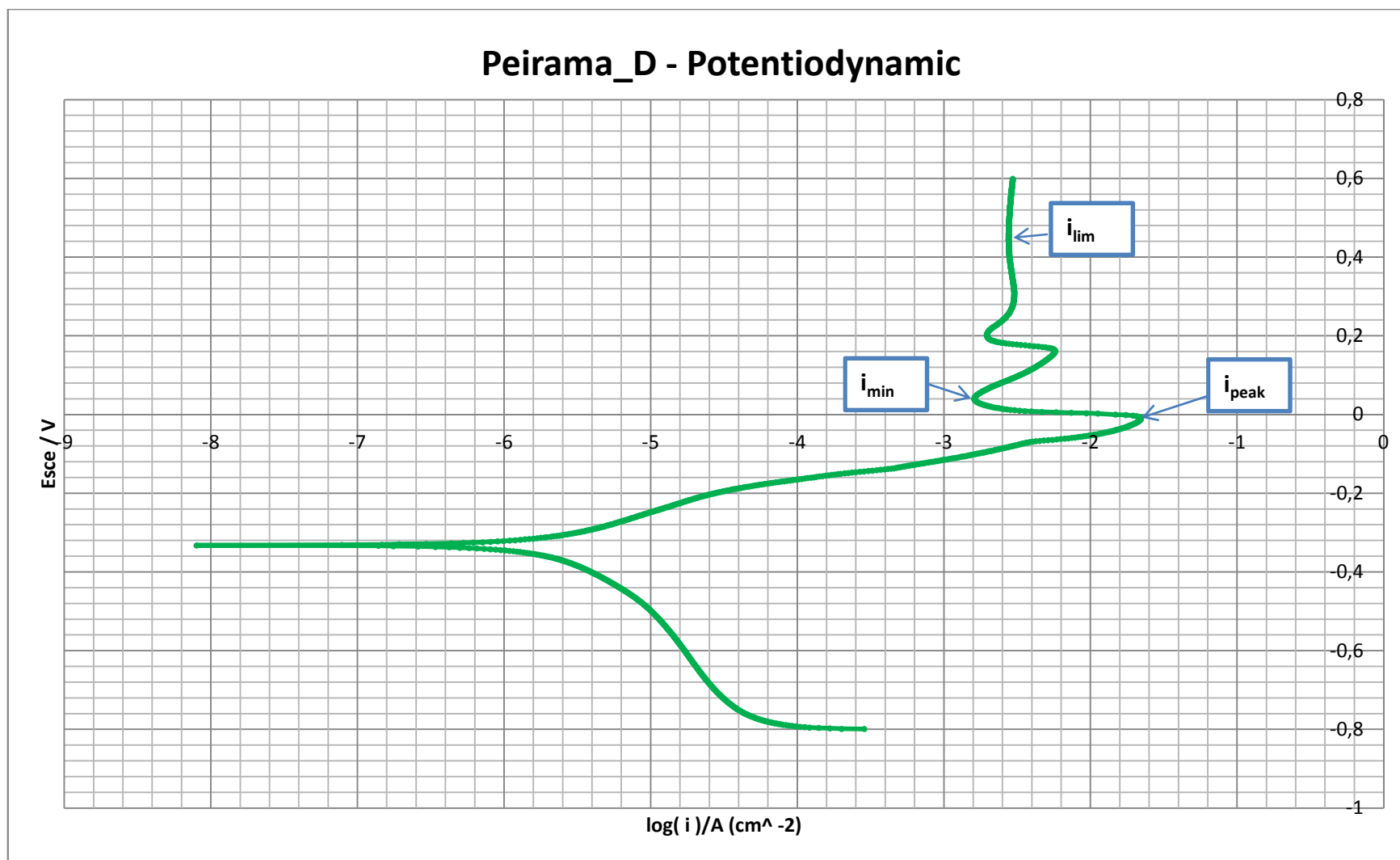


Figure 130 : Peirama\_D – Treated surface- Potentiodynamic Curve

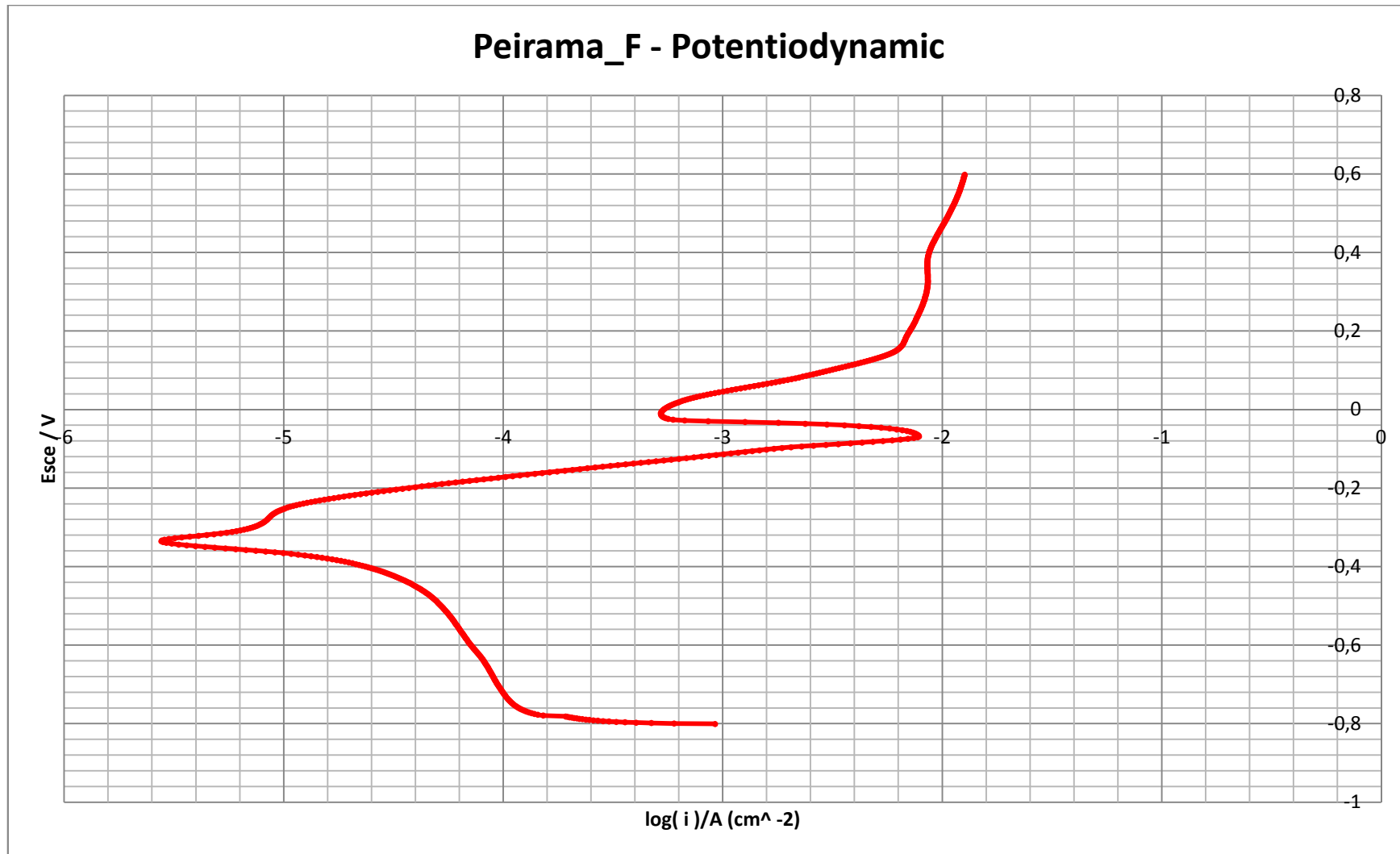


Figure 131 : Peirama\_F –Bare Copper Surface- Potentiodynamic Curve

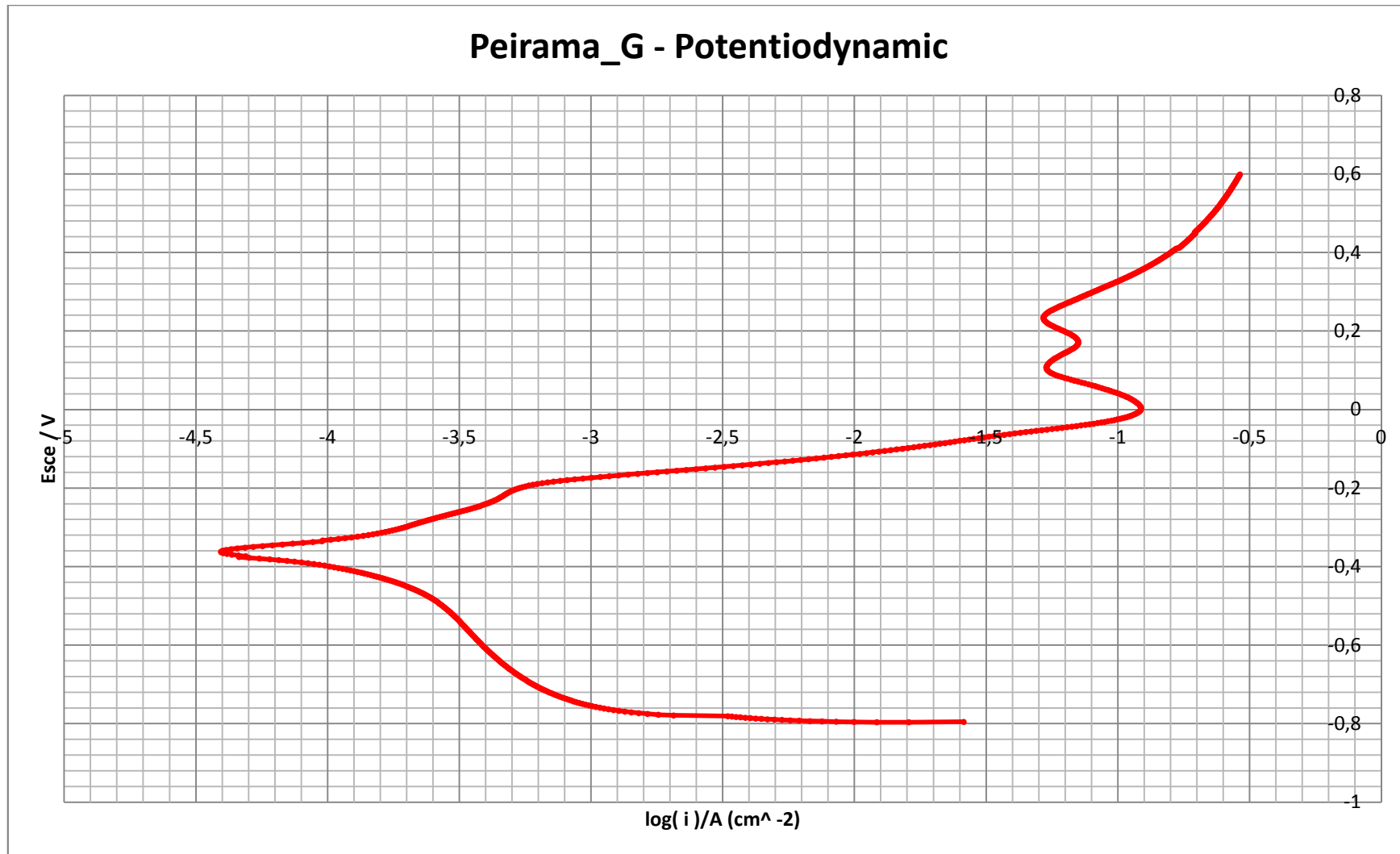


Figure 132 : Peirama\_G – Bare Copper Surface- Potentiodynamic Curve

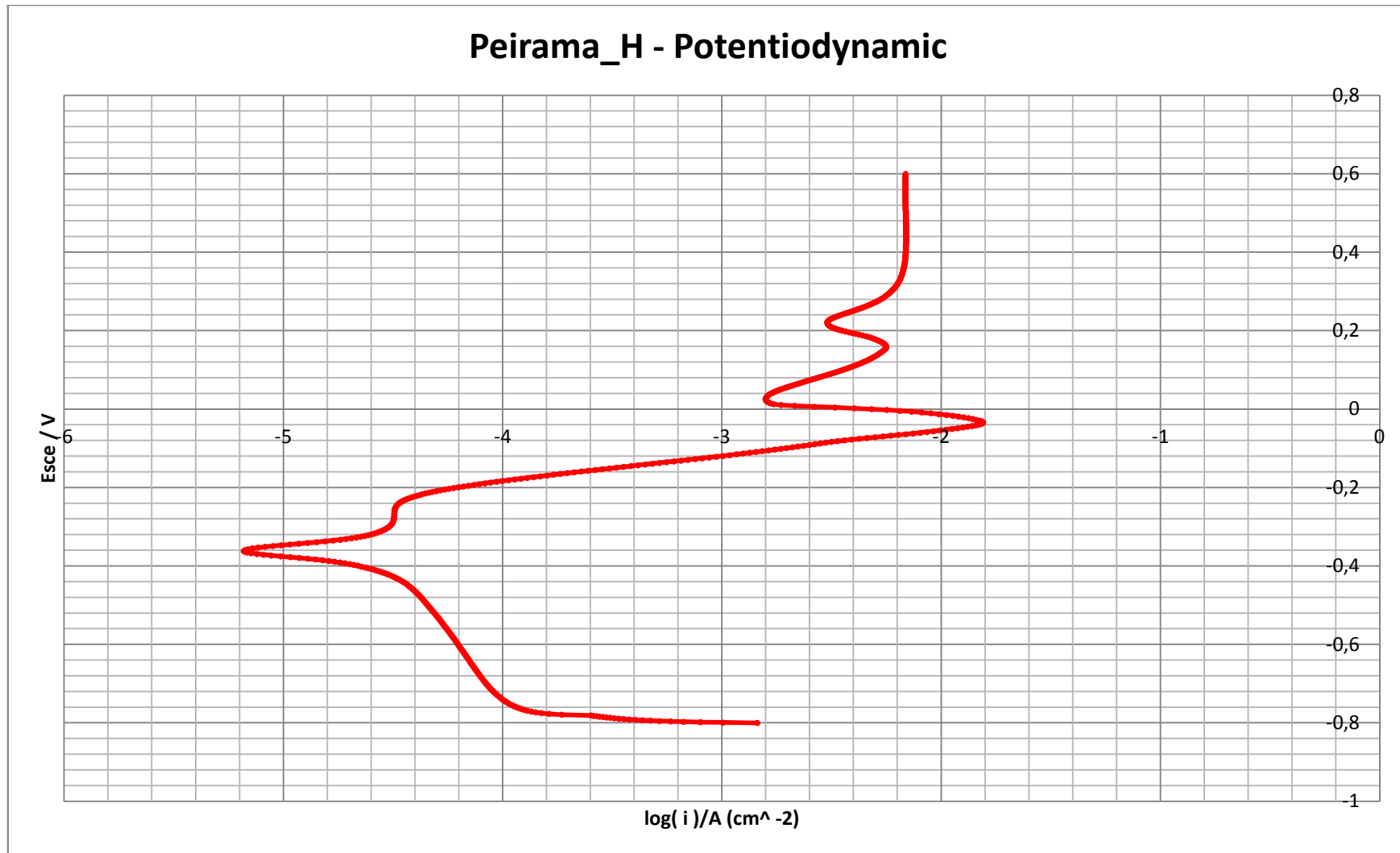


Figure 133 : Peirama\_H – Bare Copper Surface- Potentiodynamic Curve



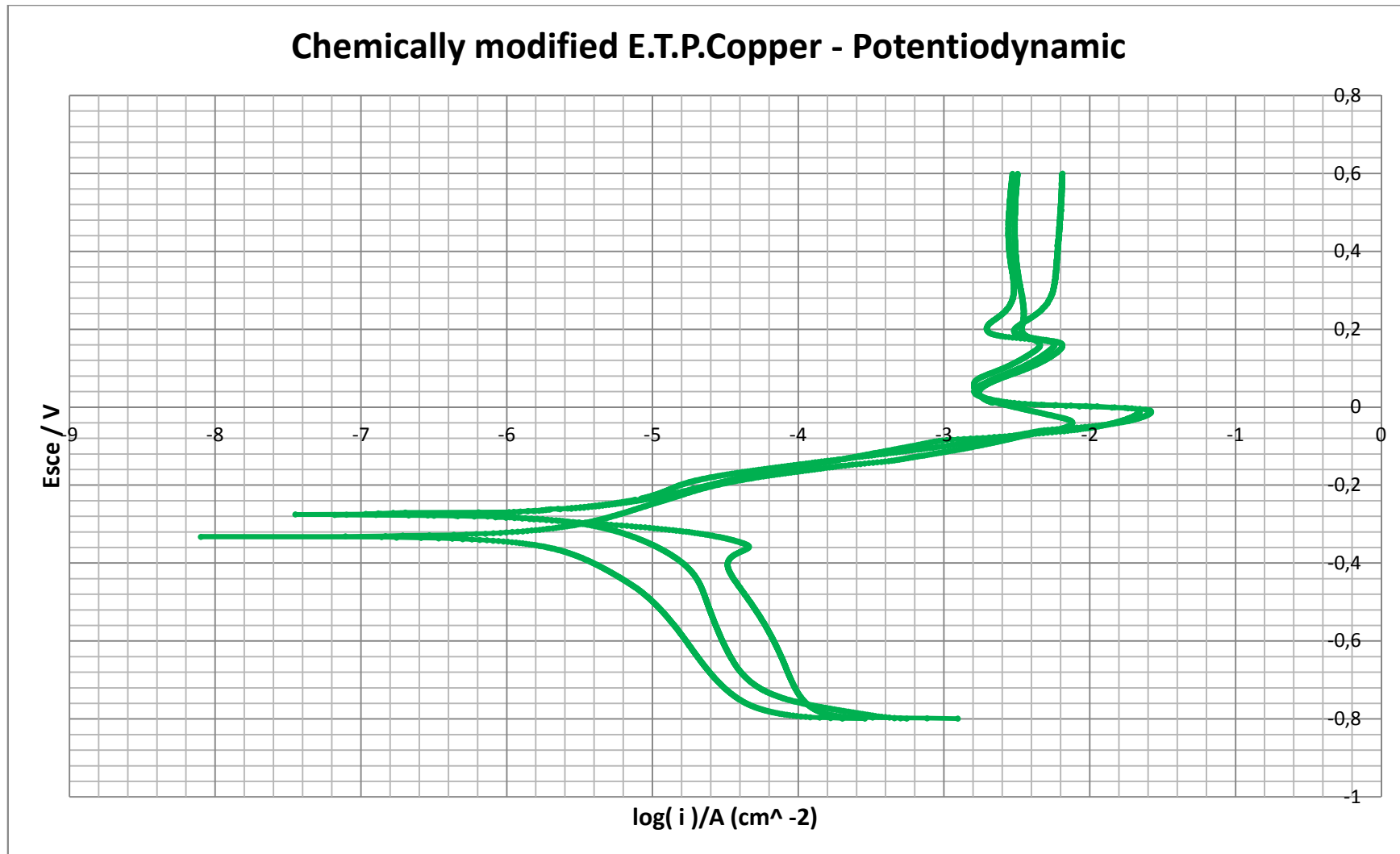


Figure 134 : Chemically modified E.T.P.Copper – Potentiodynamic Curves

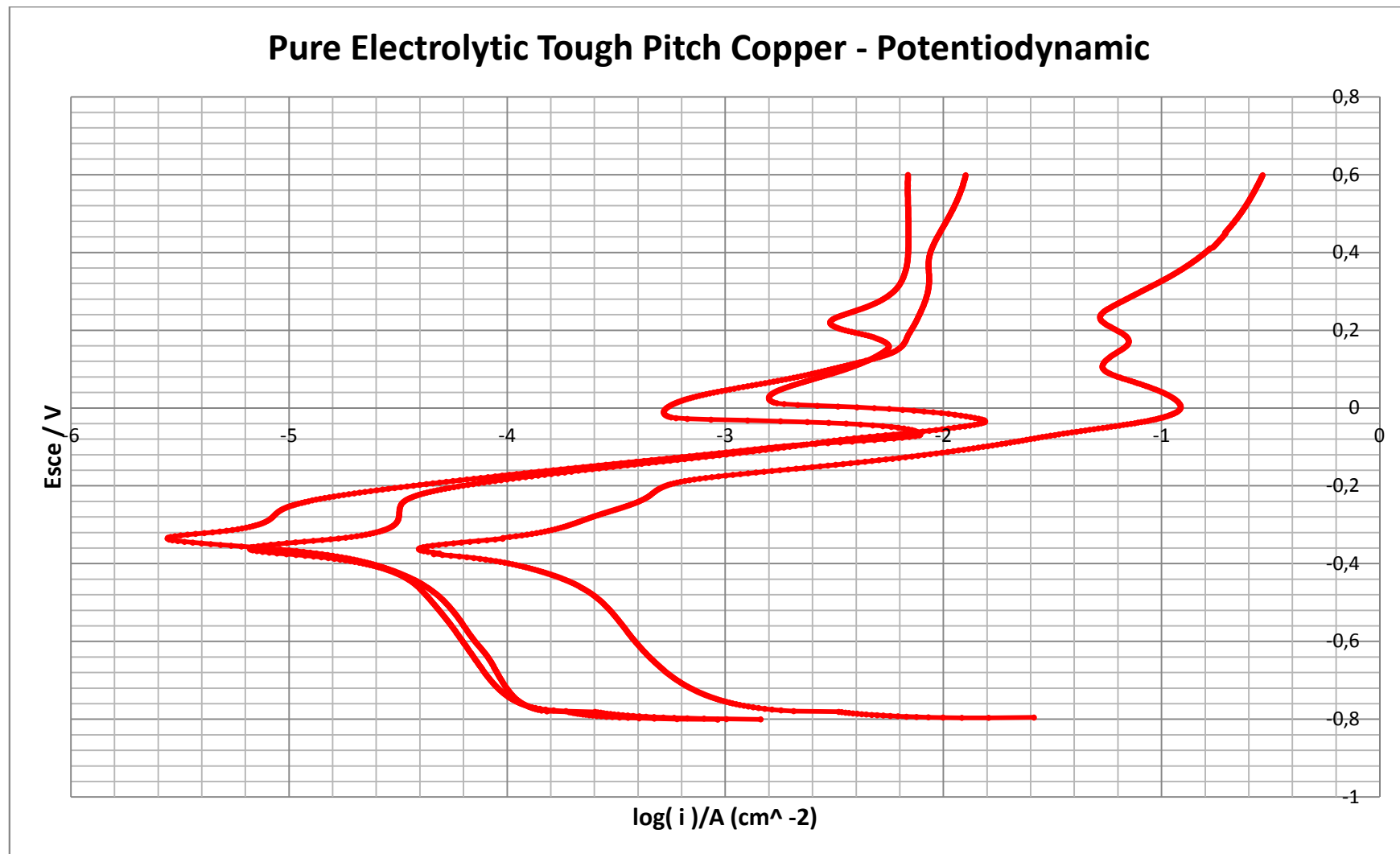


Figure 135: Pure Electrolytic Tough Pitch Copper – Potentiodynamic Curves

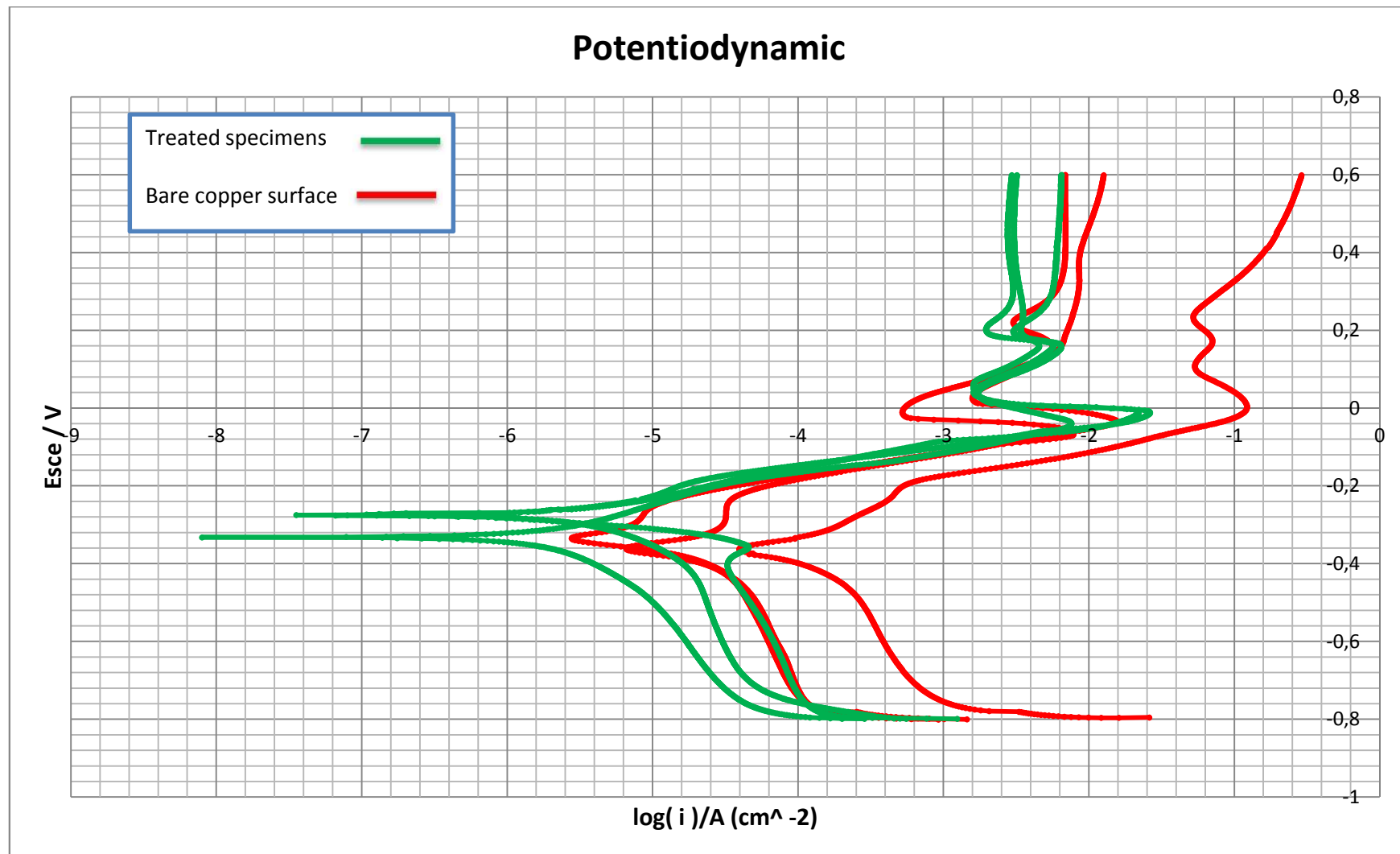


Figure 136 : Potentiodynamic Curves

## 5.8 Anticorrosion mechanism

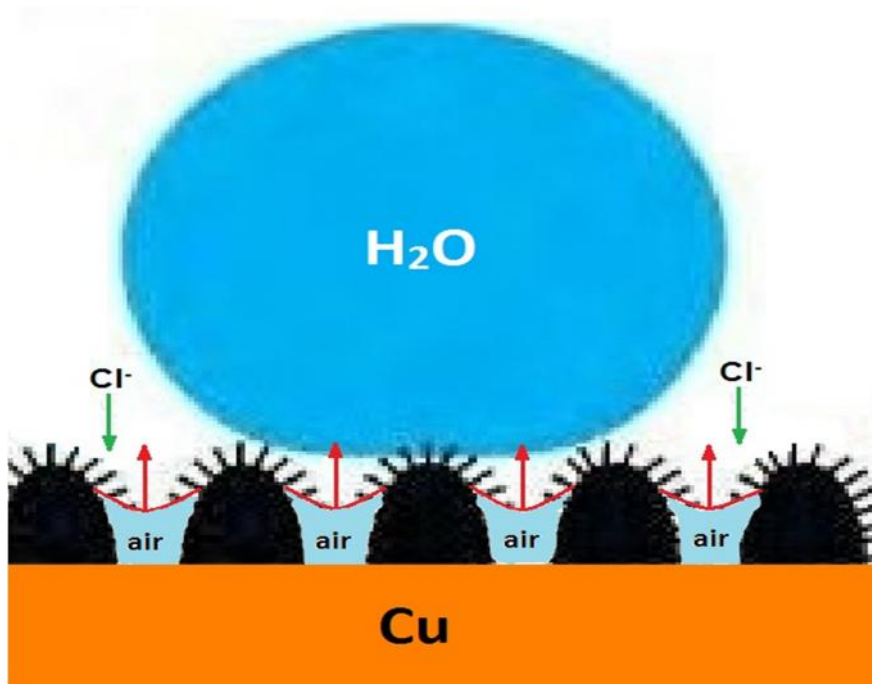


Figure 137: Model of the interface between super-hydrophobic surface and solution

The structure of super-hydrophobic surface can be simulated simply and elementarily to the interface model (Fig. 137). The super-hydrophobic surface composed of mountains (solid portion of the surface) can easily trap gas within the ‘valleys’ between the mountains. Therefore, the  $\text{Cl}^-$  can hardly reach the bare surface for the obstructive effect of ‘air valleys’.

Another important reason why the modified surface can improve the anticorrosion of copper is ‘capillarity’. As we know, when a vertical cylindrical tube is placed in liquid, the liquid rises and forms a concave surface, called a *meniscus* if the tube is hydrophilic; otherwise the liquid is depressed, if the tube is hydrophobic. The height of the water column within the tube can be calculated by the following equation:

$$h = \frac{2 * \gamma * \cos\theta}{\rho * g * R}$$

where,  $R$  is the radius of the cylindrical tube,  $\theta$  contact angle,  $\gamma$  surface tension and  $\rho$  is density of liquid. The capillary descend ( $h < 0$ ) is very obvious when the pore diameter ( $R$ ) is shorter than  $3\mu\text{m}$  and contact angle is approximately  $160^\circ$ . Then water transport against gravity is easy in such porous structure. As a result, the seawater can be pushed out from the pores of the superhydrophobic film by the Laplace pressure. Then the specimen could be protected perfectly in the seawater.

## 6 Conclusions

A novel super-hydrophobic film was prepared by *n*-tetradecanoic acid chemically adsorbed onto the copper sample. This method is a simple and inexpensive method to create super-hydrophobic surface on copper. Initially the copper surface was carefully prepared (grinded up to 1500 SiC) and etched with HNO<sub>3</sub> and consequently the specimens were immersed for 10 days with concentration of around 0.06M. This time and the procedure are ideal for the formation of stable flowerlike structure.

Contact Angle measurements revealed an obvious difference between the treated and the clean surface, more than two times. The measurements obtained for SHT are typical, and in accordance to the literature for super-hydrophobic treatments. When the coating was removed, the measured contact is still high, more than 100, implying that may be there is another layer, which still provides hydrophobic properties to the surface.

Scanning Electron Microscopy observations revealed a stable “*flowerlike structure*” of the surface, with mountain and valley areas. These observations combined with the results of the AFM images, prove that the structure of the *n*-tetradecanoic layer is a hierarchical structure (micro roughness covered with nano roughness). That hierarchical structure was not only necessary to have high contact angle but is also essential for the stability of the composite interface (water-solid and water- air).

Electrochemical experiments, Open Circuit and Potentiodynamic Polarization proved present superior behavior for the treated specimens against corrosion, comparing to the bare surface of the copper. The values for  $E_{corr}$  for treated specimens are shifted towards more positive values, albeit slightly, proving that they present lower corrosion susceptibility, from thermodynamic point of view. Moreover, Polarization Resistance ( $R_p$ ) values are obviously higher for the treated specimens. Finally the Tafel fit elaboration of the curves proved significantly lower values for the treated samples, denoting lower values for Corrosion Rate.

In conclusion, within our study a composite interface formed by the flower-like surface nanostructures, water droplet and air trapped in the crevices is responsible for the superior water-repellent property. The study of SEM, AFM, Contact Angle Measurements and Electrochemical analyze provide evidences that hydrophobicity plays an important role in corrosion behavior.

All experimental results proved that the super-hydrophobic surface can improve the corrosion resistance of copper significantly. It is believed that this method should be easily applied to large-scale production of super-hydrophobic engineering materials with ocean and naval industrial applications.

## 7 Bibliography

- [1] Παντελής, Δ.Ι., Χρυσουλάκης, Γ. Δ., *Επιστήμη και Τεχνολογία Μεταλλικών Υλικών*, Παπασωτηρίου, Αθήνα, 1996
- [2] Παντελής, Δ.Ι., Τσιούρβα Θ., *Διάβρωση και Προστασία Ναυπηγικών Κατασκευών*, Πανεπιστημιακές Εκδόσεις ΕΜΠ, 2012.
- [3] Denny A.Jones, "Principles and prevention of corrosion", second edition, Prentice Hall 1996
- [4] J. Chamberlain, K. Trethewey, "Corrosion for science and engineering", Longman Group limited 1995
- [5] Tian He a, Yuanchao Wang, Yijian Zhang a, Qun Lv a, Tugen Xu a, Tao Liu b, "Super-hydrophobic surface treatment as corrosion protection for aluminum in seawater", *Corrosion Science* 51 (2009) 1757–1761.
- [6] Tao Liu a, Yansheng Yin a, Shougang Chen, Xueting Chang, Sha Cheng, "Super-hydrophobic surfaces improve corrosion resistance of copper in seawater", *Electrochimica Acta* 52 (2007) 3709–3713
- [7] Shougang Chen, Yan Chen, Yanhua Lei, Yansheng Yin, "Novel strategy in enhancing stability and corrosion resistance for hydrophobic functional films on copper surfaces", *Electrochemistry Communications* 11 (2009) 1675–1679
- [8] Tao Liu, Shougang Chen, Sha Cheng, Jintao Tian, Xueting Chang, Yansheng Yin, "Corrosion behavior of super-hydrophobic surface on copper in seawater", *Electrochimica Acta* 52 (2007) 8003–8007
- [9] A. Dafali, B. Hammouti, R. Mokhlisse, S. Kertit, "Substituted uracils as corrosion inhibitors for copper in 3% NaCl solution", *Corrosion Science* 45 (2003) 1619–1630
- [10] K. Rahmouni, M. Keddou, A. Srhiri, H. Takenouti, "Corrosion of copper in 3% NaCl solution polluted by sulphide ions", *Corrosion Science* 47 (2005) 3249–3266
- [11] Rosa Vera, Patricia Verdugo, Marco Orellana, Eduardo Mupoz, "Corrosion of aluminium in copper–aluminium couples under a marine environment: Influence of polyaniline deposited onto copper", *Corrosion Science* 52 (2010) 3803–3810
- [12] Weihua Li, Lichao Hub, Shengtao Zhang, Baorong Hou, "Effects of two fungicides on the corrosion resistance of copper in 3.5% NaCl solution under various conditions", *Corrosion Science* 53 (2011) 735–745
- [13] Bharat Bhushan, "Biomimetics: lessons from nature-an overview", Royal Society Publishing, 2009

- [14] J. Newman, "Electrochemical Systems", Chaps. 3, 8, 11 and 16, Prentice-Hall Inc. (1973) and later editions.
- [15] P. Marcus, "Corrosion Mechanisms in Theory & Practice", 2nd Ed, Chaps. 1, 6, 8, Marcel Dekker (2002)
- [16] J. Scully, "The Fundamentals of Corrosion", 2nd Ed., Chap. 2, Pergamon Press (1981)
- [17] P. Atkins, "Physical Chemistry", Chap. 29, pp. 326 – 331, W. H. Freeman (1978)
- [18] Colin R. Crick, "The Chemistry and CVD of Hydrophobic Surfaces", University College London 2011
- [19] Daewoo Han, Andrew Steckl "Superhydrophobic and Oleophobic Fibers by Coaxial Electrospinning", Langmuir 20 April 2009
- [20] Balamurali Balu, Jong Suk Kim, Victor Breedveld and Dennis W. Hess "Design of Superhydrophobic Paper/Cellulose Surfaces via Plasma Enhanced Etching and Deposition", School of Chemical and Biomolecular Engineering, Georgia Institute of Technology
- [21] H.M. Shang, Y. Wang, S.J. Limmer, T.P. Chou, K. Takahashi, G.Z. Cao, "Optically transparent superhydrophobic silica-based films", Thin Solid Films 472 (2005) 37– 43
- [22] John T. Simpson, Alex DeTrana, "Superhydrophobic Materials", Oak Ridge National Laboratory, U.S Department of Energy
- [23] George F. Vander Voort, "ASM Handbook - Vol 09 – "Metallography and Microstructures" ", ASM International Handbook Committee, 2004
- [24] Lawrence J. Korb, Rockwell International and David L. Olson, Colorado School of Mines, "ASM Handbook - Vol 13 –, "Corrosion" ", ASM International Handbook Committee, 1992
- [25] Stephen D. Cramer and Bernard S. Covino, Jr., "ASM Handbook - Vol 13A – "Corrosion - Fundamentals, Testing, and Protection" ", ASM International Handbook Committee, 2003
- [26] Copper Development Association, "Copper – The Vital Metal", CDA Publication 121, 1998
- [27] Bruce L. Bramfitt, Arlan O. Benscoter, "Metallographer's Guide Practices and Procedures for Irons and Steels", ASM International 2002
- [28] K. L. Mittal, "Contact angle, wettability and adhesion", Volume 3, VSP, 2003
- [29] E. M. Sherif and Su-Moon Park, "Inhibition of Copper Corrosion in 3.0% NaCl Solution by N-Phenyl-1,4-phenylenediamine", Journal of The Electrochemical Society, 152(10) B428-B433 (2005).